Positivity-preserving cell-centered Lagrangian schemes for multi-material compressible flows: From first-order to high-orders

François Vilar, Chi-Wang Shu, P.H. Maire

Positivity-preserving cell-centered Lagrangian schemes for multi-material compressible flows: From first-order to high-orders

François Vilar[a,*], Chi-Wang Shu[a], Pierre-Henri Maire[b]

[a] *Division of Applied Mathematics, Brown University, Providence, RI 02912, USA*
[b] *CEA/CESTA, 15 Avenue des Sablières CS 6001 33 116 Le Barp cedex France*

Abstract

One of the main issues in the field of numerical schemes is to ally robustness with accuracy. Considering gas dynamics, numerical approximations may generate negative density or pressure, which may lead to nonlinear instability and crash of the code. This phenomenon is even more critical using a Lagrangian formalism, the grid moving and being deformed during the calculation. Furthermore, most of the problems studied in this framework contain very intense rarefaction and shock waves. In this paper, the admissibility of numerical solutions obtained by high-order finite-volume-scheme-based methods, such as the discontinuous Galerkin (DG) method, the essentially non-oscillatory (ENO) and the weighted ENO (WENO) finite volume schemes, is addressed in this Lagrangian gas dynamics framework. To this end, we first focus on the one-dimensional case. After briefly recalling how to derive Lagrangian forms of the gas dynamics system of equations, a discussion on positivity-preserving approximate Riemann solvers, ensuring first-order finite volume schemes to be positive, is then given. This study is conducted for both ideal gas and non ideal gas equations of state (EOS), such as the Jones-Wilkins-Lee (JWL) EOS or the Mie-Grüneisen (MG) EOS. It enables us to derive time step conditions ensuring the desired positivity property, as well as L_1 stability of the specific volume and total energy over the domain. Then, making use of the work presented in [74, 75, 15], this positivity study is extended to high-orders of accuracy, where new time step constraints are obtained, and proper limitation is required. This whole analysis is finally applied to the two-dimensional case, and shown to fit a wide range of numerical schemes in the literature, such as the GLACE scheme [12], the EUCCLHYD scheme [55], the GLACE scheme on conical meshes [8], and the LCCDG method [72]. Through this new procedure, scheme robustness is highly improved and hence new problems can be tackled. Numerical results are provided to demonstrate the effectiveness of these methods. Finally, let us emphasize that even if this paper is concerned with purely Lagrangian schemes, the theory developed is of fundamental importance for any methods relying on a purely Lagrangian step, as ALE methods or non-direct Euler schemes.

Keywords: positivity-preserving high-order methods, cell-centered Lagrangian schemes, updated and total Lagrangian formulations, Godunov-type method, unstructured moving grid, multi-material compressible flows, equations of state, Riemann solver

*Corresponding author
Email addresses: francois_vilar@brown.edu (François Vilar), shu@dam.brown.edu (Chi-Wang Shu), maire@celia.u-bordeaux1.fr (Pierre-Henri Maire)

1. Introduction

We aim at demonstrating the positivity-preservation property of methods solving two-dimensional Lagrangian gas dynamics equations, from first-order to high-orders of accuracy, under suitable constraints. It is well known that fluid dynamics relies on two kinematics descriptions: the Eulerian or spatial description and the Lagrangian or material description, refer for instance to [36, 32]. In the former, the conservation laws are written using a fixed reference frame whereas in the latter they are written through the use of a time dependent reference frame that follows the fluid motion. The Lagrangian representation is particularly well adapted to describe the time evolution of fluid flows contained in regions undergoing large shape changes due to strong compressions or expansions. Further, in this approach, there is no mass flux across the boundary surface of a control volume moving with the fluid velocity. Thus, Lagrangian representation provides a natural framework to track accurately material interfaces in multi-material compressible flows. Moreover, such a representation avoids the appearance of numerical diffusion resulting from the discretization of the convection terms present in the Eulerian framework.

In the Lagrangian description, the gas dynamics system may be derived in two different but consistent formulations, namely the updated Lagrangian formulation based on the moving configuration, and the total Lagrangian formulation based on the fixed initial configuration. In this latter approach, the physical conservation laws are written employing the Lagrangian coordinates which refer to the initial configuration of the fluid flow. Moreover, in these equations the divergence and gradient operators are expressed by means of the Piola transformation [36], which requires the knowledge of the deformation gradient tensor, *i.e.* the Jacobian matrix associated to the Lagrange-Euler flow map. The deformation gradient tensor characterizes the time evolving deformation and is governed by a partial differential equation named the geometric conservation law (GCL). To ensure the consistency between the initial and the current configurations, the deformation gradient tensor has to satisfy an involutive constraint [64], which implies the Piola compatibility condition. The total Lagrangian approach is very well known in the solid mechanics community wherein it is extensively used to model solid dynamics undergoing large deformations [36]. In contrast to the total Lagrangian formulation, the updated Lagrangian formulation is a moving domain method, which is widely employed in fluid mechanics. In this approach, the gas dynamics equations are written employing the Eulerian coordinates. They refer to the current configuration of the fluid flow. The time derivative of the physical variables is taken following the path of the fluid particles: this is the material derivative. The integral formulation of the conservation laws is readily obtained by employing the Reynolds transport formula over an arbitrary moving control volume. The time rate of change of a zone volume is governed by a partial differential equation which is the updated Lagrangian form of the GCL.

Two approaches are mainly employed to solve updated Lagrangian formulations of the gas dynamics equations, namely the cell-centered and staggered approaches. In the cell-centered hydrodynamics, a cell-centered placement of all hydrodynamic variables is employed. However, the referential being assumed to move as the fluid flows, one needs to advect the grid points. Also, this has to be done with respect to the GCL, which means that the new volume computed through the new position of the grid nodes has to be the same as the one derived from the discretization of the governing equation of the specific volume. Furthermore, in the multi-dimensional case, due to the large number of neighboring cells sharing a node, one cannot apply in a straightforward manner

one-dimensional solvers to define uniquely the grid point velocity. The staggered hydrodynamics has been developed to avoid such complications. In this framework, a staggered discretization is employed such that the kinematic variables (vertex position, velocity) are located at the nodes whereas the thermodynamic variables (density, pressure, internal energy) are defined at the cell centers. The conversion of kinetic energy into internal energy through shock waves, consistent with the second law of thermodynamics, is ensured by adding an artificial viscosity term. The staggered grid schemes employed in most hydro-codes have been remarkably successful over the past decades in solving complex multi-dimensional compressible fluid flows, refer for instance to [33, 73, 10, 11, 45]. However, they clearly have some theoretical and practical deficiencies such as mesh imprinting and symmetry breaking. In addition, the fact that all variables are not conserved over the same space can make these schemes difficult to handle when one wants to assess analytical properties of the numerical solution. For all these reasons, this paper focuses on the cell-centered approach. Different techniques may be employed to build the numerical fluxes and move the grid through the use of approximate Riemann solvers, with respect to the GCL. The interested readers may refer to the following papers [1, 12, 13, 52, 63, 8, 41, 70, 3, 9, 7, 72] for a more detailed description of this approach and its variants. In the section dedicated to the two-dimensional case, a general procedure to develop first-order finite volume schemes on general polygonal meshes is presented. Such formulation will cover the numerical methods introduced in [12, 55, 8, 70, 72].

Although a wide range of purely Lagrangian formulations are available, together with the different advantages associated to them, it is well known these descriptions admit a severe drawback in some situations. In the presence of intense vortexes or shear flows, Lagrangian methods suffer from a lack of robustness which may lead to the appearance of non-convex, or even tangled, cells. This is a consequence of the fundamental assumption that the referential moves as the fluid flows. A remedy for this type of problems may be the use of an Arbitrary Lagrangian Eulerian (ALE) method, where generally the explicit Lagrangian phase is combined with a rezoning phase in which a new grid is defined by improving the geometric quality of the cells, and a remapping phase in which the Lagrangian solution is conservatively interpolated onto the new grid. This ALE description, initially introduced in the seminal paper [39], has been the object of many papers and will not be addressed in this article. We focus here on the purely Lagrangian phase and how to ensure the numerical solution to remain admissible. Because, even before facing the extreme case where the mesh tangles, Lagrangian methods, just as any other numerical schemes, may produce non-physical solutions, with for instance negative density or pressure. This work is thus of crucial significance not only for Lagrangian schemes, but also for any methods relying on a purely Lagrangian step, as ALE methods or non-direct Euler schemes based on a Lagrangian step plus a projection. Let us note that there exist other type of ALE methods which are not based on a Lagrangian phase, along with rezoning and remapping steps. These so-called direct ALE schemes take into account, in the system of equations itself, the grid velocity which can be different if needed from the fluid velocity. For instance in [7, 24, 25], the authors developed high-order ALE one-step WENO finite volume schemes.

The issue of robustness is fundamental for numerical schemes. Considering gas dynamics for instance, numerical approximations may generate negative density or pressure, which may lead to nonlinear instability or crash of the code. This phenomenon is even more critical using a Lagrangian formalism, the grid moving and being deformed during the calculation. Furthermore,

most of the problems studied in this framework contain very intense rarefaction and shock waves. These phenomena are the consequence of the lack of a particular property, often referred as positively conservation or positivity preservation. For instance, it has been proven in [28] that for some class of Riemann problems, any linearization would yield nonphysical negative density or pressure. This is the case of, for example, the Roe scheme, [66]. This issue of positivity is generally addressed for the Eulerian case, see [28, 61, 62, 4, 6], but very few papers exist on this topic for the Lagrangian formulation. Contrary to the Eulerian case where non-admissible states may appear in low density regions, in the Lagrangian frame it is in regions of high compression that the scheme may fail and produce negative specific volume or internal energy. In [59], Munz assessed the positivity preservation property of the HLL (Harten, Lax, van Leer) scheme [38] and the HLLE (HLL Einfeldt) scheme [27] in the Lagrangian framework. For the HLL solver, he derived particular definitions of the left and right wavespeeds ensuring the positivity of the specific volume. In [15], Cheng and Shu employed the HLLC (HLL contact) solver [69] to develop positivity-preserving Lagrangian schemes in a direct ALE point of view, namely not making use of the Lagrangian mass coordinates generally adopted in the one-dimensional Lagrangian framework. Suitable choices in the left and right wavespeeds are also required to ensure the positivity of the numerical solution. Let us also mention the positive and entropic schemes developed in [31, 21] for a general class of Lagrangian systems including gas dynamics and magnetohydrodynamics.

In this paper, the numerical schemes presented rely on a solver widely used in the Lagrangian community and generally referred as the two-states solver, see [21, 53]. It can be seen as the counterpart of the HLLC solver in term of Lagrangian mass coordinate, and reduces in its simplest version to the Godunov acoustic scheme [35]. This solver will prove to be positivity preserving under particular definitions of the left and right wavespeeds. Furthermore, we will also demonstrate how to relax any wavespeed condition, and thus allowing us to make use of the Godunov acoustic scheme, but still ensuring the positivity of the numerical solution. To that purpose, an additional time step constraint has to be used, along with the correct CFL condition.

The question is then how to extend this positivity property to higher-order accuracy. In the Eulerian framework, earlier positivity-preserving schemes have been designed up to second-order, see for instance [61, 62, 29, 48]. More recently, Zhang and Shu developed in a series of papers, [74, 75, 76, 77], a general technique to extend the positivity-preserving property to high-order schemes based on finite-volume-like discretizations, such as the discontinuous Galerkin (DG) method, and the essentially non-oscillatory (ENO) and the weighted ENO (WENO) finite volume schemes. This is the technique used by Cheng and Shu in [15] to prove the high-order Lagrangian schemes developed are positivity-preserving. This is also the technique used in this paper, and adapted in the two-dimensional case, to assess the positivity of the high-order Lagrangian schemes presented here.

To this end, the remainder of this paper is organized as follows: In Section 2, we focus on the one-dimensional case. After briefly recalling how to derive Lagrangian forms of the gas dynamics system of equations, a discussion on positivity-preserving approximate Riemann solvers, ensuring first-order finite volume scheme to be positive, is given. This study is conducted for both ideal gas and non ideal gas equations of state (EOS), such as the Jones-Wilkins-Lee (JWL) EOS and the Mie-Grüneisen (MG) EOS. Then, making use of the work presented in [74, 75, 15], this positivity study is extended to higher-order accuracy, where new time step constraints are obtained, and proper

limitation is required. In Section 3, the positivity-preserving analysis is finally applied to the two-dimensional case, and is shown to fit a wide range of numerical schemes in the literature, such as the GLACE scheme [12], the EUCCLHYD scheme [55], the Lagrangian finite volume scheme on conical meshes [8], and the LCCDG method [72]. Through this new procedure, scheme robustness is highly improved and hence new problems can be tackled. Numerical results, provided in Section 4, demonstrate the effectiveness of these methods.

2. One-dimensional case

Most of the ingredients and techniques used in the multi-dimensional case being based on those developed in the 1D case, this first section is then dedicated to the one-dimensional case only. For the sake of clarity, we first recall the local forms of the gas dynamics governing equations in updated, total and mass Lagrangian frameworks in one dimension. The interested reader may refer to [32, 67, 26, 36, 21, 53, 72] for further details.

2.1. Governing equations

Let us first recall the standard one-dimensional compressible Euler system, constituted of the continuity equation, the momentum and total energy conservation laws

$$\frac{\partial \rho}{\partial t} + \frac{\partial \rho u}{\partial x} = 0, \tag{1a}$$

$$\frac{\partial \rho u}{\partial t} + \frac{\partial (\rho u^2 + p)}{\partial x} = 0, \tag{1b}$$

$$\frac{\partial \rho e}{\partial t} + \frac{\partial (\rho u e + p u)}{\partial x} = 0. \tag{1c}$$

In this system, ρ represents the density of the fluid, u its velocity, e its total energy and p its pressure. To obtain the counterpart of these equations in a Lagrangian framework, a moving reference has to be considered. To that end, let X be the position of a point of the fluid in its initial configuration. X is called the (initial) Lagrangian coordinate. Through the fluid flow, the fluid particle initially located at X will lie at $x(X,t)$ at time t. x is named the (moving) Eulerian coordinate. The trajectory equation, $\frac{\partial}{\partial t}x(X,t) = u(X,t)$, emphasizes the fact that the particles move as the fluid flows, where $u(X,t)$ is nothing but the fluid velocity. The Jacobian J, associated with the fluid flow, is defined as $J = \frac{\partial x}{\partial X}$. We assume $J > 0$ at all time so that the flow map is invertible. To move the fixed reference frame to a moving one following the fluid flow, we introduce here the definition of the material derivative. Let f be a fluid variable with sufficient smoothness. For the sake of conciseness, the same notation is used to denote the value of the physical quantity regardless the employed description

$$f = f(x,t) = f(x(X,t),t) = f(X,t).$$

Then, the time rate of change of f following a fluid particle along its motion writes

$$\frac{\mathrm{d}}{\mathrm{d}t} f(x,t) \equiv \frac{\partial}{\partial t} f(X,t) = \frac{\partial}{\partial t} f(x,t) + u(x,t)\, \frac{\partial}{\partial x} f(x,t). \tag{2}$$

This definition, along with basic algebraic manipulations, enables us to get the one-dimensional gas dynamics equations (1) in an updated Lagrangian form as follows

$$\rho \frac{\mathrm{d}\,\mathsf{U}}{\mathrm{d}t} + \frac{\partial\,\mathsf{F}(\mathsf{U})}{\partial x} = \mathsf{0}. \tag{3}$$

Here $\mathsf{U} = (\tau, u, e)^{\mathrm{t}}$ is the vector of the mass conservative quantities and $\mathsf{F}(\mathsf{U}) = (-u,\, p,\, p\,u)^{\mathrm{t}}$ the flux, where $\tau = \frac{1}{\rho}$ denotes the specific volume. System (3) is said to be mass conservative because the conserved quantity is $\rho\,\mathsf{U} = (1, \rho\,u, \rho\,e)^{\mathrm{t}}$. Indeed, thanks to the mass conservation relation $\frac{\partial\,\rho\,J}{\partial t} = 0$, integrating equation (3) over the control volume $\omega = [x_L, x_R]$ leads to the conservative integral form

$$\frac{\partial}{\partial t}\int_{\omega} \rho\,\mathsf{U}\,\mathrm{d}x + \mathsf{F}(\mathsf{U}_R) - \mathsf{F}(\mathsf{U}_L) = 0, \tag{4}$$

where $\mathsf{U}_{L/R} = \mathsf{U}(x_{L/R}, t)$. Another Lagrangian formalism, more often used in solid dynamics, is the total Lagrangian form which is based on the initial coordinate. The counterpart of system (3) in the initial configuration can be easily obtained for one dimension through the use of the simple derivative relation $\frac{\partial f}{\partial x} = J^{-1}\,\frac{\partial f}{\partial X}$, which writes

$$\rho^0 \frac{\partial\,\mathsf{U}}{\partial t} + \frac{\partial\,\mathsf{F}(\mathsf{U})}{\partial X} = \mathsf{0}, \tag{5}$$

where ρ^0 refers to the initial density. This system is the local form of the total Lagrangian gas dynamics equations. Its integral conservative form reads

$$\frac{\partial}{\partial t}\int_{\Omega} \rho^0\,\mathsf{U}\,\mathrm{d}X + \mathsf{F}(\mathsf{U}_R) - \mathsf{F}(\mathsf{U}_L) = 0, \tag{6}$$

where $\mathsf{U}_{L/R} = \mathsf{U}(x(X_{L/R}, t), t)$. Formulations (3) and (5) are perfectly equivalent under the assumption $J > 0$, and they both write the same in a mass Lagrangian formulation as follows

$$\frac{\mathrm{d}\,\mathsf{U}}{\mathrm{d}t} + \frac{\partial\,\mathsf{F}(\mathsf{U})}{\partial m} = \mathsf{0}, \tag{7}$$

where $\partial m = \rho^0\,\partial X = \rho\,\partial x$ is referred as the mass coordinate. The use of such coordinate, generally employed in the Lagrangian community, is restricted to the one-dimensional case. In its non-conservative form, this system yields

$$\frac{\mathrm{d}\,\mathsf{U}}{\mathrm{d}t} + \mathsf{A}(\mathsf{U})\,\frac{\partial\,\mathsf{U}}{\partial m} = 0, \tag{8}$$

where the flux Jacobian matrix $\mathsf{A}(\mathsf{U})$ has $\lambda = \{-z, 0, z\}$ as eigenvalues, where $z = \rho\,a$ denotes the acoustic impedance and a the thermodynamic sound speed.

The thermodynamic closure of these systems is given by expressing the pressure p and the temperature T in terms of the density ρ, the specific entropy S, and the internal energy $\varepsilon = e - \frac{u^2}{2}$ through the equation of state

$$p = \rho^2\,\frac{\partial \varepsilon}{\partial \rho}|_S \quad \text{and} \quad T = \frac{\partial \varepsilon}{\partial S}|_\rho.$$

This constitutive equation is consistent with the fundamental Gibbs relation

$$T\,\mathrm{d}S = \mathrm{d}\varepsilon + p\,\mathrm{d}\tau. \tag{9}$$

We also assume that the specific entropy is a concave function with respect to the specific volume τ and the internal energy ε. We note that the equation of state can also be written under the so-called incomplete form $p = p(\rho, \varepsilon)$. Finally, the thermodynamic sound speed is defined as $a^2 = \frac{\partial p}{\partial \rho}|_S$. Obviously, a^2 has to remain positive at all time. A numerical scheme not ensuring this property may lead to crash of the code. This remark will be the guiding principle of this paper, for the different equations of state studied.

2.2. Equations of state

In this paper, we consider several widely assessed multi-material problems with general equations of state. In practice, we make use of four different EOS, from the simple ideal gas one, to the more complex Mie-Grüneisen EOS for solids. Further details can be found in Appendix A.

Gamma gas law for perfect gas

For perfect gas, we define the thermodynamic pressure as

$$p = \rho(\gamma - 1)\varepsilon, \tag{10}$$

where $\gamma > 1$ is the polytropic index of the gas.

Stiffened gas EOS

This equation of state, generally used for water under very high pressures, is more generic than the ideal one. Furthermore, prefect gas is a special case of stiffened gas. Here, the pressure reads

$$p = \rho(\gamma - 1)\varepsilon - \gamma\, p_s, \tag{11}$$

where p_s is a positive constant representing the molecular attraction between water molecules.

Jones-Wilkins-Lee (JWL) EOS for detonation-product gas

This equation of state is used to describe explosions. Here, the pressure reads

$$p = \rho(\gamma - 1)\varepsilon + f_j(\rho), \tag{12}$$

where the definition of the positive function $f_j(\rho)$ can be found in Appendix A.3.

Mie-Grüneisen EOS for solids

Even if this paper is concerned with solving gas dynamics problems, one can decide to plug equations of state generally used in solid mechanics into the studied system. Here, we make use of the Mie-Grüneisen equation of state for shock-compressed solids. In this case, the pressure reads

$$p = \rho_0\,\Gamma_0\,\varepsilon + \rho_0\,a_0^2\,f_m(\eta), \tag{13}$$

where $\eta = \frac{\rho}{\rho_0}$, ρ_0 being the density of the unstressed material. The physical meaning of the constants involved in (13), as well as the definition of $f_m(\eta)$, can be found in Appendix A.4.

These different definitions of pressure yield different domains of validity. Indeed, physically the fluid flow has the positivity property for some variables such as density, internal energy, or the quantity inside the square root to define the sound speed. Let us note that it is not always the case of the pressure, which can yield negative values for the stiffened gas EOS for instance. In Appendix A, we prove that a sufficient condition for the solution to be physical writes as follows

$$(\rho, \widehat{\varepsilon}) \in]\rho_{min}, \rho_{max}[\times]\varepsilon_{min}, +\infty],$$

where $\widehat{\varepsilon} = \varepsilon - p_s\,\tau$ in the stiffened EOS case and $\widehat{\varepsilon} = \varepsilon$ otherwise, and ρ_{min}, ρ_{max} and ε_{min} are positive constants depending on the EOS. Furthermore, if the solution lies in this validity domain then one can know for sure that $a^2 > 0$. That being said, we now aim at ensuring that the numerical schemes under consideration produce solutions lying in this validity domain. But before exploring the case of a generic order of accuracy in space, one needs to ensure that the first-order scheme preserves the desired property. The first-order scheme will provide the healthy base on which one can build an high-order approximation.

2.3. First-order schemes

The cell-centered discretization of Lagrangian gas dynamics equations is quite well-known and has been the subject of many seminal papers, see for instance [65, 46, 23, 59, 34, 20, 21, 5, 31, 71, 53] and the references within. Let us briefly recall the general framework of these methods. First, let $\Omega = [X_b, X_e]$ be the domain filled by the fluid in its initial configuration. Its image through the flow map is the considered domain $\omega = [x_b, x_e]$ at time t. These domains are partitioned into I non-overlapping cells, respectively $\Omega_i = [X_{i-\frac{1}{2}}, X_{i+\frac{1}{2}}]$ and $\omega_i = [x_{i-\frac{1}{2}}, x_{i+\frac{1}{2}}]$, where ω_i is the image of cell Ω_i through the fluid flow. This relation is given by the trajectory equation $\frac{\mathrm{d}}{\mathrm{d}t} x_{i+\frac{1}{2}} = \overline{u}_{i+\frac{1}{2}}$, where $\overline{u}_{i+\frac{1}{2}}$ denotes the vertex velocity. $X_{\frac{1}{2}}$ identifies the left boundary X_b of the initial domain, and $X_{I+\frac{1}{2}}$ the right boundary X_e. Similarly, $x_{\frac{1}{2}}$ and $x_{I+\frac{1}{2}}$ identify the left and right boundaries, x_b and x_e, of the actual domain. Let us define the constant mass m_i of cell ω_i as

$$m_i = \int_{\Omega_i} \rho^0(X)\,\mathrm{d}X = \int_{\omega_i} \rho(x,t)\,\mathrm{d}x. \tag{14}$$

We introduce now the mass averaged value of function ϕ as

$$\phi_i = \frac{1}{m_i}\int_{\Omega_i} \rho^0(X)\,\phi(X,t)\,\mathrm{d}X = \frac{1}{m_i}\int_{\omega_i} \rho(x,t)\,\phi(x,t)\,\mathrm{d}x. \tag{15}$$

This definition corresponds to a classical average operator weighted by the density. Through (15), let U_i be the mass averaged solution vector U on cell ω_i. Then, integrating on the control volume $\omega_i = [x_{i-\frac{1}{2}}, x_{i+\frac{1}{2}}]$ either system (3), (5) or (7) yields the following semi-discrete first-order finite volume scheme

$$m_i \frac{\mathrm{d}\,\mathsf{U}_i}{\mathrm{d}t} + \overline{\mathsf{F}}(\mathsf{U}_i, \mathsf{U}_{i+1}) - \overline{\mathsf{F}}(\mathsf{U}_{i-1}, \mathsf{U}_i) = \mathsf{0}, \tag{16}$$

where $\overline{\mathsf{F}}(\mathsf{U}_i, \mathsf{U}_{i+1}) \equiv \overline{\mathsf{F}}_{i+\frac{1}{2}} = (-\overline{u}_{i+\frac{1}{2}}, \overline{p}_{i+\frac{1}{2}}, \overline{p}_{i+\frac{1}{2}}\,\overline{u}_{i+\frac{1}{2}})^{\mathrm{t}}$ denotes the numerical flux at the node $x_{i+\frac{1}{2}}$, with the intercell values $\overline{u}_{i+\frac{1}{2}}$ and $\overline{p}_{i+\frac{1}{2}}$ computed from the left and right states U_i and U_{i+1}. Different ways of computing these intercell values yield different numerical fluxes and different first

order schemes. Let $0 = t^0 < t^1 < \cdots < t^N = T$ be a partition of the time domain $[0, T]$, and $\Delta t^n = t^{n+1} - t^n$ denotes the n^{th} time increment. Then, applying a standard forward Euler scheme as time integrator on system (16), one gets the time discrete version of the previous first-order finite volume scheme as follows

$$\mathsf{U}_i^{n+1} = \mathsf{U}_i^n - \frac{\Delta t^n}{m_i} \left[\overline{\mathsf{F}}(\mathsf{U}_i^n, \mathsf{U}_{i+1}^n) - \overline{\mathsf{F}}(\mathsf{U}_{i-1}^n, \mathsf{U}_i^n) \right]. \tag{17}$$

Similar time integration of the trajectory equation enables us to advance in time the grid position, as $x_{i+\frac{1}{2}}^{n+1} = x_{i+\frac{1}{2}}^n + \Delta t^n \, \overline{u}_{i+\frac{1}{2}}^n$. The numerical scheme lies in the choice of the numerical flux function $\overline{\mathsf{F}}(\mathsf{U}_i^n, \mathsf{U}_{i+1}^n) = \overline{\mathsf{F}}_{i+\frac{1}{2}}^n$. Such function is generally obtained by exactly or approximately solving the Riemann problem at the cell interface $x_{i+\frac{1}{2}}$ with U_i^n and U_{i+1}^n as the left and right states respectively. The resolution of such problems has been addressed in many references [65, 23, 59, 34, 5, 21, 53] and thus will not be fully detailed here. In the following, we merely present a single approximate Riemann solver, which is widely used in the Lagrangian community and is generally referred to as the two-states solver. This solver will reduce in some simple cases either to the Godunov acoustic scheme, or to a linearized approximate Riemann solver in a Roe flux style. It can also be seen as the counterpart of the HLLC solver in terms of the Lagrangian mass coordinate.

2.4. Two-states Riemann solvers

We present here an approximate Riemann solver associated with a simple Riemann problem. In [31], Gallice defines a simple Riemann solver as a Riemann solution consisting of $(m+1)$ constant states, separated by m discontinuities. This notion is not new since Roe [66], HLL [38], HLLE [27] and HLLC [69] solvers are all simple Riemann solvers. Now, the simple Riemann problem to be solved comes from a linearization of system (8) around two mean states $\widetilde{\mathsf{U}}_L$ and $\widetilde{\mathsf{U}}_R$. This is why this solver is referred as a two-states solver. The associated Riemann problem is defined as follows

$$\frac{\mathrm{d}\,\mathsf{U}}{\mathrm{d}t} = -\begin{cases} \mathsf{A}(\widetilde{\mathsf{U}}_L)\,\dfrac{\partial\,\mathsf{U}}{\partial m} & \text{for } m\text{-}m_i < 0, \\ \mathsf{A}(\widetilde{\mathsf{U}}_R)\,\dfrac{\partial\,\mathsf{U}}{\partial m} & \text{for } m\text{-}m_i > 0, \end{cases} \tag{18a}$$

$$\mathsf{U}(m,0) = \begin{cases} \mathsf{U}_L & \text{for } m\text{-}m_i < 0, \\ \mathsf{U}_R & \text{for } m\text{-}m_i > 0. \end{cases} \tag{18b}$$

This Riemann problem is said to be simple because its solutions can be put into the following form

$$\mathsf{U}(m,t) = \begin{cases} \mathsf{U}_L & \text{for } m\text{-}m_i < \text{-}\widetilde{z}_L\,t, \\ \overline{\mathsf{U}}^- & \text{for } \text{-}\widetilde{z}_L\,t < m\text{-}m_i < 0, \\ \overline{\mathsf{U}}^+ & \text{for } \widetilde{z}_R\,t > m\text{-}m_i > 0, \\ \mathsf{U}_R & \text{for } m\text{-}m_i > \widetilde{z}_R\,t, \end{cases} \tag{19}$$

where $\overline{\mathsf{U}}^-$ and $\overline{\mathsf{U}}^+$ are the left and right intermediate states. This solution definition is emphasized in Figure 1. Naturally, the left and right wavespeeds, $\widetilde{z}_L = \widetilde{\rho}_L\,\widetilde{a}_L$ and $\widetilde{z}_R = \widetilde{\rho}_R\,\widetilde{a}_R$, are some local approximations of the acoustic impedance. The Rankine-Hugoniot relations on the gas dynamics system tell us that the pressure and the velocity are continuous across a contact discontinuity, *i.e.*

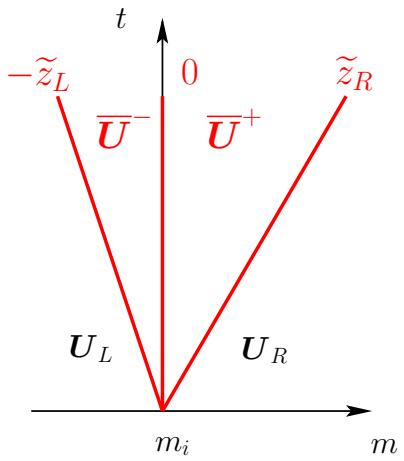

Figure 1: Two-states approximate Riemann fan.

$\overline{u}^- = \overline{u}^+ = \overline{u}$ and $\overline{p}^- = \overline{p}^+ = \overline{p}$. These relations enable us to fully determine the intermediate states associated with this two-states Riemann problem

$$\overline{\mathsf{U}}^- = \mathsf{U}_L - \frac{\overline{\mathsf{F}} - \mathsf{F}(\mathsf{U}_L)}{\widetilde{z}_L} \quad \text{and} \quad \overline{\mathsf{U}}^+ = \mathsf{U}_R + \frac{\overline{\mathsf{F}} - \mathsf{F}(\mathsf{U}_R)}{\widetilde{z}_R}, \tag{20}$$

where $\overline{\mathsf{F}} = (-\overline{u},\, \overline{p},\, \overline{p}\,\overline{u})^{\mathrm{t}}$. These definitions give us the associated numerical fluxes

$$\overline{u} = \frac{\widetilde{z}_L\, u_L + \widetilde{z}_R\, u_R}{\widetilde{z}_L + \widetilde{z}_R} - \frac{1}{\widetilde{z}_L + \widetilde{z}_R}(p_R - p_L), \tag{21a}$$

$$\overline{p} = \frac{\widetilde{z}_R\, p_L + \widetilde{z}_L\, p_R}{\widetilde{z}_L + \widetilde{z}_R} - \frac{\widetilde{z}_L\, \widetilde{z}_R}{\widetilde{z}_L + \widetilde{z}_R}(u_R - u_L), \tag{21b}$$

which, by the construction of the solver itself, preserves contact discontinuities. In the particular case where $\widetilde{z}_L = \widetilde{z}_R = \widetilde{z}$, one recovers the so-called one-state solver. This latter Riemann solver results from a linearization of the Riemann problem, and thus can be obtained by means of a Roe scheme [66]. Furthermore, a particular definition of $\widetilde{z}$ will lead to the recovery of the scheme introduced by Munz in [59]. In the general case where $\widetilde{z}_L \neq \widetilde{z}_R$, the two-states linearization makes this solver difficult to be interpreted as a Roe scheme. Different choices on the wave speeds $\widetilde{z}_L$ and $\widetilde{z}_R$ are possible and yield different properties, see [59, 21, 31] for more details. The simplest one, and certainly the most widely used, is the acoustic approximation where the wave speeds are set to be the left and right acoustic impedances, *i.e.* $\widetilde{z}_L = \rho_L\, a_L$ and $\widetilde{z}_R = \rho_R\, a_R$. In this particular case, this two-states solver is nothing but the Godunov acoustic solver.

Formula (21), derived as the solution of the two-states approximate Riemann problem, enable us to end the construction of the first-order finite volume scheme (17), by defining the numerical flux $\overline{\mathsf{F}}_{i+\frac{1}{2}} = \overline{\mathsf{F}}(\mathsf{U}_i, \mathsf{U}_{i+1})$. In this definition, the left and right wavespeeds are denoted respectively by $\widetilde{z}^-_{i+\frac{1}{2}}$ and $\widetilde{z}^+_{i+\frac{1}{2}}$. This particular choice in the numerical flux leads to a semi-discrete production of entropy. This statement is emphasized in the following remark.

Remark 2.1. *The first-order scheme in its semi-discrete form,* (16)*, provided with the two-states Riemann solver as numerical fluxes,* (21)*, ensures a semi-discrete production of entropy, see for instance [21, 53, 71]. Indeed, by means of the Gibbs identity* (9)*, it follows that the use of scheme* (16) *implies*

$$\begin{aligned} m_i\, T_i \frac{\mathrm{d}\, S_i}{\mathrm{d}t} &= m_i \frac{\mathrm{d}\, e_i}{\mathrm{d}t} + u_i\, m_i \frac{\mathrm{d}\, u_i}{\mathrm{d}t} + p_i\, m_i \frac{\mathrm{d}\, \tau_i}{\mathrm{d}t}, \\ &= \widetilde{z}^{-}_{i+\frac{1}{2}} \left(\overline{u}_{i+\frac{1}{2}} - u_i\right)^2 + \widetilde{z}^{+}_{i-\frac{1}{2}} \left(\overline{u}_{i-\frac{1}{2}} - u_i\right)^2 \geq 0. \end{aligned} \tag{22}$$

2.5. Godunov-type scheme

To assess the preservation of the numerical solution admissibility along the time, we would like to express the updated solution U_i^{n+1} as a convex combination of some admissible intermediate states. Because the presented method is a Godunov-like scheme, it is possible to write it as the combination of the two approximate Riemann solvers located at nodes $x_{i-\frac{1}{2}}$ and $x_{i+\frac{1}{2}}$. To that end, adding and subtracting $\frac{\Delta t^n}{m_i}\mathsf{F}(\mathsf{U}_i^n)$ in equation (17), along with basic algebraic manipulation, enable us to rewrite U_i^{n+1} as

$$\begin{aligned} \mathsf{U}_i^{n+1} &= \mathsf{U}_i^n - \frac{\Delta t^n}{m_i}(\overline{\mathsf{F}}^n_{i+\frac{1}{2}} - \overline{\mathsf{F}}^n_{i-\frac{1}{2}}) \ \pm \frac{\Delta t^n}{m_i}\mathsf{F}(\mathsf{U}_i^n), \\ &= (1-\lambda_i)\mathsf{U}_i^n + \lambda^-_{i+\frac{1}{2}}\, \overline{\mathsf{U}}^-_{i+\frac{1}{2}} + \lambda^+_{i-\frac{1}{2}}\, \overline{\mathsf{U}}^+_{i-\frac{1}{2}}, \end{aligned} \tag{23}$$

where $\lambda_i = \lambda^-_{i+\frac{1}{2}} + \lambda^+_{i-\frac{1}{2}}$ with $\lambda^{\mp}_{i\pm\frac{1}{2}} = \frac{\Delta t^n}{m_i}\widetilde{z}^{\mp}_{i\pm\frac{1}{2}}$. In equation (23), $\overline{\mathsf{U}}^-_{i+\frac{1}{2}}$ and $\overline{\mathsf{U}}^+_{i-\frac{1}{2}}$ read as follows

$$\overline{\mathsf{U}}^-_{i+\frac{1}{2}} = \mathsf{U}_i^n - \frac{\overline{\mathsf{F}}^n_{i+\frac{1}{2}} - \mathsf{F}(\mathsf{U}_i^n)}{\widetilde{z}^-_{i+\frac{1}{2}}} \quad \text{and} \quad \overline{\mathsf{U}}^+_{i-\frac{1}{2}} = \mathsf{U}_i^n + \frac{\overline{\mathsf{F}}^n_{i-\frac{1}{2}} - \mathsf{F}(\mathsf{U}_i^n)}{\widetilde{z}^+_{i-\frac{1}{2}}}, \tag{24}$$

which are nothing but the intermediate states defined in (20). This convex decomposition of the first-order Godunov-type scheme presented is depicted in Figure 2. Finally, to avoid the interaction of left and right waves, and thus to ensure (23) is indeed a convex combination, the condition $\lambda_i \leq 1$ has to be respected, which rewrites

$$\Delta t^n \leq \sigma_e\, \frac{m_i}{\widetilde{z}^-_{i+\frac{1}{2}} + \widetilde{z}^+_{i-\frac{1}{2}}}, \tag{25}$$

with the CFL coefficient $\sigma_e = 1$. This simple analysis provides us with the correct definition of the CFL condition. Only in the case of the acoustic approximation, *i.e.* $\widetilde{z}^{\mp}_{i\pm\frac{1}{2}} \equiv z_i^n = \rho_i^n\, a_i^n$, that we recover the following classical condition

$$\Delta t^n \leq \frac{\sigma_e}{2}\frac{\Delta x_i^n}{a_i^n}. \tag{26}$$

The purpose of this paper is to ensure that the numerical solution remains in an admissible state to be defined. Given equation (23), we can reasonably hope that if U_i^n, as well as $\overline{\mathsf{U}}^-_{i-\frac{1}{2}}$ and $\overline{\mathsf{U}}^+_{i-\frac{1}{2}}$, are admissible, the new numerical solution U_i^{n+1} will also be admissible. This would be the case if the admissible set is convex.

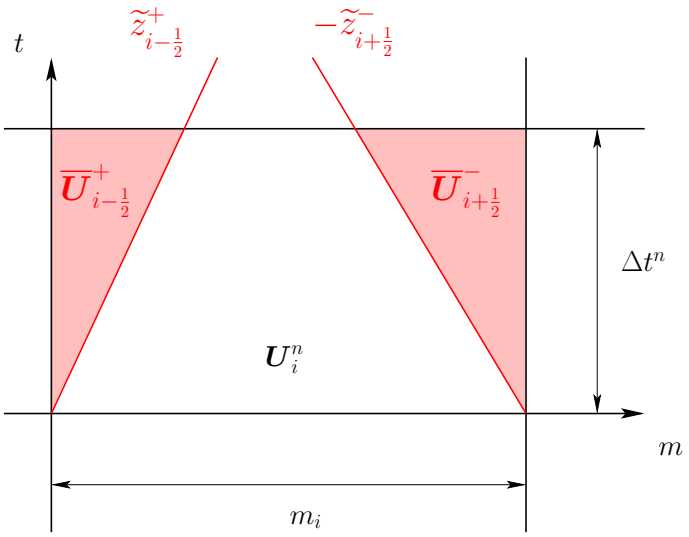

Figure 2: Illustration of the Lagrangian scheme with the two-states solver.

2.6. First-order positivity-preserving schemes

We have seen in section 2.2 dedicated to the equations of state, that the solution may lie in a domain of validity of the form, $\rho \in]\rho_{min}, \rho_{max}[$ and $\widehat{\varepsilon} > \varepsilon_{min}$, where $\widehat{\varepsilon} = \varepsilon - p^\star \tau$ in the stiffened EOS case and $\widehat{\varepsilon} = \varepsilon$ otherwise, see Appendix A for further details. One can easily check that the related admissible set

$$G = \left\{ \mathsf{U} = \begin{pmatrix} \tau \\ u \\ e \end{pmatrix}, \quad \tau \in]\tau_{min}, \tau_{max}[\ \text{ and } \ \widehat{\varepsilon}(\mathsf{U}) > \varepsilon_{min} \right\}, \tag{27}$$

is convex, where $\tau_{min/max} = \frac{1}{\rho_{min/max}}$. We will thus seek for numerical solution in G at all time. Such solution will be referred as admissible in the remainder of the article. Thanks to equation (23), assuming $\mathsf{U}^n_i \in G$, a sufficient condition to ensure $\mathsf{U}^{n+1}_i \in G$ is to have $\overline{\mathsf{U}}^{\mp}_{i\pm\frac{1}{2}} \in G$. Making use of definition (20), we are able to express the left and right intermediate specific volumes as

$$\overline{\tau}^{\mp}_{i\pm\frac{1}{2}} = \tau^n_i \pm \frac{\overline{u}_{i\pm\frac{1}{2}} - u^n_i}{\widetilde{z}^{\mp}_{i\pm\frac{1}{2}}}, \tag{28}$$

and introducing $v_{i\pm\frac{1}{2}} = \pm\frac{\overline{u}_{i\pm\frac{1}{2}} - u^n_i}{a^n_i}$, for the sake of conciseness, expression (28) rewrites into

$$\overline{\tau}^{\mp}_{i\pm\frac{1}{2}} = \tau^n_i \Big(1 + \frac{z^n_i}{\widetilde{z}^{\mp}_{i\pm\frac{1}{2}}} \, v_{i\pm\frac{1}{2}} \Big). \tag{29}$$

Similarly, definition (20) allows us to get the intermediate specific internal energy expressions

$$\overline{\varepsilon}^{\mp}_{i\pm\frac{1}{2}} = \overline{e}^{\mp}_{i\pm\frac{1}{2}} - \frac{1}{2}(\overline{u}_{i\pm\frac{1}{2}})^2 = \varepsilon^n_i - p^n_i \tau^n_i \frac{z^n_i}{\widetilde{z}^{\mp}_{i\pm\frac{1}{2}}} \, v_{i\pm\frac{1}{2}} + \frac{a^n_i}{2} v^2_{i\pm\frac{1}{2}}. \tag{30}$$

In [31], the author proved that the numerical solver defined in (20) ensures the intermediate states (29) and (30) to be positive, for large enough $\widetilde{z}^{\mp}_{i\pm\frac{1}{2}}$. This property has been obtained in the limit regime $\widetilde{z}^{\mp}_{i\pm\frac{1}{2}} \longrightarrow +\infty$. But does this property hold for realistic values of $\widetilde{z}^{\mp}_{i\pm\frac{1}{2}}$? Actually, in light of equation (29), it is clear the Godunov acoustic solver is NOT positivity-preserving. Indeed, in this case where $\widetilde{z}^{\mp}_{i\pm\frac{1}{2}} = z^n_i$, the intermediate specific volumes rewrite $\overline{\tau}^{\mp}_{i\pm\frac{1}{2}} = \tau^n_i(1 + v_{i\pm\frac{1}{2}})$. And for instance, if $\overline{u}_{i\pm\frac{1}{2}} > u^n_i + a^n_i$ then $\overline{\tau}^{-}_{i+\frac{1}{2}} < 0$. That being noted, one may want to determine the constant $\widetilde{z}^{\mp}_{i\pm\frac{1}{2}}$ ensuring the intermediate specific volume and internal energy to be positive. A simple quadratic analysis of definition (30) tells us that if $\widetilde{z}^{\mp}_{i\pm\frac{1}{2}} > \frac{p^n_i}{\sqrt{2\,\varepsilon^n_i}}$ then $\overline{\varepsilon}^{\mp}_{i\pm\frac{1}{2}} > 0$. Let us note this condition is nothing but the one obtained in the HLLC solver case in [15]. Now, a similar analysis of equation (29), to assess the positivity of the intermediate specific volume, tells us that the constant $\widetilde{z}^{\mp}_{i\pm\frac{1}{2}}$ has to yield $\widetilde{z}^{\mp}_{i\pm\frac{1}{2}} > -z^n_i\, v_{i\pm\frac{1}{2}}$, for any value of $v_{i\pm\frac{1}{2}} \in \mathbb{R}$. This is obviously impossible, and we can conclude that $\widetilde{z}^{\mp}_{i\pm\frac{1}{2}}$ has to be a function of $v_{i\pm\frac{1}{2}}$.

A solution to overcome this difficulty is the use of the shock Hugoniot approximation introduced in [23] by Dukowicz. This particular characterization of the shocks, along with a two-shock approximation, allows us to define the wavespeeds $\widetilde{z}^{\mp}_{i\pm\frac{1}{2}}$ as

$$\widetilde{z}^{\mp}_{i\pm\frac{1}{2}} = z^n_i \left(1 + \Gamma \left|v_{i\pm\frac{1}{2}}\right|\right). \tag{31}$$

The two-shock approximation, initially employed in a Riemann solver by Colella in [19], treats rarefaction waves as shocks. This particular approximation, along with the two-states solver (21) and wavespeed definition (31), constituted the technique employed by Maire in [53]. The constant $\Gamma \geq 1$ in (31) is determined in [23] to recover the exact shock Hugoniot in the regime of infinitely strong strength. Thus, in the ideal gas case, the exact Riemann solution tells us that

$$\lim_{v_{i-\frac{1}{2}}\to\infty} \frac{\overline{\tau}^{+}_{i-\frac{1}{2}}}{t^n_i} = \frac{\gamma-1}{\gamma+1} \quad \Longrightarrow \quad \Gamma = \frac{\gamma+1}{2}.$$

It is then relatively easy to prove this particular definition of wavespeeds, (31), always yields strictly positive intermediate specific volumes and internal energies. However, even if for a theoretical matter, to have $\tau > 0$ and $\varepsilon > 0$ is enough in the ideal gas case, it might not be true for numerical applications. Indeed, numerically $1.E$-20 can be interpreted as -$1.E$-20 in double precision. Thus it would be reasonable to rather impose $\tau > 1.E$-15 and $\varepsilon > 1.E$-15. Another issue arising from the use of the wavespeed (31) lies on the definition of the appropriate constant Γ in more complex equations of state. Furthermore, we have seen with the four EOS considered that the desired condition in the general case might rather be $(\tau, \varepsilon) \in \,]\tau_{min}, \tau_{max}[\times]\varepsilon_{min}, +\infty]$. These different problems will be treated in the following by two different and independent techniques, first by a modification of the constant Γ in the Dukowicz solver, second by adding a constraint on the time step but relaxing the wavespeeds definition.

2.6.1. Modified Dukowicz solver

We define the modified Dukowicz wavespeeds as follows

$$\widetilde{z}^{\mp}_{i\pm\frac{1}{2}} = z^n_i \left(1 + \widetilde{\Gamma} \left|v_{i\pm\frac{1}{2}}\right|\right), \tag{32}$$

where $\widetilde{\Gamma} = \sigma_v^{-1} > 0$ is a constant to be determined. The constant σ_v is introduced here for consistence with the next section. Definition (32) is perfectly equivalent to (31) in the particular case $\widetilde{\Gamma} = \Gamma$. Firstly, let us ensure that $\overline{\tau}^{\mp}_{i\pm\frac{1}{2}} > \tau_{min} \geq 0$. Simple algebraic manipulations allow us to rewrite $\overline{\tau}^{\mp}_{i\pm\frac{1}{2}}$ as

$$\overline{\tau}^{\mp}_{i\pm\frac{1}{2}} - \tau_{min} = (\tau_i^n - \tau_{min}) \left(1 + \left(\frac{\tau_i^n}{\tau_i^n - \tau_{min}} \right) \frac{z_i^n}{\widetilde{z}^{\mp}_{i\pm\frac{1}{2}}} \, v_{i\pm\frac{1}{2}} \right), \tag{33}$$

which, assuming $\tau_i^n > \tau_{min}$ and substituting $\widetilde{z}^{\mp}_{i\pm\frac{1}{2}}$ by its definition, equation (32), leads to the following inequality

$$\overline{\tau}^{\mp}_{i\pm\frac{1}{2}} - \tau_{min} > (\tau_i^n - \tau_{min}) \left(1 - \left(\frac{\tau_i^n}{\tau_i^n - \tau_{min}} \right) \sigma_v \right).$$

Finally, if $\sigma_v \leq 1 - \frac{\tau_{min}}{\tau_i^n}$ then $\overline{\tau}^{\mp}_{i\pm\frac{1}{2}} > \tau_{min}$. A similar procedure for the condition $\overline{\tau}^{\mp}_{i\pm\frac{1}{2}} < \tau_{max} \leq +\infty$ yields a similar conclusion, *i.e.* assuming $\tau_i^n < \tau_{max}$, if $\sigma_v \leq \frac{\tau_{max}}{\tau_i^n} - 1$ then $\overline{\tau}^{\mp}_{i\pm\frac{1}{2}} < \tau_{max}$. In the end, one can state the following result

Remark 2.2. *If* $\tau_i^n \in]\tau_{min}, \tau_{max}[$ *then* $\sigma_v \leq (1 - \frac{\tau_{min}}{\tau_i^n}, \frac{\tau_{max}}{\tau_i^n} - 1)$ *in* (32) *implies* $\overline{\tau}^{\mp}_{i\pm\frac{1}{2}} \in]\tau_{min}, \tau_{max}[$.

For the ideal gas equation of state, the physical bounds are $\tau_{min} = 0$ and $\tau_{max} = +\infty$, and thus this constraint reduces to $\sigma_v \leq 1$. In practice, we set these bounds to be $\tau_{min} = \epsilon$ and $\tau_{max} = \frac{1}{\epsilon}$, where $\epsilon > 0$ is a very small constant generally set to 10^{-14} in our numerical applications.

Now, we perform a similar analysis for the condition $\widehat{\overline{\varepsilon}}^{\mp}_{i\pm\frac{1}{2}} > \varepsilon_{min} \geq 0$. Let us recall that for stiffened gas we have defined $\widehat{\varepsilon} = \varepsilon - p_s \, \tau$ and $\widehat{p} = p + p_s$, while for the other EOS studied $\widehat{\varepsilon} = \varepsilon$ and $\widehat{p} = p$, see Appendix A for more details. It is easy to prove $\widehat{\overline{\varepsilon}}^{\mp}_{i\pm\frac{1}{2}}$ can be split into two terms as

$$\widehat{\overline{\varepsilon}}^{\mp}_{i\pm\frac{1}{2}} - \varepsilon_{min} = (\widehat{\varepsilon}_i^n - \varepsilon_{min}) \, A_{i\pm\frac{1}{2}} + B_{i\pm\frac{1}{2}}, \tag{34}$$

where the quantity $A_{i\pm\frac{1}{2}}$ writes

$$A_{i\pm\frac{1}{2}} = 1 - \left(\frac{\widehat{\varepsilon}_i^n}{\widehat{\varepsilon}_i^n - \varepsilon_{min}} \right) \frac{\tau_i^n \, \widehat{p}_i^n}{\widehat{\varepsilon}_i^n} \, \frac{z_i^n}{\widetilde{z}^{\mp}_{i\pm\frac{1}{2}}} \, v_{i\pm\frac{1}{2}}, \tag{35}$$

and $B_{i\pm\frac{1}{2}}$ is defined as follows

$$B_{i\pm\frac{1}{2}} = \frac{1}{2} (a_i^n)^2 \, v^2_{i\pm\frac{1}{2}}. \tag{36}$$

Because $B_{i\pm\frac{1}{2}} \geq 0$, a sufficient condition to ensure the desired property is $A_{i\pm\frac{1}{2}} > 0$. Similarly to what has been done previously, assuming $\widehat{\varepsilon}_i^n > \varepsilon_{min}$, if $\sigma_v \leq (1 - \frac{\varepsilon_{min}}{\widehat{\varepsilon}_i^n}) \, \frac{\rho_i^n \, \widehat{\varepsilon}_i^n}{\widehat{p}_i^n}$ then $\widehat{\overline{\varepsilon}}^{\mp}_{i\pm\frac{1}{2}} > \varepsilon_{min}$. Finally, we emphasize these results in the following proposition.

Proposition 2.3. *The first-order scheme* (17) *provided with the numerical fluxes* (21) *and the particular wavespeeds definition* (32) *ensures an admissible solution under the CFL condition* (25) *with* $\sigma_e \leq 1$ *and if*

$$\sigma_v \leq \min\left(1 - \frac{\tau_{min}}{\tau_i^n}, \frac{\tau_{max}}{\tau_i^n} - 1, (1 - \frac{\varepsilon_{min}}{\widehat{\varepsilon}_i^n})\,\frac{\rho_i^n\,\widehat{\varepsilon}_i^n}{\widehat{p}_i^n}\right).$$

In the perfect gas and stiffened gas cases, provided with the physical bounds $\tau_{min} = 0$, $\tau_{max} = +\infty$ and $\varepsilon_{min} = 0$, this constraint reads $\sigma_v \leq \min(1, \frac{1}{\gamma-1})$.

In this subsection, we have shown how to modify the Dukowicz wavespeed definition to ensure the numerical solution remains in the admissible set G at all time. Nonetheless, due to the relative complexity as well as the non-linearity of these formula, (31) and (32), generally solved by means of an iterative algorithm such as fixed point method, one may want to use the simple Godunov acoustic solver. In the following, we will show how to ensure the numerical solution remains in G, for any definition of positive wavespeeds, $\widetilde{z}^{\mp}_{i\pm\frac{1}{2}}$, which includes the particular case of the Godunov acoustic solver.

2.6.2. Generic wavespeeds

In the previous section, we have seen that we cannot ensure the intermediate states $\overline{\mathsf{U}}^{\mp}_{i\pm\frac{1}{2}}$ to be in the admissible set without particular constraints on the wavespeeds. Thus, instead of working on $\overline{\mathsf{U}}^{\mp}_{i\pm\frac{1}{2}}$ as it is generally done, we now directly operate on U_i^{n+1}. To make that possible, we make use of an additional constraint on the time step widely used in the Lagrangian community. This constraint permits to control the relative variation of cell volume during a time step such as

$$\Big|\frac{\Delta V}{V}\Big| \equiv \frac{|\Delta x_i^{n+1} - \Delta x_i^n|}{\Delta x_i^n} < \sigma_v, \tag{37}$$

which rewrites

$$\Delta t^n < \sigma_v\,\frac{\Delta x_i^n}{|\overline{u}_{i+\frac{1}{2}} - \overline{u}_{i-\frac{1}{2}}|}. \tag{38}$$

In (38), σ_v is a positive constant that will prove to be the same as the one defined in the modified Dukowicz solver section. Practically, we first determine under which conditions $\tau_i^n \in]\,\tau_{min}, \tau_{max}[$ implies $\tau_i^{n+1} \in]\tau_{min}, \tau_{max}[$. Making use of system (17) and recalling that $\Delta V = \Delta t^n(\overline{u}_{i+\frac{1}{2}} - \overline{u}_{i-\frac{1}{2}})$, we are able to rewrite τ_i^{n+1} as

$$\tau_i^{n+1} - \tau_{min} = (\tau_i^n - \tau_{min})\,\left(1 - \frac{\Delta V}{V}\Big(\frac{\tau_i^n}{\tau_i^n - \tau_{min}}\Big)\right). \tag{39}$$

Consequently, assuming $\tau_i^n > \tau_{min}$, the following sufficient condition ensures $\tau_i^{n+1} > \tau_{min}$

$$\Big|\frac{\Delta V}{V}\Big| < 1 - \frac{\tau_{min}}{\tau_i^n},$$

which is equivalent to the volume variation condition (38) with $\sigma_v \leq 1 - \frac{\tau_{min}}{\tau_i^n}$. A similar procedure in the case of $\tau_i^{n+1} < \tau_{max}$ yields that σ_v has to be such that $\sigma_v \leq \frac{\tau_{max}}{\tau_i^n} - 1$. In the end, one can state the following result.

Remark 2.4. *If* $\tau_i^n \in]\tau_{min}, \tau_{max}[$ *then* $\sigma_v \leq (1 - \frac{\tau_{min}}{\tau_i^n}, \frac{\tau_{max}}{\tau_i^n} - 1)$ *in* (38) *implies* $\overline{\tau}_i^{n+1} \in]\tau_{min}, \tau_{max}[$.

This remark provides us with a sufficient condition for the first-order scheme (17) to be positivity-preserving, and actually more generally maximum-principle-satisfying, for the specific volume and thus the density.

We may now assess the required constraints to ensure $\widehat{\varepsilon}_i^{n+1} > \varepsilon_{min}$. By means of the first-order scheme (17) and basic manipulations, $\widehat{\varepsilon}_i^{n+1}$ can be split into two terms

$$\widehat{\varepsilon}_i^{n+1} - \varepsilon_{min} = (\widehat{\varepsilon}_i^n - \varepsilon_{min})\, A_i + B_i, \tag{40}$$

where the quantity A_i reads as follows

$$A_i = 1 - \frac{\Delta V}{V} \left(\frac{\widehat{\varepsilon}_i^n}{\widehat{\varepsilon}_i^n - \varepsilon_{min}} \right) \frac{\tau_i^n\, \widehat{p}_i^n}{\widehat{\varepsilon}_i^n}, \tag{41}$$

while B_i is defined as

$$B_i = \frac{\Delta t^n}{m_i} \Big[\widetilde{z}^-_{i+\frac{1}{2}} w^2_{i+\frac{1}{2}} + \widetilde{z}^+_{i-\frac{1}{2}} w^2_{i-\frac{1}{2}} - \frac{\Delta t^n}{2m_i} (\widetilde{z}^-_{i+\frac{1}{2}} w_{i+\frac{1}{2}} + \widetilde{z}^+_{i-\frac{1}{2}} w_{i-\frac{1}{2}})^2 \Big], \tag{42}$$

with $w_{i\pm\frac{1}{2}} = \overline{u}_{i\pm\frac{1}{2}} - u_i^n$. As we did in the previous section, if we manage to prove that $B_i \geq 0$ at all time, it is then sufficient to ensure $A_i > 0$. The time step constraint (38) with $\sigma_v \leq (1 - \frac{\varepsilon_{min}}{\widehat{\varepsilon}_i^n}) \frac{\rho_i^n \widehat{\varepsilon}_i^n}{\widehat{p}_i^n}$ enforces A_i to remain strictly positive. Now for B_i, let us note this quadratic term can be put into a matrix-vector form as

$$B_i = \frac{\Delta t^n}{m_i} \begin{pmatrix} \widetilde{z}^+_{i-\frac{1}{2}} (1 - \frac{\Delta t^n}{2m_i} \widetilde{z}^+_{i-\frac{1}{2}}) & -\frac{\Delta t^n}{2m_i} \widetilde{z}^+_{i-\frac{1}{2}} \widetilde{z}^-_{i+\frac{1}{2}} \\ -\frac{\Delta t^n}{2m_i} \widetilde{z}^+_{i-\frac{1}{2}} \widetilde{z}^-_{i+\frac{1}{2}} & \widetilde{z}^-_{i+\frac{1}{2}} (1 - \frac{\Delta t^n}{2m_i} \widetilde{z}^-_{i+\frac{1}{2}}) \end{pmatrix} \begin{pmatrix} w_{i-\frac{1}{2}} \\ w_{i+\frac{1}{2}} \end{pmatrix} \cdot \begin{pmatrix} w_{i-\frac{1}{2}} \\ w_{i+\frac{1}{2}} \end{pmatrix}, \tag{43}$$

$$\equiv \frac{\Delta t^n}{m_i}\, \mathsf{M}_i\, \mathsf{W} \cdot \mathsf{W}. \tag{44}$$

It can be proven that the matrix M_i is positive semi-definite if and only if

$$\Delta t^n \leq 2\, \frac{m_i}{\widetilde{z}^-_{i+\frac{1}{2}} + \widetilde{z}^+_{i-\frac{1}{2}}}.$$

We have then recovered the CFL condition (25) with a twice bigger CFL number σ_e. In the Godunov acoustic solver case, this condition reads $\Delta t^n \leq \frac{\Delta x_i^n}{a_i^n}$.

Let us emphasize that the quantity B_i corresponds to an approximation of the time discrete counterpart of the semi-discrete entropy production $T_i \dfrac{\mathrm{d}\, S_i}{\mathrm{d}t} \geq 0$ of equation (22). Indeed, B_i rewrites as

$$B_i = \varepsilon_i^{n+1} - \varepsilon_i^n + p_i^n \left(\tau_i^{n+1} - \tau_i^n \right). \tag{45}$$

Nevertheless, to have $B_i \geq 0$ will not ensure the scheme to produce entropy at the discrete level. Actually, one can prove from the concavity of the specific entropy function S that

$$\frac{1}{T_i^{n+1}} \left[\varepsilon_i^{n+1} - \varepsilon_i^n + p_i^{n+1} \left(\tau_i^{n+1} - \tau_i^n \right) \right] \leq S(\mathsf{U}_i^{n+1}) - S(\mathsf{U}_i^n) \leq \frac{B_i}{T_i^n}, \tag{46}$$

under the assumption that both U_i^n and U_i^{n+1} lie in the admissible set G. Consequently, to prove any increase in the entropy, one has to determine a time step $\Delta t^n > 0$ such that the left-hand side of inequality (46) is positive. Such demonstration has been done by Després in [21], in which the solution is assumed to be positive. In the end, even if $B_i \geq 0$ will not ensure the scheme to be entropic at the discrete level, it provides us with a sufficient condition for the positivity of the internal energy.

Finally, let us emphasize the condition of admissibility of the numerical solution in the following proposition.

Proposition 2.5. *The first-order scheme* (17) *provided with the numerical fluxes* (21) *for any definition of positive wavespeeds ensures an admissible solution under the CFL condition* (25) *with* $\sigma_e \leq 2$ *and the volume variation constraint* (38) *with*

$$\sigma_v \leq \min\left(1 - \frac{\tau_{min}}{\tau_i^n}, \frac{\tau_{max}}{\tau_i^n} - 1, (1 - \frac{\varepsilon_{min}}{\widehat{\varepsilon}_i^n})\,\frac{\rho_i^n\,\widehat{\varepsilon}_i^n}{\widehat{p}_i^n}\right).$$

This proposition holds for any definition of positive wavespeed $\widetilde{z}^{\mp}_{i\pm\frac{1}{2}} > 0$, and thus for the particular case of the Godunov acoustic solver, $\widetilde{z}^{\mp}_{i\pm\frac{1}{2}} = z_i^n$. Furthermore, we have seen the coefficient σ_v involved in the control volume variation time step constraint (38), can be chosen similarly to the one in the modified Dukowicz solver definition (32).

Summary. Due to the large number of equations introduced, let us summarize the main features of this work so far. The problem is to determine conditions for which the first-order finite volume Lagrangian scheme

$$\mathsf{U}_i^{n+1} = \mathsf{U}_i^n - \frac{\Delta t^n}{m_i}\left[\overline{\mathsf{F}}^n_{i+\frac{1}{2}} - \overline{\mathsf{F}}^n_{i-\frac{1}{2}}\right],$$

where the numerical flux $\overline{\mathsf{F}}^n_{i+\frac{1}{2}} = (-\overline{u}^n_{i+\frac{1}{2}}, \overline{p}^n_{i+\frac{1}{2}}, \overline{p}^n_{i+\frac{1}{2}}\,\overline{u}^n_{i+\frac{1}{2}})^{\mathrm{t}}$ is evaluated through the two-states solver

$$\overline{u}^n_{i+\frac{1}{2}} = \frac{\widetilde{z}^-_{i+\frac{1}{2}}\,u_i^n + \widetilde{z}^+_{i+\frac{1}{2}}\,u_{i+1}^n}{\widetilde{z}^-_{i+\frac{1}{2}} + \widetilde{z}^+_{i+\frac{1}{2}}} - \frac{1}{\widetilde{z}^-_{i+\frac{1}{2}} + \widetilde{z}^+_{i+\frac{1}{2}}}(p_{i+1}^n - p_i^n),$$

$$\overline{p}^n_{i+\frac{1}{2}} = \frac{\widetilde{z}^+_{i+\frac{1}{2}}\,p_i^n + \widetilde{z}^-_{i+\frac{1}{2}}\,p_{i+1}^n}{\widetilde{z}_L + \widetilde{z}_R} - \frac{\widetilde{z}^-_{i+\frac{1}{2}}\,\widetilde{z}^+_{i+\frac{1}{2}}}{\widetilde{z}^-_{i+\frac{1}{2}} + \widetilde{z}^+_{i+\frac{1}{2}}}(u_{i+1}^n - u_i^n),$$

ensures numerical solutions to be admissible, namely at all time in the admissible set

$$G = \left\{\mathsf{U} = (\tau,\, u,\, e)^{\mathrm{t}}, \quad \tau \in \,]\tau_{min}, \tau_{max}[\ \text{ and }\ \widehat{\varepsilon}(\mathsf{U}) > \varepsilon_{min}\right\}.$$

To that end, two different techniques are employed. The first one relies on ensuring the intermediate states involved in the approximate Riemann solver to be in G. And it has been seen that the wavespeeds $\widetilde{z}^{\mp}_{i\pm\frac{1}{2}}$ have to necessarily be a function of $\overline{u}^n_{i\pm\frac{1}{2}}$. We have then made use of the following definition

$$\widetilde{z}^{\mp}_{i\pm\frac{1}{2}} = \rho_i^n\,\left(a_i^n + \sigma_v^{-1}\left|\overline{u}_{i\pm\frac{1}{2}} - u_i^n\right|\right).$$

Finally, a sufficient condition to ensure the numerical solution to be in G is the use of such wavespeed definition with $\sigma_v \leq \min\left(1-\frac{\tau_{min}}{\tau_i^n}, \frac{\tau_{max}}{\tau_i^n}-1, (1-\frac{\varepsilon_{min}}{\widehat{\varepsilon}_i^n})\frac{\rho_i^n \widehat{\varepsilon}_i^n}{\widehat{p}_i^n}\right)$, and the following CFL condition with $\sigma_e \leq 1$

$$\Delta t^n \leq \sigma_e \frac{m_i}{\widetilde{z}_{i+\frac{1}{2}}^- + \widetilde{z}_{i-\frac{1}{2}}^+}.$$

The second technique relaxes this particular definition of the wavespeeds. The approximate Riemann intermediate states will not necessarily to be in G this time, only U_i^{n+1} will. To that purpose, in addition to the previous CFL condition with $\sigma_e \leq 2$, we make use of a supplementary time step constraint relative to the volume variation as follows

$$\Delta t^n < \sigma_v \frac{\Delta x_i^n}{|\overline{u}_{i+\frac{1}{2}} - \overline{u}_{i-\frac{1}{2}}|}.$$

Finally, if $\sigma_v \leq \min\left(1-\frac{\tau_{min}}{\tau_i^n}, \frac{\tau_{max}}{\tau_i^n}-1, (1-\frac{\varepsilon_{min}}{\widehat{\varepsilon}_i^n})\frac{\rho_i^n \widehat{\varepsilon}_i^n}{|\widehat{p}_i^n|}\right)$, the scheme is ensured to produce solutions in G. These two techniques involve a constant σ_v which has proved to be the same.

In the end, one can now wonder how constraining this new time step condition (38) is in comparison with the CFL condition (25). Let us consider the modified Dukowicz solver case. Then, by means of $\widetilde{z}_{i\pm\frac{1}{2}}^{\mp}$ definition (32), one can write

$$\begin{aligned}\widetilde{z}_{i+\frac{1}{2}}^- + \widetilde{z}_{i-\frac{1}{2}}^+ &= \frac{m_i}{\Delta x_i^n}\left[2a_i^n + \sigma_v^{-1}(|\overline{u}_{i+\frac{1}{2}}^n - u_i^n| + |\overline{u}_{i-\frac{1}{2}}^n - u_i^n|)\right], \\ &> \frac{m_i}{\sigma_v}\frac{|\overline{u}_{i+\frac{1}{2}}^n - \overline{u}_{i-\frac{1}{2}}^n|}{\Delta x_i^n}.\end{aligned}$$

Thanks to this last relation, one can state that

$$\frac{m_i}{\widetilde{z}_{i+\frac{1}{2}}^- + \widetilde{z}_{i-\frac{1}{2}}^+} < \sigma_v \frac{\Delta x_i^n}{|\overline{u}_{i+\frac{1}{2}}^n - \overline{u}_{i-\frac{1}{2}}^n|}. \tag{47}$$

This second method seems then to be optimal in term of simplicity and time step, the CFL number σ_e being twice bigger and the new time step condition (38) being always less constraining than the CFL condition in the Dukowicz or modified Dukowicz solver cases. Of course, only the purpose of positivity has been tackled here. There might be quality resolution differences between the original Dukowicz solver, the modified one and the Godunov acoustic scheme, especially in strong shock regime. However, as it will be shown in the numerical results section, this difference is dramatically reduced going to higher-order accuracy.

The additional time step restriction technique does not seem limited to the numerical flux used in this paper. A similar procedure can potentially be applied to any other Riemann solvers in the Lagrangian framework. For instance, such technique could ensure the positivity of the Roe scheme, or relax any wavespeed constraint required in the HLLC solver. It might thus be applied in a straightforward manner to the schemes presented in [15]. Furthermore, it seems reasonable to say the two positivity-preserving techniques developed here could be generalized to other Lagrangian system of equations, as those involved in the magneto-hydrodynamics or elastic-plastic flow simulation for instance.

2.7. High-order schemes

We now consider a general high-order extension of the first-order scheme presented in the previous section, equation (17). Such extension can be obtained by means of a large number of different methods as, among others, the Monotonic Upstream-Centered Scheme for Conservation Laws (MUSCL) method [46, 47], the essentially non-oscillatory (ENO) finite volume schemes [37, 68], the weighted ENO (WENO) finite volume schemes [50, 42], or the discontinuous Galerkin (DG) method [17, 18]. The only fundamental assumption is the high-order scheme must satisfy the following equation on the mass averaged values

$$\mathsf{U}_i^{n+1} = \mathsf{U}_i^n - \frac{\Delta t^n}{m_i} \left[\overline{\mathsf{F}}(\mathsf{U}^-_{i+\frac{1}{2}}, \mathsf{U}^+_{i+\frac{1}{2}}) - \overline{\mathsf{F}}(\mathsf{U}^-_{i-\frac{1}{2}}, \mathsf{U}^+_{i-\frac{1}{2}}) \right], \tag{48}$$

where $\mathsf{U}^+_{i-\frac{1}{2}}$ and $\mathsf{U}^-_{i+\frac{1}{2}}$ are the high-order values respectively within cell ω_i at points $x_{i-\frac{1}{2}}$ and $x_{i+\frac{1}{2}}$ in an updated Lagrangian frame, and within cell Ω_i at points $X_{i-\frac{1}{2}}$ and $X_{i+\frac{1}{2}}$ in a total Lagrangian frame. In these two different frameworks, let us introduce $\mathsf{U}^n_{h,i}(x)$ and $\mathsf{U}^n_{h,i}(X)$ the piecewise polynomial solutions of degree K on respectively cells ω_i and Ω_i. These polynomials can either be reconstructed from the cell averages of neighboring cells in a finite volume method or evolved in a DG method. Let us highlight that working in a total Lagrangian frame, as it is done for instance in [71, 70, 72], the polynomial $\mathsf{U}^n_{h,i}(X)$ in the initial configuration may not be a polynomial in the actual configuration $\mathsf{U}^n_{h,i}(X(x,t))$. From now on, for sake of conciseness, when not specified, x should be replaced by X in a total Lagrangian frame, as well as ω by Ω. Then, the high-order values at the cell boundaries read as $\mathsf{U}^+_{i-\frac{1}{2}} = \mathsf{U}^n_{h,i}(x_{i-\frac{1}{2}})$ and $\mathsf{U}^-_{i+\frac{1}{2}} = \mathsf{U}^n_{h,i}(x_{i+\frac{1}{2}})$. Working on the moving configuration, the grid position is still advanced in time such that $x^{n+1}_{i+\frac{1}{2}} = x^n_{i+\frac{1}{2}} + \Delta t^n \, \overline{u}^n_{i+\frac{1}{2}}$. Let us emphasize that the high-order in space scheme (48) still relies on a first-order forward Euler time integration. The issue of high-order time integration will be addressed in section 2.11.

Let us note that different techniques can be employed to get high-order accuracy. For instance, because the high-order point values are only required in the numerical fluxes $\overline{\mathsf{F}}(\mathsf{U}^-_{i+\frac{1}{2}}, \mathsf{U}^+_{i+\frac{1}{2}}) = (-\overline{u}_{i+\frac{1}{2}}, \overline{p}_{i+\frac{1}{2}}, \overline{p}_{i+\frac{1}{2}} \, \overline{u}_{i+\frac{1}{2}})^{\mathrm{t}}$, defined through solver (21), one might be tempted to choose to build the high-order approximation only on the flux variables, namely the velocity and pressure. This is however only possible for up to second order accuracy, as one does not know the cell averages of these flux variables, only those of the conserved variables (mass, momentum and energy). Within this flux variable high-order reconstruction, the specific volume and the total energy remain constant inside the cells. To avoid this second-order accuracy bound, the high-order reconstruction may be applied on the conserved variables. In both cases, the reconstructions could be obtained from the averaged values on the neighboring cells ω_{i-1}, ω_i and ω_{i+1}, by either an ENO, a WENO or a simple least square method, see [12, 56] for this latter choice in the Lagrangian case. See [13, 14, 49, 15, 16] for examples of second and third orders ENO and WENO reconstructions in the gas dynamics Lagrangian framework. Finally, one can opt for a discontinuous Galerkin discretization. We have previously used such discretization in the total Lagrangian framework, namely working on the initial configuration, system (5), to develop third-order methods, see [71]. In this case, the conserved variables are approximated through polynomial basis functions, for which the corresponding moments are evolved through the governing equations. The pressure is then defined pointwisely through the use of the equation of state.

Now, for high-order finite volume schemes on the moving configuration, such as those presented in [12, 56, 13], the following relation between the high-order polynomial approximation and the averaged value holds

$$\mathsf{U}_i^n = \frac{1}{\Delta x_i^n} \int_{\omega_i} \mathsf{U}_{h,i}^n(x)\,\mathrm{d}x. \tag{49}$$

For the total Lagrangian DG method introduced in [71], this relation writes

$$\mathsf{U}_i^n = \frac{1}{m_i} \int_{\Omega_i} \rho^0(X)\,\mathsf{U}_{h,i}^n(X)\,\mathrm{d}X. \tag{50}$$

These relations will help us to extend the positivity-preserving proof to the high-orders of accuracy. To this end, we make use of the seminal work of Zhang and Shu presented in a series of papers, [74, 75, 76, 77], which has also been used by Cheng and Shu in [15]. This method relies on a decomposition of high-order discretization as a convex combination of first-order schemes. Provided with a particular limitation, the numerical solution can be ensured to be positive while maintaining its originally designed high order accuracy. For this purpose, let us first introduce the following high-order quadrature rule on $[-1, 1]$

$$\int_{-1}^{1} \phi(y)\,\mathrm{d}y = \sum_{\alpha=1}^{N} w_\alpha\,\phi(y_\alpha), \tag{51}$$

where $\{(w_\alpha, y_\alpha)\}_{\alpha=1,\dots,N}$ are the N positive quadrature weights and quadrature points, with $y_0 = -1$ and $y_N = 1$. For practical applications, we employ Gauss-Lobatto rules which are exact for polynomial of degree up to $2N-3$, see Figure 3.

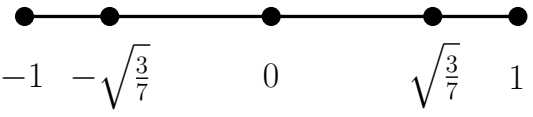

Figure 3: Five points Gauss-Lobatto quadrature rule.

Because we need the quadrature rule to be exact for relations (49) and (50), for high-order finite volume schemes on the moving configuration (51) has to be exact for polynomial up to degree K, hence $N \geq \frac{K+3}{2}$, while for the total Lagrangian DG method it has to be exact up to degree $2K$, hence $N \geq K + \frac{3}{2}$. Through the use of (51) on definitions (49) and (50), the following relation can be derived

$$\mathsf{U}_i^n = \frac{1}{m_i} \sum_{\alpha=1}^{N} m_{\alpha\,i}\,\mathsf{U}_{\alpha\,i}, \tag{52}$$

where, for finite volume schemes on moving cell, $m_{\alpha\,i} = w_\alpha\,m_i$, $\mathsf{U}_{\alpha\,i} = \mathsf{U}_{h,i}^n(x_\alpha)$ and $x_\alpha = x_{i-\frac{1}{2}} + \frac{1}{2}(y_\alpha + 1)\,(x_{i+\frac{1}{2}} - x_{i-\frac{1}{2}})$, while for the DG scheme on initial cell, $m_{\alpha\,i} = w_\alpha\,\rho^0(X_\alpha)\,\Delta X_i$, $\mathsf{U}_{\alpha\,i} =$

$\mathsf{U}^n_{h,i}(X_\alpha)$ and $X_\alpha = X_{i-\frac{1}{2}} + \frac{1}{2}(y_\alpha + 1)\,(X_{i+\frac{1}{2}} - X_{i-\frac{1}{2}})$. Noticing that $\mathsf{U}_{1\,i} = \mathsf{U}^+_{i-\frac{1}{2}}$ and $\mathsf{U}_{N\,i} = \mathsf{U}^-_{i+\frac{1}{2}}$, equation (52) immediately rewrites

$$\begin{aligned}\mathsf{U}^n_i &= \frac{1}{m_i}\sum_{\alpha=2}^{N-1} m_{\alpha\,i}\,\mathsf{U}_{\alpha\,i} + \frac{m_{1\,i}}{m_i}\,\mathsf{U}^+_{i-\frac{1}{2}} + \frac{m_{N\,i}}{m_i}\,\mathsf{U}^-_{i+\frac{1}{2}},\\ &= \frac{m^\star_i}{m_i}\,\mathsf{U}^\star_i + \frac{m_{1\,i}}{m_i}\,\mathsf{U}^+_{i-\frac{1}{2}} + \frac{m_{N\,i}}{m_i}\,\mathsf{U}^-_{i+\frac{1}{2}},\end{aligned} \tag{53}$$

where $m^\star_i = \sum_{\alpha=2}^{N-1} m_{\alpha\,i}$ and $\mathsf{U}^\star_i = \frac{1}{m^\star_i}\sum_{\alpha=2}^{N-1} m_{\alpha\,i}\,\mathsf{U}_{\alpha\,i}$. This last equation expresses U^n_i as a convex combination. Now, substituting (53) into the high-order scheme (48), along with adding and subtracting the artificial flux $\overline{\mathsf{F}}(\mathsf{U}^+_{i-\frac{1}{2}}, \mathsf{U}^-_{i+\frac{1}{2}})$ yields

$$\begin{aligned}\mathsf{U}^{n+1}_i &= \mathsf{U}^n_i - \frac{\Delta t^n}{m_i}\left[\overline{\mathsf{F}}(\mathsf{U}^-_{i+\frac{1}{2}}, \mathsf{U}^+_{i+\frac{1}{2}}) - \overline{\mathsf{F}}(\mathsf{U}^-_{i-\frac{1}{2}}, \mathsf{U}^+_{i-\frac{1}{2}})\right] \pm \frac{\Delta t^n}{m_i}\overline{\mathsf{F}}(\mathsf{U}^+_{i-\frac{1}{2}}, \mathsf{U}^-_{i+\frac{1}{2}}),\\ &= \frac{m^\star_i}{m_i}\,\mathsf{U}^\star_i + \frac{m_{1\,i}}{m_i}\,\mathsf{V}^+_{i-\frac{1}{2}} + \frac{m_{N\,i}}{m_i}\,\mathsf{V}^-_{i+\frac{1}{2}},\end{aligned} \tag{54}$$

where $\mathsf{V}^+_{i-\frac{1}{2}}$ and $\mathsf{V}^-_{i+\frac{1}{2}}$ are defined as follows

$$\mathsf{V}^+_{i-\frac{1}{2}} = \mathsf{U}^+_{i-\frac{1}{2}} - \frac{\Delta t^n}{m_{1\,i}}\left[\overline{\mathsf{F}}(\mathsf{U}^+_{i-\frac{1}{2}}, \mathsf{U}^-_{i+\frac{1}{2}}) - \overline{\mathsf{F}}(\mathsf{U}^-_{i-\frac{1}{2}}, \mathsf{U}^+_{i-\frac{1}{2}})\right], \tag{55a}$$

$$\mathsf{V}^-_{i+\frac{1}{2}} = \mathsf{U}^-_{i+\frac{1}{2}} - \frac{\Delta t^n}{m_{N\,i}}\left[\overline{\mathsf{F}}(\mathsf{U}^-_{i+\frac{1}{2}}, \mathsf{U}^+_{i+\frac{1}{2}}) - \overline{\mathsf{F}}(\mathsf{U}^+_{i-\frac{1}{2}}, \mathsf{U}^-_{i+\frac{1}{2}})\right]. \tag{55b}$$

The use of the artificial flux $\overline{\mathsf{F}}(\mathsf{U}^+_{i-\frac{1}{2}}, \mathsf{U}^-_{i+\frac{1}{2}}) = (-\mathfrak{u}_i, \mathfrak{p}_i, \mathfrak{p}_i\,\mathfrak{u}_i)^{\mathrm{t}}$, where $\mathfrak{u}_i$ plays the role of some artificial velocity and $\mathfrak{p}_i$ some artificial pressure, has allowed us to decompose U^{n+1}_i as a new convex combination (54). Then, recalling the definition of the admissible set G

$$G = \left\{\mathsf{U} = (\tau,\, u,\, e)^{\mathrm{t}}, \quad \tau \in \,]\tau_{min}, \tau_{max}[\;\text{ and }\; \widehat{\varepsilon}(\mathsf{U}) > \varepsilon_{min}\right\},$$

we can state that to have $\mathsf{U}^\star_i$, $\mathsf{V}^+_{i-\frac{1}{2}}$ and $\mathsf{V}^-_{i+\frac{1}{2}}$ in the convex admissible set G implies U^{n+1}_i, the updated numerical solution in average, to be in G. Furthermore, in light of definitions (55a) and (55b), $\mathsf{V}^+_{i-\frac{1}{2}}$ and $\mathsf{V}^-_{i+\frac{1}{2}}$ perfectly identify with the first-order scheme (17), namely they both write as $\mathsf{V} = \mathsf{U} - \frac{\Delta t}{m}(\overline{\mathsf{F}}(\mathsf{U}, \mathsf{X}) - \overline{\mathsf{F}}(\mathsf{Y}, \mathsf{U}))$. Consequently, to ensure $\mathsf{V}^\mp_{i\pm\frac{1}{2}}$ to be in G, one can apply the exact same techniques as the ones presented in the first-order case.

2.8. High-order positivity-preserving schemes

In this subsection, we focus on the conditions to enforce $\mathsf{V}^\mp_{i\pm\frac{1}{2}} \in G$. Similarly to the first-order case, one may choose to use particular non-linear definitions of the local acoustic impedances, or simply an additional time step constraint.

2.8.1. Modified Dukowicz solver

The high-order extension of the original and modified Dukowicz definitions of $\widetilde{z}^{\mp}_{i\pm\frac{1}{2}}$, introduced in (31) and (32), can be expressed as follows

$$\widetilde{z}^{\mp}_{i\pm\frac{1}{2}} = \rho^{\mp}_{i\pm\frac{1}{2}} \left(a^{\mp}_{i\pm\frac{1}{2}} + \widetilde{\Gamma} \left| \overline{u}_{i\pm\frac{1}{2}} - u^{\mp}_{i\pm\frac{1}{2}} \right| \right), \tag{56}$$

where $\rho^{\mp}_{i\pm\frac{1}{2}}$, $a^{\mp}_{i\pm\frac{1}{2}}$ and $u^{\mp}_{i\pm\frac{1}{2}}$ are the high-order values of the density, sound speed and fluid velocity at node $x_{i\pm\frac{1}{2}}$ within cell ω_i, respectively at $X_{i\pm\frac{1}{2}}$ within Ω_i in a total Lagrangian frame. In the case where $\widetilde{\Gamma} = \Gamma$, one recovers the high-order extension of the Dukowicz solver, while for $\widetilde{\Gamma} = \sigma_v^{-1}$, equation (56) reads as the extension of the modified one. Given (55) where the artificial flux $\overline{\mathsf{F}}(\mathsf{U}^{+}_{i-\frac{1}{2}}, \mathsf{U}^{-}_{i+\frac{1}{2}}) = (-\mathfrak{u}_i, \mathfrak{p}_i, \mathfrak{p}_i\,\mathfrak{u}_i)^{\mathrm{t}}$ has been introduced, we also need to define the artificial local wavespeeds relative to this term, $z^{\mp,\mathfrak{u}}_{i\pm\frac{1}{2}}$, as

$$z^{\mp,\mathfrak{u}}_{i\pm\frac{1}{2}} = \rho^{\mp}_{i\pm\frac{1}{2}} \left(a^{\mp}_{i\pm\frac{1}{2}} + \widetilde{\Gamma} \left| \mathfrak{u}_i - u^{\mp}_{i\pm\frac{1}{2}} \right| \right), \tag{57}$$

where the artificial velocity $\mathfrak{u}_i$ reads

$$\mathfrak{u}_i = \frac{z^{+,\mathfrak{u}}_{i-\frac{1}{2}}\, u^{+}_{i-\frac{1}{2}} + z^{-,\mathfrak{u}}_{i+\frac{1}{2}}\, u^{-}_{i+\frac{1}{2}}}{z^{+,\mathfrak{u}}_{i-\frac{1}{2}} + z^{-,\mathfrak{u}}_{i+\frac{1}{2}}} - \frac{p^{-}_{i+\frac{1}{2}} - p^{+}_{i-\frac{1}{2}}}{z^{+,\mathfrak{u}}_{i-\frac{1}{2}} + z^{-,\mathfrak{u}}_{i+\frac{1}{2}}}. \tag{58}$$

Each element of equations (55) having been defined explicitly, one may now apply in a straightforward manner the analysis performed on the first-order scheme. But before, let us first make the following remark.

Remark 2.6. *In the first-order case, the original Dukowicz wavespeed definition* (31)*, for which the constant* Γ *has been determined in the strong shock limit, has proved to ensure the positivity of the intermediate specific volumes and internal energies. This proof relies on the fact that pressure and sound speed are explicitly defined through the equation of state, namely in the ideal gas case* $p^n_i = (\gamma - 1)\,\rho^n_i\,\varepsilon^n_i$ *and* $a^n_i = \sqrt{\gamma(\gamma-1)\varepsilon^n_i}$*. This is no more the case when the high-order polynomial reconstruction is performed on the flux variables. In this particular case, the EOS is only ensured in mean value, and thus* $p^{\mp}_{i\pm\frac{1}{2}} \neq p(\mathsf{U}^{\mp}_{i\pm\frac{1}{2}})$*. This is the reason why, for schemes employing slope reconstruction on the flux variables, as in [12, 56], one cannot hope the high-order extension of the Dukowicz wavespeed* (56) *to ensure the positivity of the intermediate states. Nonetheless, the modified version of it,* (57)*, introduced in this paper, is ensured to produce intermediate states in the admissible set, by construction of the constant* $\widetilde{\Gamma} = \sigma_v^{-1}$*.*

Proposition 2.7. *For any high-order discretization relying on* (48)*, assuming* $\mathsf{U}^n_i \in G$ *along with* $\mathsf{U}^{\star}_i, \mathsf{U}^{+}_{i-\frac{1}{2}}, \mathsf{U}^{-}_{i+\frac{1}{2}} \in G$*, the averaged value* U^{n+1}_i *is ensured to be admissible provided the numerical fluxes* (21) *and the particular wavespeeds definition* (57) *with* $\widetilde{\Gamma} = \sigma_v^{-1}$ *under the following time step limitation*

$$\Delta t \leq \sigma_e\, \frac{m_{1\,i}}{\widetilde{z}^{+}_{i-\frac{1}{2}} + z^{+,\mathfrak{u}}_{i-\frac{1}{2}}} \quad \text{and} \quad \Delta t \leq \sigma_e\, \frac{m_{N\,i}}{\widetilde{z}^{-}_{i+\frac{1}{2}} + z^{-,\mathfrak{u}}_{i+\frac{1}{2}}},$$

where $\sigma_e \leq 1$ *and if*

$$\sigma_v \leq \min\left(1-\frac{\tau_{min}}{\tau^{\mp}_{i\pm\frac{1}{2}}}, \frac{\tau_{max}}{\tau^{\mp}_{i\pm\frac{1}{2}}}-1, \left(1-\frac{\varepsilon_{min}}{\widehat{\varepsilon}^{\mp}_{i\pm\frac{1}{2}}}\right)\frac{\rho^{\mp}_{i\pm\frac{1}{2}}\,\widehat{\varepsilon}^{\mp}_{i\pm\frac{1}{2}}}{|\widehat{p}^{\mp}_{i\pm\frac{1}{2}}|}\right).$$

Now, if one rather wants to use a simpler solver as the acoustic Godunov one, or any specific definitions of wavespeeds as for example $\widetilde{z}^{\mp}_{i\pm\frac{1}{2}} = \rho^n_i\left(a^n_i + \Gamma\,|\overline{u}_{i\pm\frac{1}{2}} - u^{\mp}_{i\pm\frac{1}{2}}|\right)$, which is generally used in the high-order extension of the Dukowicz solver, one needs to add additional limitations on the time step.

2.8.2. Generic wavespeeds

In this case, the choice in $\widetilde{z}^{\mp}_{i\pm\frac{1}{2}} > 0$ is free. Thus, one can either use z^n_i or $\rho^n_i\left(a^n_i + \widetilde{\Gamma}\,|\overline{u}_{i\pm\frac{1}{2}} - u^{\mp}_{i\pm\frac{1}{2}}|\right)$ or even $\rho^{\mp}_{i\pm\frac{1}{2}}\left(a^{\mp}_{i\pm\frac{1}{2}} + \widetilde{\Gamma}\,|\overline{u}_{i\pm\frac{1}{2}} - u^{\mp}_{i\pm\frac{1}{2}}|\right)$ for any $\widetilde{\Gamma}$, or any other definition. The artificial wavespeeds $z^{\mp,\mathfrak{u}}_{i\pm\frac{1}{2}}$ have to be chosen consistently. Similarly to the first-order case, we can state

Proposition 2.8. *For any high-order discretization presented earlier, assuming* $\mathsf{U}^n_i \in G$ *along with* $\mathsf{U}^\star_i, \mathsf{U}^+_{i-\frac{1}{2}}, \mathsf{U}^-_{i+\frac{1}{2}} \in G$*, the averaged value* U^{n+1}_i *is ensured to be admissible provided the numerical fluxes* (21) *for any positive wavespeed definition* $\widetilde{z}^{\mp}_{i\pm\frac{1}{2}}$ *under the following time step limitations*

$$\Delta t \leq \sigma_e\,\frac{m_{1\,i}}{\widetilde{z}^{+}_{i-\frac{1}{2}} + z^{+,\mathfrak{u}}_{i-\frac{1}{2}}} \quad \textit{and} \quad \Delta t \leq \sigma_e\,\frac{m_{N\,i}}{\widetilde{z}^{-}_{i+\frac{1}{2}} + z^{-,\mathfrak{u}}_{i+\frac{1}{2}}},$$

with $\sigma_e \leq 2$*, as well as*

$$\Delta t \leq \sigma_v\,\frac{\tau^{+}_{i-\frac{1}{2}}\,m_{1\,i}}{|\overline{u}_{i-\frac{1}{2}} - \mathfrak{u}_i|} \quad \textit{and} \quad \Delta t \leq \sigma_v\,\frac{\tau^{-}_{i+\frac{1}{2}}\,m_{N\,i}}{|\overline{u}_{i+\frac{1}{2}} - \mathfrak{u}_i|},$$

where σ_v *has to be such that*

$$\sigma_v \leq \min\left(1-\frac{\tau_{min}}{\tau^{\mp}_{i\pm\frac{1}{2}}}, \frac{\tau_{max}}{\tau^{\mp}_{i\pm\frac{1}{2}}}-1, \left(1-\frac{\varepsilon_{min}}{\widehat{\varepsilon}^{\mp}_{i\pm\frac{1}{2}}}\right)\frac{\rho^{\mp}_{i\pm\frac{1}{2}}\,\widehat{\varepsilon}^{\mp}_{i\pm\frac{1}{2}}}{|\widehat{p}^{\mp}_{i\pm\frac{1}{2}}|}\right).$$

The remark claiming that the second technique is optimal in term of time step still holds in this high-order case. Indeed, in the modified Dukowicz solver case, thanks to definitions (56) and (57), it is very easy to prove that

$$\frac{m_{1/N\,i}}{\widetilde{z}^{\mp}_{i\pm\frac{1}{2}} + z^{\mp,\mathfrak{u}}_{i\pm\frac{1}{2}}} < \sigma_v\,\frac{\tau^{\mp}_{i\pm\frac{1}{2}}\,m_{1/N\,i}}{|\overline{u}_{i\pm\frac{1}{2}} - \mathfrak{u}_i|}. \tag{59}$$

So far, we have proved that assuming $\mathsf{U}^n_i, \mathsf{U}^\star_i$, $\mathsf{U}^+_{i-\frac{1}{2}}$ and $\mathsf{U}^-_{i+\frac{1}{2}}$ lie in the admissible set, there exists a time step ensuring the new numerical solution U^{n+1}_i to be admissible in averaged value. To ensure the required assumptions, we make use of the particular limitation introduced in [75].

2.9. Positivity-preserving limiter

In the remainder, x should be replaced by X in a total Lagrangian frame. At time level n, the averaged value U_i^n is assumed to be in G. Then, we modify the polynomial reconstruction $\mathsf{U}_{h,i}^n$ to ensure the desired properties, as follows

$$\widetilde{\mathsf{U}_{h,i}^n}(x) = \mathsf{U}_i^n + \theta\,(\mathsf{U}_{h,i}^n(x) - \mathsf{U}_i^n), \tag{60}$$

where $\theta \in [0,1]$ is to be determined. Obviously, such a constant exists because in the worst case, with $\theta = 0$, one recovers the first-order scheme with $\mathsf{U}_i^n \in G$. However, the strategy to choose θ below will ensure the original high order accuracy of the solution polynomial is not destroyed. The purpose of the limiter is to yield $\widetilde{\mathsf{U}}_{i-\frac{1}{2}}^{+} \equiv \widetilde{\mathsf{U}_{h,i}^n}(x_{i-\frac{1}{2}}^{+})$, $\widetilde{\mathsf{U}}_{i+\frac{1}{2}}^{-} \equiv \widetilde{\mathsf{U}_{h,i}^n}(x_{i+\frac{1}{2}}^{-})$ and $\widetilde{\mathsf{U}}_i^{\star} \equiv \frac{1}{m_i^{\star}} \sum_{\alpha=2}^{N-1} m_{\alpha\, i}\, \widetilde{\mathsf{U}_{h,i}^n}(x_\alpha)$ in the admissible set G. Let us note that ensuring $\widetilde{\mathsf{U}_{h,i}^n}(x_\alpha) \in G$, for all $\alpha = 2, \ldots, N-1$, will imply to have $\widetilde{\mathsf{U}}_i^{\star} \in G$. However, this procedure being over-limiting regarding the requirement, the enforcement of only $\widetilde{\mathsf{U}}_i^{\star}$ in the admissible set has been preferred. First, let us enforce the admissibility of the specific volume as follows

$$\widetilde{\tau_{h,i}^n}(x) = \tau_i^n + \theta_\tau\,(\tau_{h,i}^n(x) - \tau_i^n), \tag{61}$$

where the coefficient $\theta_\tau = \min(\theta_\tau^{min}, \theta_\tau^{max})$ is computed such that

$$\theta_\tau^{min} = \min\Big(1, \frac{\tau_i^n - \tau_{min}}{\tau_i^n - \tau_m^{min}}\Big) \quad \text{with} \quad \tau_m^{min} = \min(\tau_{i-\frac{1}{2}}^{+}, \tau_{i+\frac{1}{2}}^{-}, \tau_i^{\star}),$$
$$\theta_\tau^{max} = \min\Big(1, \frac{\tau_{max} - \tau_i^n}{\tau_m^{max} - \tau_i^n}\Big) \quad \text{with} \quad \tau_m^{max} = \max(\tau_{i-\frac{1}{2}}^{+}, \tau_{i+\frac{1}{2}}^{-}, \tau_i^{\star}).$$

Then, for the positivity of the internal energy, the limited polynomial reconstructions of the velocity and total energy are computed through

$$\widetilde{u_{h,i}^n}(x) = u_i^n + \theta_\varepsilon\,(u_{h,i}^n(x) - u_i^n), \tag{62}$$
$$\widetilde{e_{h,i}^n}(x) = e_i^n + \theta_\varepsilon\,(e_{h,i}^n(x) - e_i^n), \tag{63}$$

where θ_ε is evaluated in an optimal manner to ensure $\widetilde{\varepsilon}_m > \varepsilon_{min}$, where $\widetilde{\varepsilon}_m = \min(\widetilde{\varepsilon}_{i-\frac{1}{2}}^{+} - p_s\,\widetilde{\tau}_{i-\frac{1}{2}}^{+}, \widetilde{\varepsilon}_{i+\frac{1}{2}}^{-} - p_s\,\widetilde{\tau}_{i+\frac{1}{2}}^{-}, \widetilde{\varepsilon}_i^{\star} - p_s\,\widetilde{\tau}_i^{\star})$ for the stiffened gas EOS, and $\widetilde{\varepsilon}_m = \min(\widetilde{\varepsilon}_{i-\frac{1}{2}}^{+}, \widetilde{\varepsilon}_{i+\frac{1}{2}}^{-}, \widetilde{\varepsilon}_i^{\star})$ otherwise. In order to determine θ_ε, let us develop the limited polynomial approximation of the internal energy

$$\begin{aligned}\widetilde{\varepsilon_{h,i}^n}(x) &= \widetilde{e_{h,i}^n}(x) - \frac{1}{2}\big(\widetilde{u_{h,i}^n}(x)\big)^2, \\ &= \varepsilon_i^n + \theta_\varepsilon\,(\varepsilon_{h,i}^n(x) - \varepsilon_i^n) + \frac{\theta_\varepsilon(1-\theta_\varepsilon)}{2}\,(u_{h,i}^n(x) - u_i^n)^2.\end{aligned} \tag{64}$$

Because $\frac{\theta_\varepsilon(1-\theta_\varepsilon)}{2}\,(u_{h,i}^n(x) - u_i^n)^2 \geq 0$, one could decide to limit $\widetilde{\varepsilon_{h,i}^n}(x) \geq \varepsilon_i^n + \theta_\varepsilon\,(\varepsilon_{h,i}^n(x) - \varepsilon_i^n)$ in a similar way to the specific volume. However, such procedure will limit more than necessary, except in the case $u_{h,i}^n(x) = u_i^n$. Then, to pick θ_ε in an optimal manner for $u_{h,i}^n(x) \neq u_i^n$, in the light of equation (64), we solve the quadratic equation $\widetilde{\varepsilon_{h,i}^n}(x) = \varepsilon_{min}$. This equation leads to two roots of opposite signs. We finally set θ_ε to be the minimum between 1 and the positive root. That being said, we will presently show how the positivity of the numerical scheme yields stability properties.

2.10. Positivity-preserving stability

Let us define the piecewise polynomial numerical solution $\mathsf{U}_h(x,t)$ defined on $\omega \times [0,T]$ such that

$$\mathsf{U}_h(x,t) = \mathsf{U}_{h,i}^n(x), \quad \text{for } x \in \omega_i \text{ and } t \in [t^n, t^{n+1}[. \tag{65}$$

A similar definition can be introduced in the total Lagrangian frame by substituting in (65) x by X, and ω by Ω. We assume the following initialization of the numerical variable mean values

$$\mathsf{U}_i^0 = \frac{1}{m_i} \int_{\Omega_i} \rho^0(X)\, U^0(X)\, \mathrm{d}X, \tag{66}$$

where $U^0(X) = (\frac{1}{\rho^0(X)}, u^0(X), e^0(X))^{\mathrm{t}}$, with $\rho^0(X)$ the initial fluid density, $u^0(X)$ the initial fluid velocity and $e^0(X)$ the initial total energy. Let us introduce the L_1 and L_2 norms of a function ϕ, respectively in the case of finite volume schemes on moving frame

$$\|\phi\|_{L_1} = \frac{m_c}{\Delta x_i^n} \int_\omega |\phi(x)|\, \mathrm{d}x \quad \text{and} \quad \|\phi\|_{L_2} = \left(\frac{m_c}{\Delta x_i^n} \int_\omega (\phi(x))^2\, \mathrm{d}x \right)^{\frac{1}{2}}, \tag{67}$$

and for DG schemes in a total Lagrangian frame

$$\|\phi\|_{L_1} = \int_\Omega \rho^0(X)\, |\phi(X)|\, \mathrm{d}X \quad \text{and} \quad \|\phi\|_{L_2} = \left(\int_\Omega \rho^0(X)\, (\phi(X))^2\, \mathrm{d}X \right)^{\frac{1}{2}}. \tag{68}$$

For the sake of simplicity, we set ourselves either in a periodic boundary case, or in the particular case where $\overline{\mathsf{F}}_b = \overline{\mathsf{F}}_e = 0$, with $\overline{\mathsf{F}}_b$ and $\overline{\mathsf{F}}_e$ read for the left and right boundary fluxes. Then, summing the high-order scheme (48) on each cell leads to

$$\sum_{i=1}^{I_i} m_i\, \mathsf{U}_i^{n+1} = \sum_{i=1}^{I_i} m_i\, \mathsf{U}_i^n. \tag{69}$$

Because the high-order scheme has proved to produce positive mean values under some constraints, the polynomials τ_h and $\varepsilon_h = e_h - \frac{1}{2}(u_h)^2$ are assumed to be positive for any $x \in \omega$, which is always feasible by limiting enough. Then, by means of relation (69) we are able to derive the following L_1 stability statements on the specific volume and total energy

$$\|\tau_h\|_{L_1} = \|\frac{1}{\rho^0}\|_{L_1} \quad \text{and} \quad \|e_h\|_{L_1} = \|e^0\|_{L_1}. \tag{70}$$

No similar result can be obtained for the velocity. However, we can derive relations bounding the L_2 norm of the velocity, namely the kinetic energy $K = \frac{1}{2}u^2$. Indeed, one knows that $0 \leq K_h < e_h$. Then, making use of the Cauchy-Schwarz inequality, the following stability results can be ensured

$$\|K_h\|_{L_1} < \|e_h\|_{L_1} \quad \text{and} \quad \|u_h\|_{L_2}^2 < m_\omega + \|e_h\|_{L_2}^2, \tag{71}$$

where $m_\omega = \sum_i m_i$ corresponds to the constant total mass of the domain ω. Let us recall that only the case of the first-order time integration has been tackled so far. In the next section, the high-order time extension will be discussed.

2.11. High-order time discretization

In Section 2.7, the high-order space discretization has been used, while the time integration is carried out by a simple first-order forward Euler method. To reach a global high-order scheme, we make use of Strong Stability Preserving (SSP) Runge-Kutta method, see [68]. For instance, at the third-order, the used algorithm writes as follows

$$\begin{aligned}
\text{Stage 1)}\ & m_i\,\mathsf{U}_{h,i}^{(1)} = m_i\,\mathsf{U}_{h,i}^{n} + \Delta t^n\,\mathsf{L}(\mathsf{U}_{h,i}^{n}),\\
& x_{i+\frac{1}{2}}^{(1)} = x_{i+\frac{1}{2}}^{n} + \Delta t^n\,\overline{u}_{i+\frac{1}{2}}^{n};\\
\text{Stage 2)}\ & m_i\,\mathsf{U}_{h,i}^{(2)} = \frac{3}{4} m_i\,\mathsf{U}_{h,i}^{n} + \frac{1}{4}[m_i\,\mathsf{U}_{h,i}^{(1)} + \Delta t^n\,\mathsf{L}(\mathsf{U}_{h,i}^{(1)})],\\
& x_{i+\frac{1}{2}}^{(2)} = \frac{3}{4} x_{i+\frac{1}{2}}^{n} + \frac{1}{4}[x_{i+\frac{1}{2}}^{(1)} + \Delta t^n\,\overline{u}_{i+\frac{1}{2}}^{(1)}];\\
\text{Stage 3)}\ & m_i\,\mathsf{U}_{h,i}^{n+1} = \frac{1}{3} m_i\,\mathsf{U}_{h,i}^{n} + \frac{2}{3}[m_i\,\mathsf{U}_{h,i}^{(2)} + \Delta t^n\,\mathsf{L}(\mathsf{U}_{h,i}^{(2)})],\\
& x_{i+\frac{1}{2}}^{n+1} = \frac{1}{3} x_{i+\frac{1}{2}}^{n} + \frac{2}{3}[x_{i+\frac{1}{2}}^{(2)} + \Delta t^n\,\overline{u}_{i+\frac{1}{2}}^{(2)}];
\end{aligned}$$

where $\mathsf{L}(\mathsf{U}_{h,i})$ is the operator corresponding to the space discretization. In light of the fact that these multistage time integration methods write as convex combinations of first-order forward Euler schemes, they will be positivity-preserving as soon as the first-order steps are. Thus, the positive limitation introduced previously, in Section 2.9, has to be applied at each Runge-Kutta stage. Let us highlight that even though in the first-order time integration case time steps ensuring an admissible numerical solution have been explicitly defined, in the multistage high-order time discretization, one can only be certain that there exists a time step small enough ensuring the global high-order scheme to be positive. Consequently, for the numerical applications we make use of an iterative procedure to determine the time step to be used. Practically, at each time level n, we start from an initial time step Δt^n, for instance defined with the first-order restrictions emphasized in Propositions 2.3 and 2.5 with a smaller CFL coefficient as $\sigma_e = 0.2$. Then, after any Runge-Kutta stage, we assess the average of the new numerical solution to see if it belongs or not to the admissible set G. If it is the case, then after having applying the positivity limitation we go forward to the next Runge-Kutta stage. Otherwise, we return to time level n and take $\Delta t^n/2$ as the new time step. In propositions 2.7 and 2.8, the time step restrictions are just used for a theoretical purpose to be sure that this iterative time step selection process admits a positive limit.

So far, only the one-dimensional case has been tackled, in a quite exhaustive manner. It will help us to extend this analysis to the two-dimensional case. We will see how this work fits a wide number of already existing schemes as those presented in [12, 55, 8, 72] for instance.

3. Two-dimensional case

We will not give details in the multi-dimensional case how to derive, from the Euler equations, the different Lagrangian gas dynamics systems of equations. For a complete review of such process, the interested reader may refer to [36, 21, 53, 72]. We will just recall in the remainder the gas dynamics system in both updated and total Lagrangian formulations.

3.1. Governing equations

On a frame moving through the fluid flow, the two-dimensional gas dynamics governing equations write in an updated Lagrangian formulation as

$$\rho \frac{\mathrm{d}\,\mathsf{U}}{\mathrm{d}t} + \nabla_x \cdot \mathsf{F}(\mathsf{U}) = \mathsf{0}, \tag{72}$$

where $\mathsf{U} = (\tau, \boldsymbol{u}, e)^{\mathrm{t}}$ and $\mathsf{F}(\mathsf{U}) = (-\boldsymbol{u},\ \mathbb{1}(1)\,p,\ \mathbb{1}(2)\,p,\ p\,\boldsymbol{u})^{\mathrm{t}}$, with $\mathbb{1}(i) = (\delta_{i1}, \delta_{i2})^{\mathrm{t}}$. Similarly to the one-dimensional case, the material derivative $\frac{\mathrm{d}}{\mathrm{d}t}$ in (72) is defined through

$$\frac{\mathrm{d}}{\mathrm{d}t} f(\boldsymbol{x}, t) = \frac{\partial}{\partial t} f(\boldsymbol{x}, t) + \boldsymbol{u} \cdot \nabla_x f(\boldsymbol{x}, t), \tag{73}$$

provided that the referential moves with the fluid velocity. This statement is emphasized in the trajectory equation, $\frac{\partial}{\partial t}\boldsymbol{x}(\boldsymbol{X}, t) = \boldsymbol{u}(\boldsymbol{x}(\boldsymbol{X}, t), t)$, where $\boldsymbol{x}(\boldsymbol{X}, t)$ is a fluid particle initially located at $\boldsymbol{X}$. Integrating equation (72) on a control volume ω, and by means of the Reynolds transport formula [36, 53], one can easily get this system into its conservative integral form as

$$\frac{\partial}{\partial t} \int_\omega \rho\,\mathsf{U}\,\mathrm{d}v + \int_{\partial\omega} \mathsf{F}(\mathsf{U}) \cdot \boldsymbol{n}\,\mathrm{d}s = 0, \tag{74}$$

where $\boldsymbol{n}$ represents the unit outward normal of ω boundary. Now, the counterpart of system (72) on the initial referential, namely the system of gas dynamics equations in a total Lagrangian framework, reads as follows

$$\rho^0 \frac{\partial\,\mathsf{U}}{\partial t} + \nabla_X \cdot \big(|\mathsf{J}|\mathsf{J}^{-1}\mathsf{F}(\mathsf{U})\big) = \mathsf{0}. \tag{75}$$

In (75), $\mathsf{J} = \nabla_X \boldsymbol{x}$ identifies the Jacobian of the fluid flow, also referred as the deformation gradient tensor, and $|\mathsf{J}|$ is nothing but the determinant of J. We assume $|\mathsf{J}| > 0$ for the flow map to be invertible. Similarly to (74), one can write system (75) in an integral conservative form as

$$\frac{\partial}{\partial t} \int_\Omega \rho^0\,\mathsf{U}\,\mathrm{d}V + \int_{\partial\Omega} \mathsf{F}(\mathsf{U}) \cdot |\mathsf{J}|\mathsf{J}^{-t}\boldsymbol{N}\,\mathrm{d}S = 0, \tag{76}$$

where $\boldsymbol{N}$ represents the unit outward normal of the boundary of Ω. Obviously, if ω is the image through the fluid flow of the initial volume Ω, then $\boldsymbol{n}$ will be nothing but the image in the actual configuration of the initial normal $\boldsymbol{N}$. In this case, they are related to each other by means of the Nanson formula

$$|\mathsf{J}|\mathsf{J}^{-t}\boldsymbol{N}\,\mathrm{d}S \equiv \mathsf{J}^\star\boldsymbol{N}\,\mathrm{d}S = \boldsymbol{n}\,\mathrm{d}s, \tag{77}$$

where $\mathsf{J}^\star$ reads as the cofactor matrix of tensor J.

3.2. First-order scheme

Using the same procedure as in the one-dimensional case, let Ω be the domain filled by the fluid in its initial configuration. Its image through the flow map is the considered domain ω at time t. These domains are partitioned into non-overlapping cells, respectively Ω_c and ω_c, where ω_c is the image of cell Ω_c through the fluid flow. Then, integrating on ω_c, respectively Ω_c, the Lagrangian

gas dynamics systems presented and applying a standard forward Euler scheme as time integrator, one gets the following first-order scheme

$$\mathsf{U}_c^{n+1} = \mathsf{U}_c^n - \frac{\Delta t^n}{m_c} \int_{\partial\omega_c} \overline{\mathsf{F}} \cdot \boldsymbol{n} \, \mathrm{d}s, \tag{78}$$

where U_c^n reads as the mass averaged value of the solution vector U as

$$\mathsf{U}_c^n = \frac{1}{m_c} \int_{\Omega_c} \rho^0 \, \mathsf{U} \, \mathrm{d}V = \frac{1}{m_c} \int_{\omega_c} \rho \, \mathsf{U} \, \mathrm{d}v, \tag{79}$$

with m_c the constant mass of cell ω_c. In equation (78), $\overline{\mathsf{F}} = (-\overline{\boldsymbol{u}},\, \mathbb{1}(1)\,\overline{p},\, \mathbb{1}(2)\,\overline{p},\, \overline{p}\,\overline{\boldsymbol{u}})^{\mathrm{t}}$ reads for the numerical flux. Scheme (78) is said to be compatible, which means that both discretizations on the updated Lagrangian frame (72) and the total Lagrangian frame (75) are perfectly equivalent, under the assumptions that the Nanson formula is true at the discrete level, as well as the Piola compatibility condition ensured, see [72] for more details.

A wide number of cell-centered numerical schemes take their starting point from equation (78). The differences will then arise from the definition of the numerical flux $\overline{\mathsf{F}}$ and the treatment of the boundary integral $\int_{\partial\omega_c}$. Consequently, to avoid the positivity-preserving study to be too scheme specific, we present and make use here of a general first-order finite volume formulation that will prove to fit different existing cell-centered Lagrangian schemes, such as those presented in [12, 55, 8, 70, 72]. The general scheme relies on general polygonal cells defined either by straight line edges, Figure 4(a), conical edges, Figure 4(b), or any high-order curvilinear edges, Figure 4(c). By means

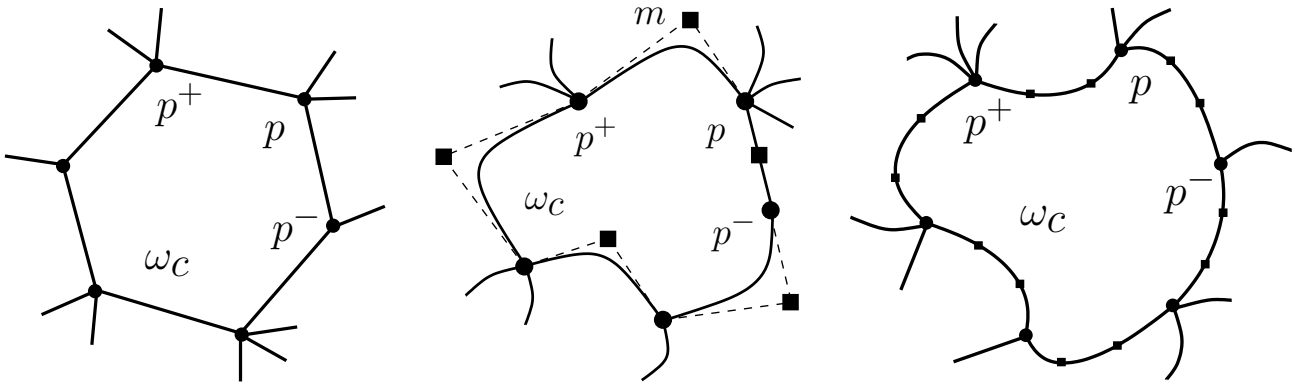

(a) Straight line edges. (b) Conical edges. (c) Polynomial edges.

Figure 4: General polygonal cells.

of quadrature rules or some approximations, the cell boundary integral present in equation (78) can be expressed as a combination of control point contributions. Following this statement, the first-order scheme (78) can be expressed as follows

$$\mathsf{U}_c^{n+1} = \mathsf{U}_c^n - \frac{\Delta t^n}{m_c} \sum_{q \in \mathcal{Q}_c} \overline{\mathsf{F}}_{qc} \cdot l_{qc} \boldsymbol{n}_{qc}, \tag{80}$$

where the $l_{qc}\boldsymbol{n}_{qc}$ correspond to some normals at time level n to be defined. In (80), $\mathcal{Q}_c$ is the chosen control point set of cell ω_c. This set has to contain the node set of the cell, *i.e.* $\mathcal{P}_c \subseteq \mathcal{Q}_c$. Indeed, the mesh has to be advected in some ways, and thus some velocity has to be allocated to all grid points. In equation (80), the control flux $\overline{\mathsf{F}}_{qc} = (-\overline{\boldsymbol{u}}_q,\, \mathbb{1}(1)\,\overline{p}_{qc},\, \mathbb{1}(2)\,\overline{p}_{qc},\, \overline{p}_{qc}\,\overline{\boldsymbol{u}}_q)^{\mathrm{t}}$ plays this role. Indeed, any grid control point q will be advected through $\boldsymbol{x}_q^{n+1} = \boldsymbol{x}_q^n + \Delta t^n\,\overline{\boldsymbol{u}}_q$. Let us emphasize that $\overline{\mathsf{F}}_{qc}$, in addition to be local to the control point q, is local the cell ω_c under consideration. This is different from the classical finite volume framework where the numerical flux on the cell boundary enforce the scheme conservation, and consequently is continuous on the edge from one cell to another. The reason a discontinuous numerical flux is considered is, as indicated previously, the cornerstone of any Lagrangian scheme is to move the mesh. We would like to do so in a similar way as in the one-dimensional case, namely by means of Riemann solvers. However, even if for a control point on a face, Figure 5(a), the two neighboring cells allow us to use a 1D Riemann solver in the normal direction, this is no more the case for nodes, Figure 5(b).

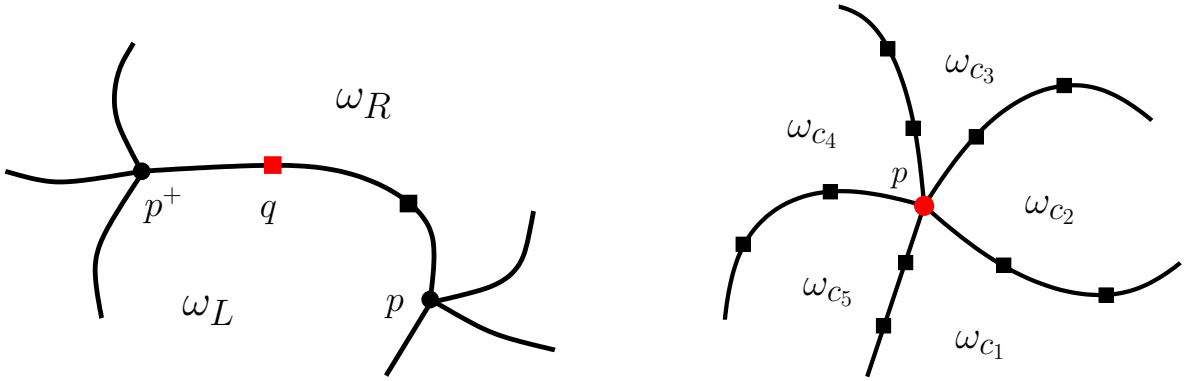

(a) Face point neighboring cells.

(b) Node neighboring cells.

Figure 5: Points neighboring cell sets.

In the 2D case, the numerical flux at node p yields three unknowns, $\overline{p}_p$ the pressure and $\overline{\boldsymbol{u}}_p$ its velocity. However, applying for instance the two-states 1D Riemann solver presented in the previous section on each edge surrounding p will produce a too large number of equations. And applying a least square or any minimizing procedure, as it was done in [2], will leads to the loss of the one-dimensional scheme properties as the entropy production or positivity.

To overcome this difficulty, the idea introduced in the GLACE scheme, [22, 12], was to break the continuity of the numerical flux pressure $\overline{p}$. Indeed, the only strong continuity requirement lies on the velocity because we do not want the nodes to split. By means of this assumption, the control point pressure $\overline{p}_q$ becomes local to the cell ω_c, namely $\overline{p}_{qc}$, and will be defined through the one-dimensional two-states solver relation (20) as follows

$$\overline{p}_{qc} = p_c^n - \widetilde{z}_{qc}\,(\overline{\boldsymbol{u}}_q - \boldsymbol{u}_c^n)\,\boldsymbol{\cdot}\,\boldsymbol{n}_{qc}, \tag{81}$$

where $\widetilde{z}_{qc} > 0$ is again a local approximation of the acoustic impedance. Let us emphasize the pressure continuity relaxation obviously leads to the loss of the scheme conservation. Nonetheless, this property will be recovered by the construction of the scheme itself. For the sake of simplicity, we

set ourselves in the simple case where no external contribution is applied on the domain boundary, *i.e.* $\int_{\partial\omega} \overline{\mathsf{F}} \cdot \boldsymbol{n}\,\mathrm{d}s = 0$. In this particular case, the scheme conservation writes

$$\sum_c m_c\,\mathsf{U}_c^{n+1} = \sum_c m_c\,\mathsf{U}_c^n. \tag{82}$$

And substituting scheme (80) in relation (82) leads to following condition on the numerical pressures

$$\sum_c \sum_{q\in\mathcal{Q}_c} \overline{p}_{qc}\,l_{qc}\boldsymbol{n}_{qc} = \boldsymbol{0}. \tag{83}$$

In the end, satisfying such relation will allow us to define explicitly the velocity for grid control points. Finally, the differences in the first-order schemes presented for instance in [12, 55, 8, 72] will arise from the type of cells considered, the definition of the control point set $\mathcal{Q}_c$ and the way condition (83) is ensured.

Let us remark that, similarly to the 1D case, the first-order scheme (80) provided with the two-states Riemann solver produces entropy at the semi-discrete level.

Remark 3.1. *Any semi-discrete scheme based on the one-dimensional two-states Riemann solver* (81)*, and which can be put in the following general form*

$$m_c\frac{\mathrm{d}\,\mathsf{U}_c}{\mathrm{d}t} = -\sum_{q\in\mathcal{Q}_c} \overline{\mathsf{F}}_{qc} \cdot l_{qc}\boldsymbol{n}_{qc}, \tag{84}$$

ensures an entropy production at the semi-discrete level. Indeed, by means of the Gibbs identity (9)*, it follows that the semi-discrete scheme* (84) *produces*

$$\begin{aligned} m_c\,T_c\frac{\mathrm{d}\,S_c}{\mathrm{d}t} &= m_c\frac{\mathrm{d}\,e_c}{\mathrm{d}t} + \boldsymbol{u}_c \cdot m_c\frac{\mathrm{d}\,\boldsymbol{u}_c}{\mathrm{d}t} + p_c\,m_c\frac{\mathrm{d}\,\tau_c}{\mathrm{d}t}, \\ &= \sum_{q\in\mathcal{Q}_c} \widetilde{z}_{qc}\,l_{qc}\left[(\overline{\boldsymbol{u}}_q - \boldsymbol{u}_c)\cdot\boldsymbol{n}_{qc}\right]^2 \geq 0. \end{aligned} \tag{85}$$

The question of the fully discrete entropy production will be addressed in the remainder of the article. Now, another essential property to be ensured in a Lagrangian frame is the accordance with the geometric conservation law. Through scheme (84) and trajectory equation $\frac{\partial}{\partial t}\boldsymbol{x}_q = \overline{\boldsymbol{u}}_q$, we know for sure that the GCL will be respected at the semi-discrete level, as soon as the integration of the boundary term in (78) has been carried out exactly, and that the domain control point set $\mathcal{Q}(\omega) = \bigcup_c \mathcal{Q}(\omega_c)$ contains all the points required to characterize the grid. This semi-discrete GCL accordance can be rewritten as $\frac{\partial}{\partial t}|\omega_c| = m_c\,\frac{\partial}{\partial t}\tau_c$. Now, to get the counterpart of this property at the fully discrete level, *i.e.* $|\omega_c| = m_c\,\tau_c$ at all time, some implicit features have to be added to the time integrator. Indeed, assuming the grid point velocity $\overline{\boldsymbol{u}}_q$ is constant during each time step, the location of the moving point $\boldsymbol{x}_q$, and hence the normals $l_{qc}\boldsymbol{n}_{qc}$, will be linear in time. So, to ensure the discrete GCL, instead of using the normals at time t^n, one should have taken for instance the normals at time $t^n + \Delta t^n/2$, or the half sum of those at time t^n and t^{n+1}, as it is generally done. However, because no theoretical positivity result holds for implicit time integration, we only use in this article explicit time discretizations. For a first-order in time scheme, the chosen normals are thus those at time level n. The GCL will then be ensured only at the semi-discrete level. Consequently, one cannot be certain that $|\omega_c|$, the true geometric volume of cell ω_c, yields $|\omega_c| = m_c\,\tau_c$. All

these considerations are no more relevant in the one-dimensional case, where the normals remain $+1$ and -1 at all time. For the sake of consistence with the 1D, let us define $|\widetilde{\omega}_c|$, such that $|\widetilde{\omega}_c| = m_c\,\tau_c$.

In this subsection, a general first-order scheme has been introduced. Particular choices in the type of cells considered, Figure 4, in the definition of the control point set $\mathcal{Q}_c$, or in the way the conservation condition (83) is ensured will enable us to recover the schemes presented in [12, 55, 8, 72]. To emphasize that, brief specifications of the schemes will now be given. But first, let us remark that the substantial progress made during the past decades on Lagrangian cell-centered schemes have been made possible thanks to the original work of Dukowicz and his co-workers on their CAVEAT code [2], and the seminal work of Loubère *et al* on high-order numerical schemes applied to the gas dynamics equations in a total Lagrangian frame [1, 51].

GLACE scheme. In the scheme introduced by Després and Mazeran in [22] and named GLACE in [12] for Godunov-type LAgrangian scheme Conservative for Energy, the moving cells under consideration are assumed to be polygons delimited by straight line edges, as in Figure 4(a). Here, the control point set $\mathcal{Q}_c$ identifies with the node set $\mathcal{P}_c$. And for any $p \in \mathcal{P}_c$, the normal $l_{pc}\boldsymbol{n}_{pc}$ stands for the cell corner normal, such that $l_{pc}\boldsymbol{n}_{pc} = \frac{1}{2}(\boldsymbol{x}_{p^+} - \boldsymbol{x}_{p^-}) \times \boldsymbol{e}_z$. Finally, to avoid any explicit coupling between the definition of node velocity, a sufficient condition ensuring the scheme conservation, relation (83), writes as follows

$$\forall p \in \mathcal{P}(\omega), \quad \sum_{c \in \mathcal{C}_p} \overline{p}_{pc}\, l_{pc}\boldsymbol{n}_{pc} = \boldsymbol{0}, \tag{86}$$

where $\mathcal{P}(\omega)$ stands for the set containing all grid nodes, and $\mathcal{C}_p = \mathcal{C}(p)$ for the neighboring cell set of node p. This previous relation says that the pressure forces are conserved around the nodes. Substituting solver relation (81) into condition (86) leads to the following equation

$$\sum_{c \in \mathcal{C}_p} \Big[p_c^n\, l_{pc}\boldsymbol{n}_{pc} - \underbrace{\widetilde{z}_{pc}\, l_{pc}\, (\boldsymbol{n}_{pc} \otimes \boldsymbol{n}_{pc})}_{\mathsf{M}_{pc}} (\overline{\boldsymbol{u}}_p - \boldsymbol{u}_c^n) \Big] = \boldsymbol{0},$$

where $\mathsf{M}_{pc} = \widetilde{z}_{pc}\, l_{pc}\, (\boldsymbol{n}_{pc} \otimes \boldsymbol{n}_{pc})$ is a projection matrix along $\boldsymbol{n}_{pc}$. This last relation allows us to uniquely define the node velocity $\overline{\boldsymbol{u}}_p$

$$\overline{\boldsymbol{u}}_p = \Big(\sum_{c \in \mathcal{C}_p} \mathsf{M}_{pc} \Big)^{-1} \sum_{c \in \mathcal{C}_p} \Big(\mathsf{M}_{pc}\boldsymbol{u}_c^n + p_c^n\, l_{pc}\boldsymbol{n}_{pc} \Big). \tag{87}$$

EUCCLHYD scheme. A thorough study of the properties of the GLACE node-centered solver reveals a strong sensitivity to cell aspect ratio. Furthermore, the fact that the matrix M_{pc} is a rank-one matrix can lead to severe numerical instabilities due to a too low entropy production, and also makes boundary conditions difficult to implement. In [55], Maire *et al* proposed an alternative scheme named EUCCLHYD for Explicit Unstructured Cell-Centered Lagrangian HYDrodynamics, that successfully solves these problems. This method relies on the same assumptions and design procedure. Thus, similar straight line edged polygonal cells are used, refer to Figure 4(a). The only difference between these two schemes lies in the way the one-dimensional Riemann solver is applied at the grid points. In the GLACE scheme, the solver is applied along the corner normal $l_{pc}\boldsymbol{n}_{pc}$, while in the EUCCLHYD scheme the one-dimensional Riemann solver is applied on each edge surrounding the node. Consequently, the node numerical flux pressure $\overline{p}_p$ is not only local

to the cell, but also local to the surrounding edges, namely $\overline{p}^-_{pc}$ and $\overline{p}^+_{pc}$. Thus, in cell ω_c, one will have two pressures per node, left and right, defined through the one-dimensional two-states solver relation (81). With this particular assumption, the control point set no longer identifies with the node cell set. Here, $\mathcal{Q}_c$ is the union of the face control point set $\mathcal{Q}(f_{pp^+}) = \{p, p^+\}$, such that $\mathcal{Q}_c = \bigcup_{p\in\mathcal{P}_c}\{p, p^+\}$. The associated normals on face f_{pp^+} identify with the face normal, $l^+_{pc}\boldsymbol{n}^+_{pc} = l^-_{p^+c}\boldsymbol{n}^-_{p^+c} = \frac{1}{2}(\boldsymbol{x}_{p^+} - \boldsymbol{x}_p)\times\boldsymbol{e}_z$. Similar to the GLACE scheme, one recovers the scheme conservation (82) assuming the pressure forces are conserved around the nodes, such that

$$\forall p \in \mathcal{P}(\omega), \quad \sum_{c\in\mathcal{C}_p}\left[\overline{p}^-_{pc}\, l^-_{pc}\boldsymbol{n}^-_{pc} + \overline{p}^+_{pc}\, l^+_{pc}\boldsymbol{n}^+_{pc}\right] = \boldsymbol{0}, \tag{88}$$

which leads to

$$\sum_{c\in\mathcal{C}_p}\Big[p^n_c\, l_{pc}\boldsymbol{n}_{pc} - \underbrace{\left(\widetilde{z}^-_{pc}\, l^-_{pc}\,(\boldsymbol{n}^-_{pc}\otimes\boldsymbol{n}^-_{pc}) + \widetilde{z}^+_{pc}\, l^+_{pc}\,(\boldsymbol{n}^+_{pc}\otimes\boldsymbol{n}^+_{pc})\right)}_{\mathsf{M}_{pc}}(\overline{\boldsymbol{u}}_p - \boldsymbol{u}^n_c)\Big] = \boldsymbol{0},$$

with $\mathsf{M}_{pc} = \widetilde{z}^-_{pc}\, l^-_{pc}\,(\boldsymbol{n}^-_{pc}\otimes\boldsymbol{n}^-_{pc}) + \widetilde{z}^+_{pc}\, l^+_{pc}\,(\boldsymbol{n}^+_{pc}\otimes\boldsymbol{n}^+_{pc})$ being the projection matrix along the two corner normals $\boldsymbol{n}^-_{pc}$ and $\boldsymbol{n}^+_{pc}$. This last relation allows us to uniquely define the node velocity $\overline{\boldsymbol{u}}_p$, similar to the GLACE scheme, as follows

$$\overline{\boldsymbol{u}}_p = \Big(\sum_{c\in\mathcal{C}_p}\mathsf{M}_{pc}\Big)^{-1}\sum_{c\in\mathcal{C}_p}\Big(\mathsf{M}_{pc}\boldsymbol{u}^n_c + p^n_c\, l_{pc}\boldsymbol{n}_{pc}\Big). \tag{89}$$

GLACE extension on conic cells. In [8], Boutin *et al* introduced an extension of the GLACE scheme on conical mesh, see Figure 4(b). In this configuration, a point $\boldsymbol{x}$ located on the conical face f_{pp^+} is defined through

$$\boldsymbol{x}_{|pp^+}(\zeta) = \frac{(1-\zeta)^2\,\boldsymbol{x}_p + 2\,\nu\zeta(1-\zeta)\,\boldsymbol{x}_m + \zeta^2\,\boldsymbol{x}_{p^+}}{(1-\zeta)^2 + 2\,\nu\zeta(1-\zeta) + \zeta^2}, \tag{90}$$

where $\zeta\in[0,1]$ is the curvilinear abscissa, m the conic control point and $\nu > 0$ the associated weight of the conic. For $\nu = 0$, one recovers a straight line, while for $\nu = 1$ the conic identifies with a Bezier curve. For the sake of conciseness, let us define $\lambda_p(\zeta) = (1-\zeta)^2/g(\zeta)$, $\lambda_m(\zeta) = 2\,\nu\zeta(1-\zeta)^2/g(\zeta)$ and $\lambda_{p^+}(\zeta) = \zeta^2/g(\zeta)$, with $g(\zeta) = (1-\zeta)^2 + 2\,\nu\zeta(1-\zeta) + \zeta^2$, so that equation (90) reformulates as

$$\boldsymbol{x}_{|pp^+}(\zeta) = \lambda_p(\zeta)\,\boldsymbol{x}_p + \lambda_m(\zeta)\,\boldsymbol{x}_m + \lambda_{p^+}(\zeta)\,\boldsymbol{x}_{p^+}. \tag{91}$$

In the GLACE conical mesh extension, the control point set is defined as the union of the nodes set and the set containing all the conic control points of cell ω_c, *i.e.* $\mathcal{Q}_c = \mathcal{P}_c\bigcup\mathcal{M}_c$ with $\mathcal{M}_c$ being the conic control point set. The associated normals are then respectively defined as

$$l_{pc}\boldsymbol{n}_{pc} = \int_{p^-}^{p}\lambda_p\,\boldsymbol{n}\,\mathrm{d}s + \int_{p}^{p^+}\lambda_p\,\boldsymbol{n}\,\mathrm{d}s,$$

as well as

$$l_{mc}\boldsymbol{n}_{mc} = \int_{p^-}^{p}\lambda_m\,\boldsymbol{n}\,\mathrm{d}s.$$

In these definitions, the normal $\boldsymbol{n}\,\mathrm{d}s$ is computed through the conic parametrization (90) such that $\boldsymbol{n}\,\mathrm{d}s = \mathrm{d}\boldsymbol{x}_{|pp^+} \times \boldsymbol{e}_z$. Finally, the scheme conservation (82) is enforced assuming that the pressure forces are conserved around the node, and around the conic control point, which can be put into the two following relations

$$\forall p \in \mathcal{P}(\omega), \quad \sum_{c\in\mathcal{C}_p} \overline{p}_{pc}\, l_{pc}\boldsymbol{n}_{pc} = \boldsymbol{0}, \tag{92}$$

$$\forall m \in \mathcal{M}(\omega), \quad (\overline{p}_{mL} - \overline{p}_{mR})\, l_{mL}\boldsymbol{n}_{mL} = \boldsymbol{0}, \tag{93}$$

with $\mathcal{M}(\omega)$ the set containing all conic control points in the domain, and for given conic control point m, ω_L and ω_R stand for the neighboring cells sharing the conical face. The first relation (92) gives the definition of the nodes velocity

$$\overline{\boldsymbol{u}}_p = \Big(\sum_{c\in\mathcal{C}_p} \mathsf{M}_{pc}\Big)^{-1} \sum_{c\in\mathcal{C}_p} \Big(\mathsf{M}_{pc}\boldsymbol{u}_c^n + p_c^n\, l_{pc}\boldsymbol{n}_{pc}\Big), \tag{94}$$

where $\mathsf{M}_{pc} = \widetilde{z}_{pc}\, l_{pc}\,(\boldsymbol{n}_{pc}\otimes\boldsymbol{n}_{pc})$. However, the problem deriving from relation (93) is not invertible, and only provides a condition on the normal component of $\overline{\boldsymbol{u}}_m$ as follows

$$\overline{\boldsymbol{u}}_m \cdot \boldsymbol{n}_{mL} = \left(\frac{\widetilde{z}_{mL}\,\boldsymbol{u}_L^n + \widetilde{z}_{mR}\,\boldsymbol{u}_R^n}{\widetilde{z}_{mL}+\widetilde{z}_{mR}}\right)\cdot \boldsymbol{n}_{mL} - \frac{p_R^n - p_L^n}{\widetilde{z}_{mL}+\widetilde{z}_{mR}}.$$

The tangential component of $\overline{\boldsymbol{u}}_m$ is then evaluated from an upwind point of view as

$$\overline{\boldsymbol{u}}_m \cdot \boldsymbol{t}_{mL} = \begin{cases} \boldsymbol{u}_L^n \cdot \boldsymbol{t}_{mL}, & \text{if } \overline{\boldsymbol{u}}_m \cdot \boldsymbol{n}_{mL} > 0, \\ \boldsymbol{u}_R^n \cdot \boldsymbol{t}_{mL}, & \text{if } \overline{\boldsymbol{u}}_m \cdot \boldsymbol{n}_{mL} < 0, \\ \left(\dfrac{\widetilde{z}_{mL}\,\boldsymbol{u}_L^n + \widetilde{z}_{mR}\,\boldsymbol{u}_R^n}{\widetilde{z}_{mL}+\widetilde{z}_{mR}}\right)\cdot \boldsymbol{t}_{mL}, & \text{if } \overline{\boldsymbol{u}}_m \cdot \boldsymbol{n}_{mL} = 0, \end{cases}$$

where $\boldsymbol{t}_{mL}$ stands for a unit vector orthogonal to $\boldsymbol{n}_{mL}$.

LCCDG scheme. Both GLACE and EUCCLHYD schemes have been extended to second-order accuracy. Nonetheless, to go further to third-order and higher, straight line edges geometry can no longer be used. Indeed, it has been proved in [14] that in this case, an implicit linear assumption is made on the fluid flow. Consequently, higher-order curved geometries are required. In [72], we have presented a general high-order cell-centered discretization of the two-dimensional Lagrangian gas dynamics equations, based a discontinuous Galerkin (DG) scheme and high-order curved polygonal cells, that we refer as LCCDG for Lagrangian Cell-Centered Discontinuous Galerkin. We recall here its first-order version, on a $(d+1)^{\text{th}}$ order polygonal cell, see Figure 4(c) for instance for a fourth-order geometry. When we refer to $(d+1)^{\text{th}}$ geometry, we mean that each edge is defined through $(d+1)$ points. The polygonal cell depicted in Figure 4(a) is then referred as a second-order geometry. In [72], the LCCDG schemes developed are based on a total Lagrangian formulation. But in its first-order version, the method is perfectly compatible between the actual and initial configurations. For the sake of simplicity, we recall such scheme on the moving cells. Here, similarly to EUCCLHYD schemes, the cell control point set is made of each face control point set, $\mathcal{Q}_c = \bigcup_{p\in\mathcal{P}_c} \mathcal{Q}(f_{pp^+})$, where $\mathcal{Q}(f_{pp^+})$ is made of the $(d+1)$ points defining the curvilinear edge which include the nodes

p and p^+. The associated normals on face f_{pp^+} are then defined as follows

$$l_{pc}^{+}\boldsymbol{n}_{pc}^{+} = \int_0^1 \lambda_p(\zeta) \sum_{k\in\mathcal{Q}(f_{pp^+})} \frac{\partial\lambda_k}{\partial\zeta}(\boldsymbol{x}_k \times \boldsymbol{e}_z)\,\mathrm{d}\zeta,$$

$$l_{p^+c}^{-}\boldsymbol{n}_{p^+c}^{-} = \int_0^1 \lambda_{p^+}(\zeta) \sum_{k\in\mathcal{Q}(f_{pp^+})} \frac{\partial\lambda_k}{\partial\zeta}(\boldsymbol{x}_k \times \boldsymbol{e}_z)\,\mathrm{d}\zeta,$$

as well as, for $q \neq p$ and $q \neq p^+$

$$l_{qc}\boldsymbol{n}_{qc} = \int_0^1 \lambda_q(\zeta) \sum_{k\in\mathcal{Q}(f_{pp^+})} \frac{\partial\lambda_k}{\partial\zeta}(\boldsymbol{x}_k \times \boldsymbol{e}_z)\,\mathrm{d}\zeta.$$

In these definitions, $\lambda_q(\zeta)$ denotes the one-dimensional Lagrangian finite element basis functions of degree d, $\zeta \in [0,1]$ the curvilinear abscissa, and $\boldsymbol{x}_k$ the actual position of the control point $k \in \mathcal{Q}(f_{pp^+})$. To recover the scheme conservation, we make use of two complementary sufficient conditions, a pressure force conservation around the grid nodes

$$\forall p \in \mathcal{P}(\omega), \quad \sum_{c\in\mathcal{C}_p} \left[\overline{p}_{pc}^{-}\, l_{pc}^{-}\boldsymbol{n}_{pc}^{-} + \overline{p}_{pc}^{+}\, l_{pc}^{+}\boldsymbol{n}_{pc}^{+}\right] = \boldsymbol{0}, \tag{95}$$

and a pressure force conservation around the face control points

$$\forall q \in \mathcal{Q}(\omega) \setminus \mathcal{P}(\omega), \quad (\overline{p}_{qL} - \overline{p}_{qR})\, l_{qL}\boldsymbol{n}_{qL} = \boldsymbol{0}, \tag{96}$$

where $\mathcal{Q}(\omega)$ denotes the set containing all control points defining the curvilinear grid. Condition (95) allows us to define the grid node velocity

$$\overline{\boldsymbol{u}}_p = \Big(\sum_{c\in\mathcal{C}_p} \mathsf{M}_{pc}\Big)^{-1} \sum_{c\in\mathcal{C}_p} \Big(\mathsf{M}_{pc}\boldsymbol{u}_c^n + p_c^n\, l_{pc}\boldsymbol{n}_{pc}\Big), \tag{97}$$

where $\mathsf{M}_{pc} = \widetilde{z}_{pc}^{-}\, l_{pc}^{-}\,(\boldsymbol{n}_{pc}^{-} \otimes \boldsymbol{n}_{pc}^{-}) + \widetilde{z}_{pc}^{+}\, l_{pc}^{+}\,(\boldsymbol{n}_{pc}^{+} \otimes \boldsymbol{n}_{pc}^{+})$. Unlike (95), condition (96) does not allow us to fully determine the face control point velocity. But, in light of the Rankine-Hugoniot relations which state that the tangential component of the velocity should be continuous across a discontinuity, see [72] for further details, the face control point velocity is defined as follows

$$\overline{\boldsymbol{u}}_q = \left(\frac{\widetilde{z}_{qL}\,\boldsymbol{u}_L^n + \widetilde{z}_{qR}\,\boldsymbol{u}_R^n}{\widetilde{z}_{qL} + \widetilde{z}_{qR}}\right) - \frac{p_R^n - p_L^n}{\widetilde{z}_{qL} + \widetilde{z}_{qR}}\,\boldsymbol{n}_{qf_{pp^+}}. \tag{98}$$

3.3. 2D extension of the Godunov-type schemes

Now, similar to the one-dimensional case, to be able to assess the scheme positivity property, we will rewrite the new averaged solution U_c^{n+1} as a convex combination of the previous solution U_c^n and some intermediate states. To that end and in the remainder of the article, we will make use extensively of the essential relation

$$\sum_{q\in\mathcal{Q}_c} l_{qc}\boldsymbol{n}_{qc} = \boldsymbol{0}, \tag{99}$$

which states that the cell control point normals sum to zero. This relation holds for any of the schemes presented previously. Thanks to (99), we are able to rewrite the first-order scheme (80) as

$$\begin{aligned}\mathsf{U}_c^{n+1} &= \mathsf{U}_c^n - \frac{\Delta t^n}{m_c} \sum_{q\in\mathcal{Q}_c} \overline{\mathsf{F}}_{qc} \cdot l_{qc}\boldsymbol{n}_{qc} + \frac{\Delta t^n}{m_c}\, \mathsf{F}(\mathsf{U}_c^n) \cdot \sum_{q\in\mathcal{Q}_c} l_{qc}\boldsymbol{n}_{qc},\\ &= (1-\lambda_c)\,\mathsf{U}_c^n + \sum_{q\in\mathcal{Q}_c} \lambda_{qc}\,\overline{\mathsf{U}}_{qc}, \end{aligned} \tag{100}$$

where $\lambda_{qc} = \frac{\Delta t^n}{m_c}\widetilde{z}_{qc}\, l_{qc}$, and $\lambda_c = \sum_{q\in\mathcal{Q}_c}\lambda_{qc}$. The intermediate state $\overline{\mathsf{U}}_{qc}$ reads

$$\overline{\mathsf{U}}_{qc} = \mathsf{U}_c^n - \frac{\left(\overline{\mathsf{F}}_{qc} - \mathsf{F}(\mathsf{U}_c^n)\right)}{\widetilde{z}_{qc}} \cdot \boldsymbol{n}_{qc}, \tag{101}$$

which is nothing but the high-dimensional extension of (24), where the $\pm$ sign has been replaced by the scalar product with $\boldsymbol{n}_{qc}$. Obviously, to ensure (100) to be a convex combination, the condition $\lambda_c \leq 1$ has to be ensured, which provides us with the two-dimensional CFL condition

$$\Delta t^n \leq \sigma_e\, \frac{m_c}{\displaystyle\sum_{q\in\mathcal{Q}_c} \widetilde{z}_{qc}\, l_{qc}}, \tag{102}$$

with the CFL coefficient $\sigma_e = 1$. In the acoustic approximation, where $\widetilde{z}_{qc} = z_c^n = \rho_c^n\, a_c^n$, this CFL condition reduces to a more classical one

$$\Delta t^n \leq \sigma_e\, \frac{|\widetilde{\omega}_c^n|}{a_c^n \displaystyle\sum_{q\in\mathcal{Q}_c} l_{qc}}, \tag{103}$$

where $|\widetilde{\omega}_c^n| = m_c/\rho_c^n$ denotes the approximated volume of the cell ω_c at time t^n introduced previously. We recall that because the time integration is explicit, the true volumes $|\omega_c^n|$ and $|\widetilde{\omega}_c^n|$ may differ. However, the differences only arising from the time error, and the problems studied in the Lagrangian framework relying on quite small characteristic computational times, the difference of these two volumes will prove to be extremely small in practice. In (102), $\sum_q l_{qc}$ yields different values depending on the scheme being studied. For instance, the CFL condition in the EUCCLHYD scheme will always be smaller than the one in the GLACE scheme. Let us now demonstrate how the discrete general scheme, equation (80), provided with the one-dimensional Riemann solver (81), produces admissible solutions under some constraints to be determined.

3.4. First-order positivity-preserving scheme

Now, similarly to the one-dimensional case, we introduce the convex admissible set we want the numerical solution to remain in

$$G = \left\{ \mathsf{U} = \begin{pmatrix} \tau \\ \boldsymbol{u} \\ e \end{pmatrix}, \quad \tau \in]\tau_{min}, \tau_{max}[\ \text{ and } \ \widehat{\varepsilon}(\mathsf{U}) > \varepsilon_{min} \right\}, \tag{104}$$

where $\widehat{\varepsilon} = \varepsilon - p^\star\tau$ in the stiffened EOS case and $\widehat{\varepsilon} = \varepsilon$ otherwise. Thus, assuming $\mathsf{U}_c^n \in G$, if one is able to prove $\forall q \in \mathcal{Q}_c$, $\overline{\mathsf{U}}_{qc} \in G$ then one can be sure that $\mathsf{U}_c^{n+1} \in G$. We will see that the one-dimensional analysis done previously can be applied in a straightforward manner to this two-dimensional case. Consequently, the same two different techniques to achieve positivity will be studied, namely the modified Dukowicz solver and the generic wave speed definition provided with an additional time step constraint.

3.4.1. Modified Dukowicz solver

Let us first show how the intermediate states $\overline{\mathsf{U}}_{qc}$ defined in equation (101) can be put into the exact same form as in the one-dimensional case. For instance, regarding the condition $\overline{\tau}_{qc} > \tau_{min}$, let us rewrite $\overline{\tau}_{qc}$ as

$$\begin{aligned}\overline{\tau}_{qc} - \tau_{min} &= \tau_c^n + \frac{\left(\overline{\boldsymbol{u}}_q - \boldsymbol{u}_c^n\right)}{\widetilde{z}_{qc}} \cdot \boldsymbol{n}_{qc} - \tau_{min}, \\ &= (\tau_c^n - \tau_{min}) \left(1 + \left(\frac{\tau_c^n}{\tau_c^n - \tau_{min}}\right) \frac{z_c^n}{\widetilde{z}_{qc}} \frac{\left(\overline{\boldsymbol{u}}_q - \boldsymbol{u}_c^n\right)}{a_c^n} \cdot \boldsymbol{n}_{qc}\right),\end{aligned} \tag{105}$$

which, introducing v_{qc} similarly to the 1D case

$$v_{qc} = \frac{\left(\overline{\boldsymbol{u}}_q - \boldsymbol{u}_c^n\right)}{a_c^n} \cdot \boldsymbol{n}_{qc}, \tag{106}$$

turns into

$$\overline{\tau}_{qc} - \tau_{min} = (\tau_c^n - \tau_{min}) \left(1 + \left(\frac{\tau_c^n}{\tau_c^n - \tau_{min}}\right) \frac{z_c^n}{\widetilde{z}_{qc}} v_{qc}\right). \tag{107}$$

This is nothing but what has been obtained in the one-dimensional case, equation (33). Same kind of relation can be derived for the condition $\overline{\tau}_{qc} < \tau_{max}$. Now, concerning $\overline{\varepsilon}_{qc} = \overline{e}_{qc} - \frac{1}{2}(\overline{\boldsymbol{u}}_{qc})^2$, let us first notice that $\overline{\boldsymbol{u}}_{qc} \neq \overline{\boldsymbol{u}}_q$. Indeed, $\overline{\boldsymbol{u}}_{qc}$ corresponds directly to one-dimensional Riemann solver at the control point q along the normal $\boldsymbol{n}_{qc}$, while $\overline{\boldsymbol{u}}_q$ would correspond to an high-dimensional extension of the one-dimensional solver. That being said, one can easily check that

$$\overline{\boldsymbol{u}}_{qc} = (\overline{\boldsymbol{u}}_q \cdot \boldsymbol{n}_{qc})\, \boldsymbol{n}_{qc} + (\boldsymbol{u}_c^n \cdot \boldsymbol{t}_{qc})\, \boldsymbol{t}_{qc}, \tag{108}$$

where $\boldsymbol{t}_{qc}$ identifies with the unit tangential vector of cell ω_c at control point q, orthogonal to $\boldsymbol{n}_{qc}$. Then, using (108), $\overline{\varepsilon}_{qc}$ can be rewritten as

$$\widehat{\overline{\varepsilon}}_{qc} - \varepsilon_{min} = (\widehat{\varepsilon}_c^n - \varepsilon_{min})\, A_{qc} + B_{qc}, \tag{109}$$

where the quantity A_{qc} writes

$$A_{qc} = 1 - \left(\frac{\widehat{\varepsilon}_c^n}{\widehat{\varepsilon}_c^n - \varepsilon_{min}}\right) \frac{\tau_c^n\, \widehat{p}_c^n}{\widehat{\varepsilon}_c^n} \frac{z_c^n}{\widetilde{z}_{qc}}\, v_{qc}, \tag{110}$$

recalling that $\widehat{p} = p + p_s$ for stiffened and $\widehat{p} = p$ otherwise, while B_{qc} is defined as follows

$$B_{qc} = \frac{1}{2}(a_c^n)^2\, v_{qc}^2. \tag{111}$$

Again, we have exactly recovered the one-dimensional expressions (34), (35) and (36). Then, to be able to apply the same analysis as the 1D case, let us define the modified Dukowicz wave speed $\widetilde{z}_{qc}$

$$\widetilde{z}_{qc} = z_c^n \left(1 + \widetilde{\Gamma} \left|v_{qc}\right|\right), \tag{112}$$

where in the case $\widetilde{\Gamma} = \Gamma$ one recovers the original Dukowicz solver, while for $\widetilde{\Gamma} = \sigma_v^{-1}$ one gets the positive modified version of it. Because the same one-dimensional analysis holds, we can state the following proposition.

Proposition 3.2. *Any scheme based on the one-dimensional two-states Riemann solver* (81) *with the particular wave speeds definition* (112)*, and which can be put into the generic form* (80) *ensures an admissible solution under the CFL condition* (102) *with* $\sigma_e \leq 1$ *and if*

$$\sigma_v \leq \min\left(1 - \frac{\tau_{min}}{\tau_c^n}, \frac{\tau_{max}}{\tau_c^n} - 1, (1 - \frac{\varepsilon_{min}}{\widehat{\varepsilon}_c^n})\,\frac{\rho_c^n\,\widehat{\varepsilon}_c^n}{\widehat{p}_c^n}\right).$$

Now, let us address the case of any positive wave speeds definition, $\widetilde{z}_{qc}$, which includes the particular case of the Godunov acoustic solver, but still ensuring the numerical solution admissibility.

3.4.2. Generic wave speeds

To make that possible, similarly to the one-dimensional case, we make use of an additional constraint on the time step permitting the control of the approximated cell volume variation, such as

$$\Big|\frac{\Delta V}{V}\Big| \equiv \frac{\big||\widetilde{\omega}_c^{n+1}| - |\widetilde{\omega}_c^n|\big|}{|\widetilde{\omega}_c^n|} < \sigma_v, \tag{113}$$

which reformulates into

$$\Delta t^n < \sigma_v\,\frac{|\widetilde{\omega}_c^n|}{\big|\sum\limits_{q\in\mathcal{Q}_c} \overline{\boldsymbol{u}}_q \cdot l_{qc}\boldsymbol{n}_{qc}\big|}. \tag{114}$$

Making use of system (80) and recalling that $\Delta V = \Delta t^n \sum_{q\in\mathcal{Q}_c} \overline{\boldsymbol{u}}_q \cdot l_{qc}\boldsymbol{n}_{qc}$, τ_c^{n+1} rewrites as

$$\tau_c^{n+1} - \tau_{min} = (\tau_c^n - \tau_{min})\,\left(1 - \frac{\Delta V}{V}\Big(\frac{\tau_c^n}{\tau_c^n - \tau_{min}}\Big)\right), \tag{115}$$

which is perfectly equivalent to relation (39) obtained in the one-dimensional case. Now, regarding the condition $\widehat{\varepsilon}_c^{n+1} > \varepsilon_{min}$, by means of the first-order scheme (80) and basic manipulations, $\widehat{\varepsilon}_c^{n+1}$ can again be split into two terms

$$\widehat{\varepsilon}_c^{n+1} - \varepsilon_{min} = (\widehat{\varepsilon}_c^n - \varepsilon_{min})\,A_c + B_c, \tag{116}$$

where the quantity A_c reads

$$A_c = 1 - \frac{\Delta V}{V}\left(\frac{\widehat{\varepsilon}_c^n}{\widehat{\varepsilon}_c^n - \varepsilon_{min}}\right)\frac{\tau_c^n\,\widehat{p}_c^n}{\widehat{\varepsilon}_c^n}, \tag{117}$$

while B_c is defined as

$$B_c = \frac{\Delta t^n}{m_c}\Big[\sum_{q\in\mathcal{Q}_c} \widetilde{z}_{qc}\,l_{qc}\,w_{qc}^2 - \frac{\Delta t^n}{2\,m_c}\Big(\sum_{q\in\mathcal{Q}_c} \widetilde{z}_{qc}\,l_{qc}\,w_{qc}\,\boldsymbol{n}_{qc}\Big)^2\Big], \tag{118}$$

with $w_{qc} = (\overline{\boldsymbol{u}}_q - \boldsymbol{u}_c^n)\cdot\boldsymbol{n}_{qc}$. Then, if we manage to prove that $B_c \geq 0$, it is then sufficient to ensure $A_c > 0$. Let us first rewrite B_c into a matrix-vector form as

$$B_c = \frac{\Delta t^n}{m_c}\,\mathsf{M}_c\,\mathsf{W}\cdot\mathsf{W}, \tag{119}$$

where $\mathsf{W} = (w_{1c}, \dots, w_{qc}, \dots, w_{N_c c})^{\mathrm{t}}$, with $N_c = |Q_c|$ the number of elements contained in Q_c, and where the generic coefficient $\mathsf{M}_c^{q\,r}$ of matrix M_c reads

$$\mathsf{M}_c^{q\,r} = \frac{\Delta t^n}{m_c} \begin{cases} \widetilde{z}_{qc}\, l_{qc}\,(1 - \dfrac{\Delta t^n}{2\,m_c}\widetilde{z}_{qc}\, l_{qc}), & \text{if } q = r, \\ -\dfrac{\Delta t^n}{2\,m_c}\widetilde{z}_{qc}\,\widetilde{z}_{rc}\, l_{qc}\, l_{rc}\,(\boldsymbol{n}_{qc}\,.\,\boldsymbol{n}_{rc}), & \text{if } q \neq r. \end{cases} \tag{120}$$

Let us recall that if M_c is symmetric diagonally dominant with non-negative diagonal entries then M_c is positive semi-definite, see [40] for instance. The matrix M_c yields non-negative diagonal entries if and only if $\Delta t^n < \frac{2\,m_c}{\widetilde{z}_{qc}\, l_{qc}}$, for any $q \in \mathcal{Q}_c$. Now, for the diagonally dominant criterion, it can be proved matrix M_c exhibits such property if and only if

$$\Delta t^n \leq \frac{2\,m_c}{\displaystyle\sum_{r \in \mathcal{Q}_c} \widetilde{z}_{rc}\, l_{rc}\, |(\boldsymbol{n}_{qc}\,.\,\boldsymbol{n}_{rc})|},$$

for any $q \in \mathcal{Q}_c$, which is always more constraining than the previous condition. Finally, to end up with only one condition per cell, and acknowledging that $|(\boldsymbol{n}_{qc}\,.\,\boldsymbol{n}_{rc})| \leq 1$, let us emphasize both conditions, M_c is with non-negative diagonal entries and symmetric diagonally dominant, are ensured under the sufficient condition

$$\Delta t^n \leq 2\,\frac{m_c}{\sum_q \widetilde{z}_{qc}\, l_{qc}}.$$

This condition is nothing but the CFL condition (102) with a CFL coefficient $\sigma_e = 2$. Let us note that, similarly to the 1D case, B_c corresponds to the approximation of the time discrete counterpart of the semi-discrete entropy production $T_c \frac{\mathrm{d}\, S_c}{\mathrm{d}t} \geq 0$ of equation (85), B_c rewriting as $B_c = \varepsilon_c^{n+1} - \varepsilon_c^n - p_c^n \left(\tau_c^{n+1} - \tau_c^n\right)$. As before, to have $B_c \geq 0$ will not ensure the scheme to produce entropy at the discrete level. However, it will help us in ensuring the internal energy positivity. Furthermore, considering a positive solution at all time, it is still possible to prove there exists a time step Δt^n small enough to ensure a discrete entropy production, see [21] for details of the proof.

Finally, noticing expression (115) is perfectly consistent with the 1D relation (39), as well as equation (117) with (41), the same analysis holds and is emphasized in the following proposition.

Proposition 3.3. *Any scheme based on the one-dimensional two-states Riemann solver* (81) *for any positive wave speeds definition, and which can be put into the generic form* (80) *ensures an admissible solution under the CFL condition* (102) *with* $\sigma_e \leq 2$ *and the volume variation constraint* (114) *with*

$$\sigma_v \leq \min\left(1 - \frac{\tau_{min}}{\tau_c^n}, \frac{\tau_{max}}{\tau_c^n} - 1, (1 - \frac{\varepsilon_{min}}{\widehat{\varepsilon}_c^n})\,\frac{\rho_c^n\,\widehat{\varepsilon}_c^n}{\widehat{p}_c^n}\right).$$

This proposition holds for any positive wavespeed definition $\widetilde{z}_{qc} > 0$, and thus for the particular case of the Godunov acoustic solver.

Summary. Let us summarize the main features of this work presented so far in the two-dimensional case. The problem is to determine conditions for the generic first-order Lagrangian scheme

$$\mathsf{U}_c^{n+1} = \mathsf{U}_c^n - \frac{\Delta t^n}{m_c} \sum_{q \in \mathcal{Q}_c} \overline{\mathsf{F}}_{qc}\,.\,l_{qc}\boldsymbol{n}_{qc},$$

where $\overline{\mathsf{F}}_{qc} = (-\overline{\boldsymbol{u}}_q,\, \mathbb{1}(1)\,\overline{p}_{qc},\, \mathbb{1}(2)\,\overline{p}_{qc},\, \overline{p}_{qc}\,\overline{\boldsymbol{u}}_q)^{\mathrm{t}}$ stands for the grid control point numerical flux and is solution of the 1D two-states Riemann solver

$$\overline{p}_{qc} = p_c^n - \widetilde{z}_{qc}\,(\overline{\boldsymbol{u}}_q - \boldsymbol{u}_c^n)\,\boldsymbol{.}\,\boldsymbol{n}_{qc},$$

to ensure numerical solutions in the admissible set

$$G = \left\{ \mathsf{U} = (\tau,\, \boldsymbol{u},\, e)^{\mathrm{t}}, \quad \tau \in \,]\tau_{min}, \tau_{max}[\;\text{ and }\; \widehat{\varepsilon}(\mathsf{U}) > \varepsilon_{min} \right\}.$$

To that end, two different techniques are employed. The first one relies on a particular definition of the wavespeeds $\widetilde{z}_{qc}$ depending on $\overline{\boldsymbol{u}}_q$, such that

$$\widetilde{z}_{qc} = \rho_c^n \,\left(a_c^n + \sigma_v^{-1} \left| (\overline{\boldsymbol{u}}_q - \boldsymbol{u}_c^n)\,\boldsymbol{.}\,\boldsymbol{n}_{qc} \right| \right).$$

Then, a sufficient condition to ensure the numerical solution admissibility is the use of a constant $\sigma_v \leq \min\left(1 - \frac{\tau_{min}}{\tau_c^n}, \frac{\tau_{max}}{\tau_c^n} - 1, (1 - \frac{\varepsilon_{min}}{\widehat{\varepsilon}_c^n})\,\frac{\rho_c^n\,\widehat{\varepsilon}_c^n}{\widehat{p}_c^n}\right)$, and the following CFL condition with $\sigma_e \leq 1$

$$\Delta t^n \leq \sigma_e\, \frac{m_c}{\displaystyle\sum_{q \in \mathcal{Q}_c} \widetilde{z}_{qc}\, l_{qc}}.$$

The second technique relaxes this particular definition of the wavespeeds. To that end, in addition to the previous CFL condition with $\sigma_e \leq 2$, we make use of a supplementary time step constraint relative to the volume variation as follows

$$\Delta t^n < \sigma_v\, \frac{|\widetilde{\omega}_c^n|}{\left| \displaystyle\sum_{q \in \mathcal{Q}_c} \overline{\boldsymbol{u}}_q\,\boldsymbol{.}\,l_{qc}\boldsymbol{n}_{qc} \right|},$$

where $|\widetilde{\omega}_c^n| = m_c\,\tau_c^n$. Finally, if $\sigma_v \leq \min\left(1 - \frac{\tau_{min}}{\tau_c^n}, \frac{\tau_{max}}{\tau_c^n} - 1, (1 - \frac{\varepsilon_{min}}{\widehat{\varepsilon}_c^n})\,\frac{\rho_c^n\,\widehat{\varepsilon}_c^n}{\widehat{p}_c^n}\right)$, the scheme is ensured to produce solutions in G. These two techniques involve a constant σ_v which has proved to be the same.

Finally, as we did for one dimension in space, we can compare the new time step constraint (114) with the CFL condition (102) in the case of the Dukowicz solver. By means of $\widetilde{z}_{qc}$ definition (112), one can write

$$\begin{aligned}
\sum_{q \in \mathcal{Q}_c} \widetilde{z}_{qc}\, l_{qc} &> \sum_{q \in \mathcal{Q}_c} \rho_c^n\, \widetilde{\Gamma}\, |(\overline{\boldsymbol{u}}_q - \boldsymbol{u}_c^n)\,\boldsymbol{.}\,l_{qc}\boldsymbol{n}_{qc}|, \\
&> \frac{m_c}{\sigma_v\, |\widetilde{\omega}_c^n|} \left| \sum_{q \in \mathcal{Q}_c} \overline{\boldsymbol{u}}_q\,\boldsymbol{.}\,l_{qc}\boldsymbol{n}_{qc} \right|.
\end{aligned}$$

And thanks to this last relation, one can state that

$$\frac{m_c}{\displaystyle\sum_{q \in \mathcal{Q}_c} \widetilde{z}_{qc}\, l_{qc}} < \sigma_v\, \frac{|\widetilde{\omega}_c^n|}{\left| \displaystyle\sum_{q \in \mathcal{Q}_c} \overline{\boldsymbol{u}}_q\,\boldsymbol{.}\,l_{qc}\boldsymbol{n}_{qc} \right|}. \tag{121}$$

This second method seems again optimal in term of simplicity and time step, the CFL number σ_e being twice bigger and the new time step condition (114) being always less constraining than the CFL condition in the Dukowicz or modified Dukowicz solver.

We have seen in the one-dimensional case that the high-order extension of the positivity-preserving proof relies directly on the work of Zhang and Shu, [75, 78]. However, in the 2D case, it is no longer possible to apply in a straightforward manner the simple 1D technique, the two-dimensional schemes presented relying on multi-dimensional Riemann solvers used at some control points of the generic polygonal, possibly curved, cells considered. The proof will yet be based on the decomposition of the high-order scheme into a convex combination of first-order schemes.

3.5. High-order schemes

A wide number of different methods can be used to extend the generic first-order formulation (80) to higher-order accuracy. The only fundamental assumption is the high-order scheme must satisfy the same equation (80) on the mass averaged values. However, in the definition of the numerical flux $\overline{\mathsf{F}}_{qc}$ through the Riemann solver (81) as well as the respecting definitions of the control point velocity $\overline{\boldsymbol{u}}_q$, (87), (89), (94), (97) and (98), the mass average U_c^n will be substituted by $\mathsf{U}_{qc} = \mathsf{U}_{h,c}^n(\boldsymbol{x}_q)$, the high-order value at point $\boldsymbol{x}_q$ within the cells ω_c, such that

$$\overline{p}_{qc} = p_{qc} - \widetilde{z}_{qc}\,(\overline{\boldsymbol{u}}_q - \boldsymbol{u}_{qc})\,.\,\boldsymbol{n}_{qc}. \tag{122}$$

Working on the inital configuration, as it is the case in a total Lagrangian formulation, the polynomial $\mathsf{U}_{h,c}^n(\boldsymbol{X})$ is defined on cell Ω_c, and $\mathsf{U}_{qc} = \mathsf{U}_{h,c}^n(\boldsymbol{X}_q)$. As before, for sake of conciseness, when not specified, $\boldsymbol{x}$ should be replaced by $\boldsymbol{X}$ in a total Lagrangian frame, as well as ω by Ω. In both updated and total Lagrangian frames, these polynomials can either be reconstructed from the cell averages of neighboring cells in a finite volume method or evolved in a DG method. To that end, as introduced in the 1D case, one can decide to perform the polynomial reconstruction of the flux variables, as it is done in [12, 56]. We recall that in this case, the specific volume and total energy remain constant inside the cells, namely $\tau_{h,c}^n(x) = \tau_c^n$ and $e_{h,c}^n(x) = e_c^n$. Because the polynomial reconstruction is performed on the flux variables, and because one only knows the cell averages of the conserved variables, this method is limited to second-order accuracy. To avoid any accuracy discrepancy, one can apply the polynomial reconstruction on the conserved variables. In this case, the pressure is defined pointwisely through the use of the EOS as $p_{h,c}^n(\boldsymbol{x}) = p(\mathsf{U}_{h,c}^n(\boldsymbol{x}))$. In [15], the authors made use of a second-order ENO method to perform the slope reconstruction, while in [16] a WENO discretization has been used. Obviously, higher order reconstructions may be considered, see for instance [13, 14, 49] for third-order ENO discretizations. Finally, one can also opt for a discontinuous Galerkin discretization. We have previously used such discretization in the total Lagrangian frame to develop generic high-order methods, referred as LCCDG schemes, see [72]. As mentioned before, the first-order version of this scheme is perfectly compatible between the actual and initial configurations. Nonetheless, in the high-order versions, the computation is only performed on the fixed referential configuration, which is assumed to yield straight line edges, even if its image through the fluid flow will admit curved edges, as in Figure 4(c). In this case, the system variables are approximated through polynomial basis functions, for which the corresponding moments are evolved through governing equations. The pressure is then defined pointwisely through the use of the equation of state.

As before, we now introduce relations between the high-order polynomial approximation and the averaged value, which for high-order finite volume schemes on the moving configuration, such as those presented in [12, 56, 13], write

$$\mathsf{U}_c^n = \frac{1}{|\omega_c|} \int_{\omega_c} \mathsf{U}_{h,c}^n(\boldsymbol{x}) \, \mathrm{d}v. \tag{123}$$

For the total Lagrangian DG methods introduced in [70, 72], this relation writes

$$\mathsf{U}_c^n = \frac{1}{m_c} \int_{\Omega_c} \rho^0(\boldsymbol{X}) \, \mathsf{U}_{h,c}^n(\boldsymbol{X}) \, \mathrm{d}V. \tag{124}$$

These relations will help us to extend the positivity-preserving proof to the high-orders of accuracy. This proof relies on the fundamental assumption that there exists a two-dimensional quadrature rule on straight line edged polygonal cell, Figure 4(a), exact for polynomial up to degree K for high-order finite volume schemes on moving cell, and $2K$ for the DG methods on the initial configuration, such that

$$\int_{\omega_c} \phi(\boldsymbol{x}) \, \mathrm{d}v = |\omega_c| \sum_{\alpha \in \Theta_c} w_\alpha \, \phi(\boldsymbol{x}_\alpha), \tag{125}$$

where $\{(w_\alpha, y_\alpha)\}_{\alpha \in \Theta_c}$ are the positive quadrature weights and quadrature points, including the cell control point set, *i.e.* $\mathcal{Q}_c \subset \Theta_c$. If no such quadrature is provided by the literature, one can always break down the polygonal cells into triangles, and then build the quadrature rule by gathering those on the triangle elements. The triangle quadrature rules developed in [78], deriving from a projection of quadrangle quadrature rules onto triangles, can be used as a starting point. Now, through the use of (125), for the different discretizations presented, the following relation holds

$$\mathsf{U}_c^n = \frac{1}{m_c} \sum_{\alpha \in \Theta_c} m_{\alpha c} \, \mathsf{U}_{\alpha c}, \tag{126}$$

where, for finite volume schemes on moving cell, $m_{\alpha c} = w_\alpha \, m_c$ and $\mathsf{U}_{\alpha c} = \mathsf{U}_{h,c}^n(\boldsymbol{x}_\alpha)$, while for the DG scheme on initial cell, $m_{\alpha c} = w_\alpha \, \rho^0(\boldsymbol{X}_\alpha) \, |\Omega_c|$ and $\mathsf{U}_{\alpha c} = \mathsf{U}_{h,c}^n(\boldsymbol{X}_\alpha)$. This last expression immediately rewrites

$$\mathsf{U}_c^n = \frac{1}{m_c} \sum_{\alpha \in \Theta_c \setminus \mathcal{Q}_c} m_{\alpha c} \, \mathsf{U}_{\alpha c} + \frac{1}{m_c} \sum_{q \in \mathcal{Q}_c} m_{qc} \, \mathsf{U}_{qc} = \frac{m_c^\star}{m_c} \, \mathsf{U}_c^\star + \frac{1}{m_c} \sum_{q \in \mathcal{Q}_c} m_{qc} \, \mathsf{U}_{qc}, \tag{127}$$

where $m_c^\star = \sum_{\alpha \in \Theta_c \setminus \mathcal{Q}_c} m_{\alpha c}$ and $\mathsf{U}_c^\star = \frac{1}{m_c^\star} \sum_{\alpha \in \Theta_c \setminus \mathcal{Q}_c} m_{\alpha c} \, \mathsf{U}_{\alpha c}$. Now, similarly to what has been done in the 1D case, we make use of U_c^n decomposition (127), as well as adding some artificial fluxes $\mathfrak{F}_{qc} = (-\mathfrak{u}_c, \, \mathbb{1}(1) \, \mathfrak{p}_{qc}, \, \mathbb{1}(2) \, \mathfrak{p}_{qc}, \, \mathfrak{p}_{qc} \, \mathfrak{u}_c)^{\mathrm{t}}$, that sum to zero, to the high-order scheme (80)

$$\mathsf{U}_c^{n+1} = \mathsf{U}_c^n - \frac{\Delta t^n}{m_c} \sum_{q \in \mathcal{Q}_c} \overline{\mathsf{F}}_{qc} \cdot l_{qc} \boldsymbol{n}_{qc} + \frac{\Delta t^n}{m_c} \sum_{q \in \mathcal{Q}_c} \mathfrak{F}_{qc} \cdot l_{qc} \boldsymbol{n}_{qc}, \tag{128}$$

under the assumption that

$$\sum_{r \in \mathcal{Q}_c} \mathfrak{F}_{rc} \cdot l_{rc} \boldsymbol{n}_{rc} = 0, \tag{129}$$

which is perfectly equivalent to

$$\sum_{r\in\mathcal{Q}_c\setminus q} \mathfrak{F}_{rc}\cdot l_{rc}\boldsymbol{n}_{rc} = -\mathfrak{F}_{qc}\cdot l_{qc}\boldsymbol{n}_{qc}. \tag{130}$$

It is easy to show equation (128) reformulates as

$$\mathsf{U}_c^{n+1} = \frac{m_c^\star}{m_c}\,\mathsf{U}_c^\star + \sum_{q\in\mathcal{Q}_c}\frac{m_{qc}}{m_c}\,\mathsf{V}_{qc}, \tag{131}$$

where the V_{qc} can be expressed as follows

$$\mathsf{V}_{qc} = \mathsf{U}_{qc} - \frac{\Delta t^n}{m_{qc}}\,\big(\overline{\mathsf{F}}_{qc} - \mathfrak{F}_{qc}\big)\cdot l_{qc}\boldsymbol{n}_{qc}. \tag{132}$$

V_{qc} defined in (132) does not yet identify with the first-order scheme (80). To that purpose, let us introduce $\overline{\mathfrak{F}}_r^q$ such that, $\forall r\in\mathcal{Q}_c$

$$\overline{\mathfrak{F}}_r^q = \begin{cases} \overline{\mathsf{F}}_{qc}, & \text{if } r = q,\\ \mathfrak{F}_{rc}, & \text{otherwise,}\end{cases} \tag{133}$$

where $\overline{\mathfrak{F}}_r^q = (-\overline{\mathfrak{u}}_r^q,\ \mathbb{1}(1)\,\overline{\mathfrak{p}}_r^q,\ \mathbb{1}(2)\,\overline{\mathfrak{p}}_r^q,\ \overline{\mathfrak{p}}_r^q\,\overline{\mathfrak{u}}_r^q)^{\mathrm{t}}$. In light of (130), definition (132) finally reads

$$\mathsf{V}_{qc} = \mathsf{U}_{qc} - \frac{\Delta t^n}{m_{qc}}\sum_{r\in\mathcal{Q}_c}\overline{\mathfrak{F}}_r^q\cdot l_{rc}\boldsymbol{n}_{rc}. \tag{134}$$

The artificial fluxes $\mathfrak{F}_{rc}$ will be built to ensure that this last expression perfectly mimics the first-order scheme (80). Substituting in the first-order Riemann solver (81), located at the control point $r\in\mathcal{Q}_c$, the mean value U_c^n with the high-order value U_{qc}, and the numerical flux with the artificial flux tells us that

$$\begin{aligned}\sum_{r\in\mathcal{Q}_c}\overline{\mathfrak{p}}_r^q\,l_{rc}\boldsymbol{n}_{rc} &= \sum_{r\in\mathcal{Q}_c}\big(p_{qc} - \widetilde{z}_{rc}^q\,(\overline{\mathfrak{u}}_r^q - \boldsymbol{u}_{qc})\cdot\boldsymbol{n}_{rc}\big)\,l_{rc}\boldsymbol{n}_{rc},\\ &= p_{qc}\sum_{r\in\mathcal{Q}_c} l_{rc}\boldsymbol{n}_{rc} - \sum_{r\in\mathcal{Q}_c}\widetilde{z}_{rc}^q\,l_{rc}\,(\boldsymbol{n}_{rc}\otimes\boldsymbol{n}_{rc})\,(\overline{\mathfrak{u}}_r^q - \boldsymbol{u}_{qc}),\\ &= -\sum_{r\in\mathcal{Q}_c}\mathsf{M}_{rc}^q\,(\overline{\mathfrak{u}}_r^q - \boldsymbol{u}_{qc}),\end{aligned}$$

where $\mathsf{M}_{rc}^q = \widetilde{z}_{rc}^q\,l_{rc}\,(\boldsymbol{n}_{rc}\otimes\boldsymbol{n}_{rc})$, and $\widetilde{z}_{rc}^q$ may depend on $\overline{\mathfrak{u}}_r^q$ as in a Dukowicz-like solver. By means of (130), this last relation rewrites

$$\begin{aligned}(\overline{p}_{qc} - \mathfrak{p}_{qc})\,l_{qc}\boldsymbol{n}_{qc} &= -\mathsf{M}_{qc}^q\,(\overline{\boldsymbol{u}}_q - \boldsymbol{u}_{qc}) - \big(\sum_{r\in\mathcal{Q}_c\setminus q}\mathsf{M}_{rc}^q\big)\,(\mathfrak{u}_c - \boldsymbol{u}_{qc}),\\ &= -\mathsf{M}_{qc}^q\,(\overline{\boldsymbol{u}}_q - \boldsymbol{u}_{qc}) - \mathsf{M}_c^q\,(\mathfrak{u}_c - \boldsymbol{u}_{qc}),\end{aligned}$$

where $\mathsf{M}_c^q = \sum_{r\setminus q}\mathsf{M}_{rc}^q$. And finally, by means of the high-order Riemann solver relation (122), we are able to define the artificial pressure $\mathfrak{p}_{qc}$ as

$$\mathfrak{p}_{qc}\,l_{qc}\boldsymbol{n}_{qc} = p_{qc}\,l_{qc}\boldsymbol{n}_{qc} + \mathsf{M}_c^q\,(\mathfrak{u}_c - \boldsymbol{u}_{qc}). \tag{135}$$

In the end, condition (129) will give us the explicit definition of the artificial velocity $\mathfrak{u}_c$

$$\mathfrak{u}_c = \Big(\sum_{q \in \mathcal{Q}_c} \mathsf{M}_c^q \Big)^{-1} \sum_{q \in \mathcal{Q}_c} \Big[\mathsf{M}_c^q \, \boldsymbol{u}_{qc} - p_{qc} \, l_{qc} \boldsymbol{n}_{qc} \Big]. \tag{136}$$

The artificial flux $\mathfrak{F}_{qc}$ which has been added to the high-order scheme (80) is now fully determined, and has allowed us to decompose U_c^{n+1} as a convex combination (131). One can thus state that to have $\mathsf{U}_c^\star$ and $\forall q \in \mathcal{Q}_c, \mathsf{V}_{qc}$ in the convex admissible set G implies to have the updated numerical solution in average U_c^{n+1} in G. Furthermore, in the light of relation (134) as well as the particular definitions of the artificial pressure and velocity, (135) and (136), V_{qc} identifies perfectly with the first-order scheme (80). Consequently, we can apply the exact same techniques as those presented in the first-order case to ensure $\mathsf{V}_{qc} \in G$.

3.6. High-order positivity-preserving schemes

In this subsection, we focus on the conditions to enforce $\mathsf{V}_{qc} \in G$. Similar to the first-order case, one may choose to use particular non-linear definitions of the local acoustic impedances, or simply an additional time step constraint.

3.6.1. Modified Dukowicz solver

The high-order extension of the modified Dukowicz definitions of $\widetilde{z}_{qc}$, introduced in (112), can be expressed as follows

$$\widetilde{z}_{qc} = \rho_{qc} \left(a_{qc} + \widetilde{\Gamma} \left| (\overline{\boldsymbol{u}}_q - \boldsymbol{u}_{qc}) \cdot \boldsymbol{n}_{qc} \right| \right), \tag{137}$$

where ρ_{qc}, a_{qc} and $\boldsymbol{u}_{qc}$ are the high-order values of the density, sound speed and fluid velocity at node $\boldsymbol{x}_{qc}$ within cell ω_c, respectively $\boldsymbol{X}_{qc}$ in Ω_c in a total Lagrangian frame. In the case where $\widetilde{\Gamma} = \Gamma$, one recovers the high-order extension of the Dukowicz solver, while for $\widetilde{\Gamma} = \sigma_v^{-1}$, equation (137) reads as the extension of the modified one. Given (134) where the artificial numerical flux $\overline{\mathfrak{F}}_r^q$ has been introduced, we also need to define the local wave speeds relative to this term, $\widetilde{z}_{rc}^q$, as

$$\widetilde{z}_{rc}^q = \rho_{qc} \left(a_{qc} + \widetilde{\Gamma} \left| (\mathfrak{u}_c - \boldsymbol{u}_{qc}) \cdot \boldsymbol{n}_{rc} \right| \right), \tag{138}$$

for $r \neq q$, while for $r = q$, $\widetilde{z}_{qc}^q$ is defined through (137). Each element of equations (134) having been defined explicitly, one may now apply in a straightforward manner the analysis performed on the first-order scheme. Furthermore, remark 2.6 made in the one-dimensional case still holds in this 2D case.

Proposition 3.4. *For any high-order discretization presented earlier, assuming* $\forall q \in \mathcal{Q}_c$, $\mathsf{U}_{qc} \in G$ *and* $\mathsf{U}_c^\star \in G$, *the averaged value* U_c^{n+1} *is ensured to be admissible provided the numerical fluxes* (122) *and the particular wave speeds definition* (138) *with* $\widetilde{\Gamma} = \sigma_v^{-1}$ *under the time step limitation*

$$\Delta t \leq \sigma_e \, \frac{m_{qc}}{\displaystyle\sum_{r \in \mathcal{Q}_c} \widetilde{z}_{rc}^q \, l_{rc}},$$

for all $q \in \mathcal{Q}_c$, *and with* $\sigma_e \leq 1$, *as well as*

$$\sigma_v \leq \min \left(1 - \frac{\tau_{min}}{\tau_{qc}}, \frac{\tau_{max}}{\tau_{qc}} - 1, (1 - \frac{\varepsilon_{min}}{\widehat{\varepsilon_{qc}}}) \, \frac{\rho_{qc} \, \widehat{\varepsilon_{qc}}}{|\widehat{p}_{qc}|} \right).$$

Now, if one rather wants to use a simpler solver as the acoustic Godunov one, or any specific definitions of wave speeds as for example $\widetilde{z}_{qc} = \rho_c^n \left(a_c^n + \Gamma \left|(\overline{\boldsymbol{u}}_q - \boldsymbol{u}_{qc}) \cdot \boldsymbol{n}_{qc}\right|\right)$, which is generally used in the high-order extension of the Dukowicz solver, one needs to add additional constraints on Δt^n.

3.6.2. Generic wave speeds

In this case, the choice in $\widetilde{z}_{qc} > 0$ is free. Thus, one can either use z_c^n or $\rho_c^n \left(a_c^n + \widetilde{\Gamma} \left|(\overline{\boldsymbol{u}}_q - \boldsymbol{u}_{qc}) \cdot \boldsymbol{n}_{qc}\right|\right)$ or even $\rho_{qc} \left(a_{qc} + \widetilde{\Gamma} \left|(\overline{\boldsymbol{u}}_q - \boldsymbol{u}_{qc}) \cdot \boldsymbol{n}_{qc}\right|\right)$ for any $\widetilde{\Gamma}$, or any other definition. The artificial wave speeds $\widetilde{z}_{rc}^q$ have to be chosen consistently. Similarly to the first-order case, one can state

Proposition 3.5. *For any high-order discretization presented earlier, assuming $\forall q \in \mathcal{Q}_c$, $\mathsf{U}_{qc} \in G$ and $\mathsf{U}_c^\star \in G$, the averaged value U_c^{n+1} is ensured to be admissible provided the numerical fluxes* (122) *for any positive wave speed definition $\widetilde{z}_{qc}$ under the following time step limitations*

$$\Delta t \leq \sigma_e \, \frac{m_{qc}}{\displaystyle\sum_{r \in \mathcal{Q}_c} \widetilde{z}_{rc}^q \, l_{rc}},$$

for all $q \in \mathcal{Q}_c$, and $\sigma_e \leq 2$, as well as

$$\Delta t \leq \sigma_v \, \frac{\tau_{qc} \, m_{qc}}{\Big| \displaystyle\sum_{r \in \mathcal{Q}_c} \overline{\mathfrak{u}}_r^q \cdot l_{rc} \boldsymbol{n}_{rc} \Big|} = \sigma_v \, \frac{\tau_{qc} \, m_{qc}}{\big|(\overline{\boldsymbol{u}}_q - \mathfrak{u}_c) \cdot l_{qc} \boldsymbol{n}_{qc}\big|},$$

for all $q \in \mathcal{Q}_c$, where σ_v has to be such that

$$\sigma_v \leq \min \left(1 - \frac{\tau_{min}}{\tau_{qc}}, \frac{\tau_{max}}{\tau_{qc}} - 1, (1 - \frac{\varepsilon_{min}}{\widehat{\varepsilon_{qc}}}) \, \frac{\rho_{qc} \, \widehat{\varepsilon_{qc}}}{|\widehat{p}_{qc}|} \right).$$

The same remark claiming that the second technique is optimal in term of time step still holds in this high-order case. Indeed, in the modified Dukowicz solver case, thanks to definitions (137) and (138), it is quite simple to prove that, $\forall q \in \mathcal{Q}_c$

$$\frac{m_{qc}}{\displaystyle\sum_{r \in \mathcal{Q}_c} \widetilde{z}_{rc}^q \, l_{rc}} < \sigma_v \, \frac{\tau_{qc} \, m_{qc}}{\Big| \displaystyle\sum_{r \in \mathcal{Q}_c} \overline{\mathfrak{u}}_r^q \cdot l_{rc} \boldsymbol{n}_{rc} \Big|}. \tag{139}$$

So far, we have proved that assuming $\forall q \in \mathcal{Q}_c$, U_{qc} and $\mathsf{U}_c^\star$ lie in the admissible set, there exist a time step ensuring the new numerical solution to be admissible in averaged value. To ensure the required assumptions, we make use of the same kind of limitation introduced in the 1D case.

3.7. Positivity-preserving limiter

In the remainder, $\boldsymbol{x}$ should be replaced by $\boldsymbol{X}$ in a total Lagrangian frame. At time level n, the averaged value U_c^n is assumed to be in G. Then, we modify the polynomial reconstruction $\mathsf{U}_{h,c}^n$ to ensure the desired properties, as follows

$$\widetilde{\mathsf{U}_{h,c}^n}(\boldsymbol{x}) = \mathsf{U}_c^n + \theta \, (\mathsf{U}_{h,c}^n(\boldsymbol{x}) - \mathsf{U}_c^n), \tag{140}$$

where $\theta \in [0,1]$ is to be determined. The property to be ensured is to yield $\forall q \in \mathcal{Q}_c,\ \widetilde{\mathsf{U}}_{qc} \equiv \widetilde{\mathsf{U}^n_{h,c}}(\boldsymbol{x}_{qc})$ and $\widetilde{\mathsf{U}}^\star_c \equiv \frac{1}{m^\star_c}\sum_{\alpha\in\Theta_c\setminus\mathcal{Q}_c} m_{\alpha c}\,\widetilde{\mathsf{U}^n_{h,c}}(\boldsymbol{x}_\alpha)$ in the admissible set G. To that end, we first enforce the admissibility of the specific volume as follows

$$\widetilde{\tau^n_{h,c}}(\boldsymbol{x}) = \tau^n_c + \theta_\tau\,(\tau^n_{h,c} - \tau^n_c), \tag{141}$$

where the coefficient $\theta_\tau = \min(\theta^{min}_\tau, \theta^{max}_\tau)$ is computed such that

$$\theta^{min}_\tau = \min\left(1, \frac{\tau^n_c - \tau_{min}}{\tau^n_c - \tau^{min}_m}\right) \quad \text{with} \quad \tau^{min}_m = \min(\tau^\star_c, \min_{q\in\mathcal{Q}_c}\tau_{qc}),$$
$$\theta^{max}_\tau = \min\left(1, \frac{\tau_{max} - \tau^n_c}{\tau^{max}_m - \tau^n_c}\right) \quad \text{with} \quad \tau^{max}_m = \max(\tau^\star_c, \max_{q\in\mathcal{Q}_c}\tau_{qc}).$$

Then, for the positivity of the internal energy, the limited polynomial reconstructions of the velocity and total energy are computed through

$$\widetilde{\boldsymbol{u}^n_{h,c}}(\boldsymbol{x}) = \boldsymbol{u}^n_c + \theta_\varepsilon\,(\boldsymbol{u}^n_{h,c} - \boldsymbol{u}^n_c), \tag{142}$$
$$\widetilde{e^n_{h,c}}(\boldsymbol{x}) = e^n_c + \theta_\varepsilon\,(e^n_{h,c} - e^n_c), \tag{143}$$

where θ_ε is evaluated in an optimal manner to ensure the required properties. For more details concerning the procedure to get an optimal θ_ε, see the related one-dimensional section 2.9.

3.8. positivity-preserving stability

Let us extend to the two-dimensional case what has been introduced in Section 2.10, namely the piecewise polynomial numerical solution $\mathsf{U}_h(\boldsymbol{x},t)$ defined on $\omega\times[0,T]$ such that

$$\mathsf{U}_h(\boldsymbol{x},t) = \mathsf{U}^n_{h,c}(\boldsymbol{x}), \quad \text{for } \boldsymbol{x}\in\omega_c \text{ and } t\in[t^n, t^{n+1}[, \tag{144}$$

the numerical variables initialization

$$\mathsf{U}^0_c = \frac{1}{m_c}\int_{\Omega_c}\rho^0(\boldsymbol{X})\,U^0(\boldsymbol{X})\,\mathrm{d}V, \tag{145}$$

and the L_1 and L_2 norms as follows

$$\|\phi\|_{L_1} = \frac{m_c}{|\omega_c|}\int_{\omega_c}|\phi(\boldsymbol{x})|\,\mathrm{d}v \quad \text{and} \quad \|\phi\|_{L_2} = \left(\frac{m_c}{|\omega_c|}\int_{\omega_c}(\phi(\boldsymbol{x}))^2\,\mathrm{d}v\right)^{\frac{1}{2}}. \tag{146}$$

In the total Lagrangian frame, definition (144) holds by substituting $\boldsymbol{x}$ by $\boldsymbol{X}$, and ω by Ω, and the L_1 and L_2 norms then write

$$\|\phi\|_{L_1} = \int_{\Omega_c}\rho^0(\boldsymbol{X})\,|\phi(\boldsymbol{X})|\,\mathrm{d}V \quad \text{and} \quad \|\phi\|_{L_2} = \left(\int_{\Omega_c}\rho^0(\boldsymbol{X})\,(\phi(\boldsymbol{X}))^2\,\mathrm{d}V\right)^{\frac{1}{2}}. \tag{147}$$

Here, the polynomials τ_h and $\varepsilon_h = e_h - \frac{1}{2}(\boldsymbol{u}_h)^2$ are assumed to be positive everywhere, which is always feasible by limiting enough. Then, in the no external contribution case (82), one can state

$$\|\tau_h\|_{L_1} = \|\frac{1}{\rho^0}\|_{L_1} \quad \text{and} \quad \|e_h\|_{L_1} = \|e^0\|_{L_1}, \tag{148}$$
$$\|K_h\|_{L_1} < \|e_h\|_{L_1} \quad \text{and} \quad \|\boldsymbol{u}_h\|^2_{L_2} < m_\omega + \|e_h\|^2_{L_2}, \tag{149}$$

where $K = \frac{1}{2}\boldsymbol{u}^2$ and m_ω correspond to the kinetic energy and the total mass of domain ω.

Although only the case of first-order time integration has been tackled for two dimensions in space, the considerations related to the high-order time extension remaining similar to the 1D case, we refer to Section 2.11. We just recall that, even if particular time step restrictions have been defined through propositions 3.4 and 3.5, for practical application the iterative procedure introduced in Section 2.11 to select time steps ensuring an admissible numerical solution will be also used in this 2D frame. By doing this, one does not have to introduce in the implementation the artificial fluxes $\mathfrak{F}_{qc}$ or the related wave speeds $\widetilde{z}^q_{rc}$, or any of the quite complex time step restrictions presented. Propositions 3.4 and 3.5 allow us to justify the chosen iterative process admits a positive limit.

4. Numerical results

In this numerical results section, we make use of several challenging test cases to demonstrate the performance and robustness of the cell-centered positivity-preserving Lagrangian schemes presented. In the previous successive sections, it has been demonstrated that for the cell-centered Lagrangian schemes considered to be positive, particular definitions of the local acoustic impedance approximation $\widetilde{z}$ have to be used, or an additional constraint on the time step has to be ensured. For the sake of simplicity and computational time, in most of cases presented we make use of the simple Godunov acoustic solver, where $\widetilde{z} = z \equiv \rho\, a$. Consequently, if it is not specified, the numerical results displayed are obtained with this acoustic approximation. For the high-order extension, the case of a DG polynomial approximation of the system variables, in a total Lagrangian formulation, will be used, as it is done in [71, 70, 72]. In the total Lagrangian frame, the whole calculation is performed on the fixed initial grid. However, for a better understanding of the numerical results, the solutions will be displayed on the actual deformed mesh.

In this paper, the conditions to ensure the averaged numerical solution to be admissible in the sens $(\tau, \widehat{\varepsilon}) \in]\tau_{min}, \tau_{max}[\times]\varepsilon_{min}, \infty]$ have been derived. For practical applications, for ideal and stiffened gas, we make use of $\tau_{min} = \varepsilon_{min} = 10^{-14}$ and $\tau_{max} = 10^{14}$, while for the detonation product gas $\tau_{min} = 0.999\,\tau_0$. Working with the Mie-Grüneisen, we employ $\tau_{min} = \frac{S_m - 1}{S_m}\,\tau_0$ and $\tau_{max} = \frac{\tau_0}{\eta^\star}$.

Even if the time step constraints developed in this paper along with the positive limitation introduced previously are enough to ensure the solution to be admissible, an additional limitation might be required in some cases. Indeed, the use of an high-order discontinuous Galerkin discretization leads, in the vicinity of discontinuities, to the apparition of strong spurious oscillations. Obviously, under the constraints derived along this article, these oscillations cannot produce non-admissible solutions. Nonetheless, strong spurious oscillations on the specific volume may lead to a drastic decrease in the time step selection if we want to maintain the admissibility of the numerical solution. To avoid such phenomenon, an additional and more classical limitation may be used. When needed or when we want to improve the global quality of the numerical solution by reducing this spurious oscillation phenomenon, we will turn on the additional limiting procedure. And even though, a simple limitation of the specific volume will succeed in avoiding the occurrence of very small time steps, we make use of a slightly more complex one. Indeed, it has been proved in [17] that to enforce the monotonicity of the system variables, the limitation has to be performed on the characteristic variables. To that purpose, we make use of a combination between the characteristic variables limitation procedure presented in [71, 72] and a standard limitation on the piecewise polynomial specific volume. Finally, for the specific volume, we choose the most limiting procedure, while for the other variables only the characteristic variable limitation is used.

4.1. One-dimensional case

For the one-dimensional case, we study the first-order and third-order cases of the cell-centered Lagrangian schemes presented, for different equations of state. Most of the test cases assessed here have been taken from those addressed in [15].

4.1.1. Numerical convergence study

To test the accuracy of these schemes, we make use of a smooth test case initially introduced in [71]. This example has been derived in the isentropic case, with the polytropic index $\gamma = 3$. In this special situation, the characteristic curves of the Euler equations become straight lines, and the governing equations reduce to two Burgers equations. It is then simple to solve analytically this problem. Similarly to [15], we modify the initial data to yield a more challenging example, as

$$\rho^0(X) = 1 + 0.9999995\sin(2\pi X), \quad u^0(X) = 0, \quad p^0(X) = \rho^0(X)^\gamma, \quad X \in [0,1],$$

provided with periodic conditions. In Figure 6, the first-order and third-order numerical solutions are depicted at time $t = 0.1$, using 50 uniform cells. In this smooth test case, the positivity limitation is not required, and when turned on has not effect whatsoever. In Table 1, we gather the global errors as well as the rates of convergence related to the third-order scheme provided with Godunov acoustic solver. The results confirm the expected third-order rate of convergence.

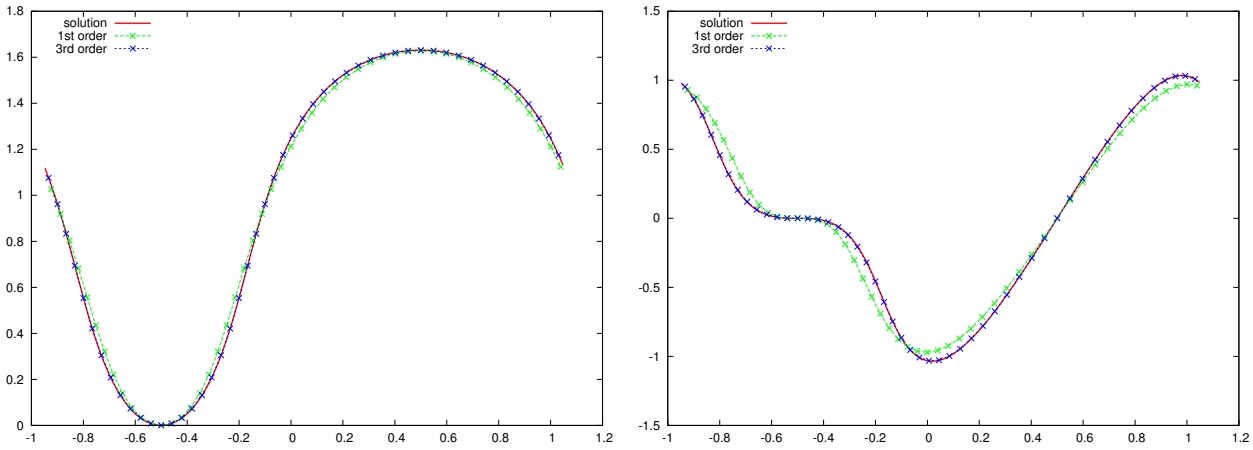

(a) Density profiles. (b) Velocity profiles.

Figure 6: Comparison between first and third-order computations on a smooth isentropic problem at time $t = 0.1$ on a 50 cells mesh.

4.1.2. The Leblanc shock tube

By means of the extreme shock tube problem, we will assess the resolution difference of the three different solvers presented, namely the acoustic solver, the Dukowicz solver and the modified Dukowicz solver. The Leblanc shock tube problem is characterized by a $[0, 9]$ domain filled by a perfect gas with $\gamma = 5/3$, and by large ratio jumps for the initial energy and density as follows

$$(\rho^0,\, u^0,\, e^0) = \begin{cases} (1,\, 0,\, 0.1), & 0 < X < 0.1, \\ (0.001,\, 0,\, 10^{-7}), & 0.1 < X < 0.9. \end{cases}$$

	L_1		L_2		L_∞	
h	$E^h_{L_1}$	$q^h_{L_1}$	$E^h_{L_2}$	$q^h_{L_2}$	$E^h_{L_\infty}$	$q^h_{L_\infty}$
$\frac{1}{50}$	9.69E-5	3.02	9.31E-5	3.01	2.75E-4	3.01
$\frac{1}{100}$	1.19E-5	3.01	1.16E-5	3.00	3.40E-5	3.01
$\frac{1}{200}$	1.48E-6	3.00	1.44E-6	3.00	4.923E-6	3.00
$\frac{1}{400}$	1.85E-7	3.00	1.80E-7	3.00	5.26E-7	3.00
$\frac{1}{800}$	2.30E-8	-	2.25E-8	-	6.56E-8	-

Table 1: Rate of convergence computed on the pressure in the case of the smooth isentropic problem at time $t = 0.1$, for the third-order Lagrangian scheme.

It is quite challenging for a gas dynamics scheme to obtain accurate positions of the contact and shock discontinuities in this severe shock tube problem. In Figure 7, the first-order density and internal energy obtained at time $t = 6$, with respectively the acoustic, Dukowicz and modified Dukowicz solvers, are depicted. One can see in Figure 7 that the Dukowicz solver yields a slightly

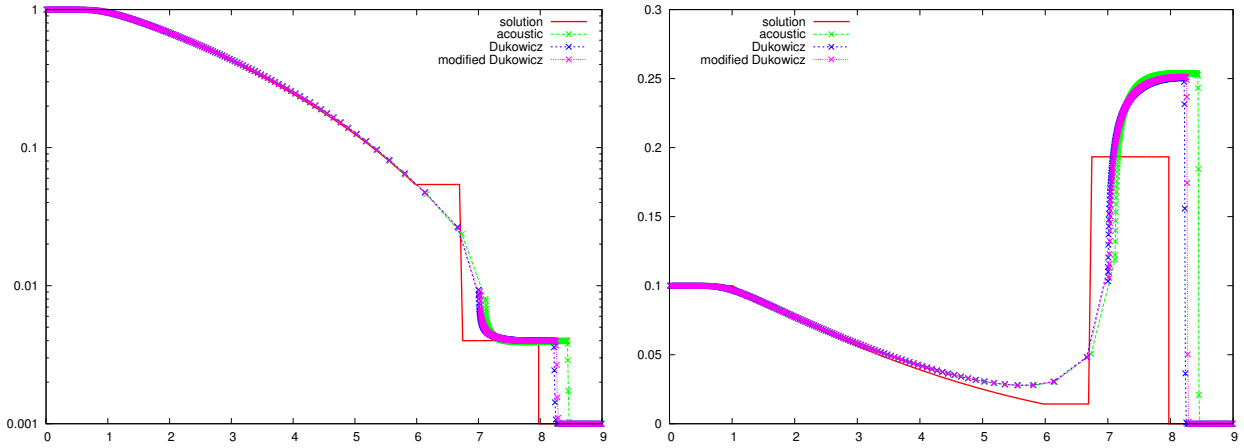

(a) Density profiles.

(b) Internal energy profiles.

Figure 7: Comparison between solvers on the Leblanc problem at time $t = 6$ on a 500 cells mesh with first-order schemes.

better resolution than the acoustic solver in this case. This comes from the fact such solver has been built to mimic the exact Godunov solver in the infinite strength limit. The Dukowicz solver should thus handle in a better way the approximation of strong shocks compared to the acoustic solver. The modified Dukowicz solver relying on the same type of definition produces similar results. However, let us note that, besides its great simplicity, the use of the acoustic solver leads to smaller computational times, see Table 2. This difference comes from the iterative fixed point procedure used in the Dukowicz and modified Dukowicz solvers to resolve the coupled system on the velocity $\overline{u}$ and the acoustic impedance local approximation $\widetilde{z}$. Furthermore, even if the difference in the solver resolutions seems substantial in Figure 7, it will dramatically be reduced when the mesh is refined, which is not the case of the difference in the computational times involved. Indeed, in Figure 8 the three different solvers yield almost the same discontinuities localization. This difference in the

	Acoustic solver	Dukowicz solver		modified Dukowicz solver	
h	Comp. time	Comp. time	Ratio ($\times$ acoustic)	Comp. time	Ratio ($\times$ acoustic)
$\frac{1}{400}$	9 sec	10 sec	1.11	10 sec	1.11
$\frac{1}{1000}$	53 sec	1 min 2 sec	1.17	1 min 2 sec	1.17
$\frac{1}{2000}$	3 min 17 sec	3 min 52 sec	1.18	3 min 51 sec	1.17

Table 2: Computational times in the case of the Leblanc shock tube problem, for the first-order Lagrangian schemes.

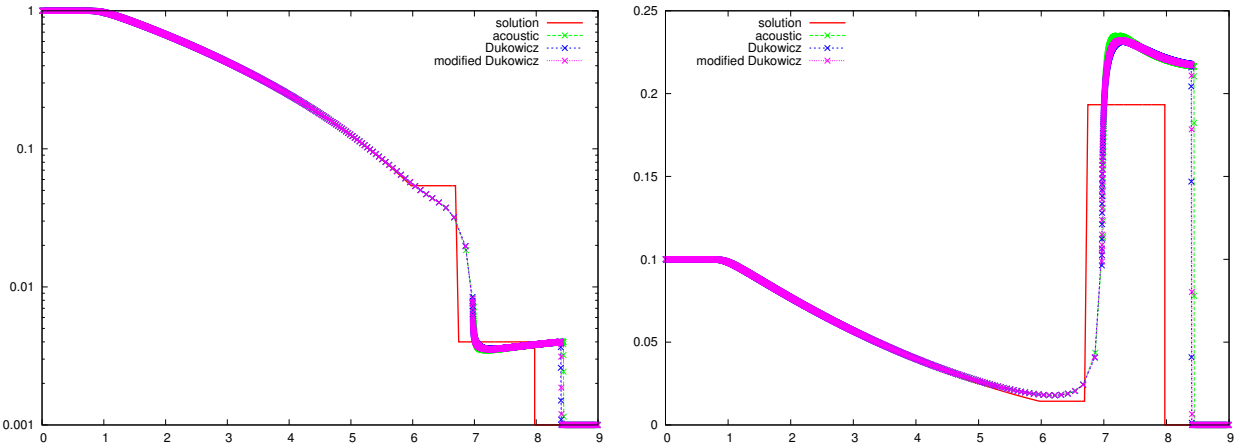

(a) Density profiles. (b) Internal energy profiles.

Figure 8: Comparison between solvers on the Leblanc problem at time $t = 6$ on a 2000 cells mesh with first-order schemes.

resolution quality will also decrease by going to high-order of accuracy. In Figure 9, limited third-

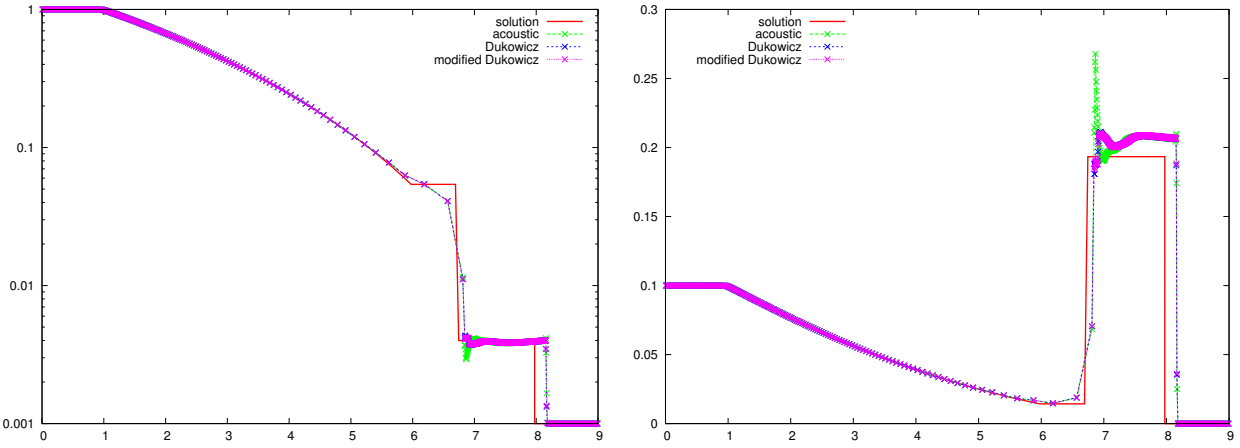

(a) Density profiles. (b) Internal energy profiles.

Figure 9: Comparison between solvers on the Leblanc problem at time $t = 6$ on a 500 cells mesh with third-order DG schemes.

order DG schemes with third-order Runge-Kutta time integration have been used on a grid made of 500 cells. And compared to Figure 7, the numerical solution obtained with the different solvers are now a lot more alike. Finally, we end this Leblanc test case section by assessing the difference in the resolution between the first-order scheme and the limited third-order scheme, in the acoustic solver case, Figure 10. As expected, the shape and position of the contact discontinuity and shock

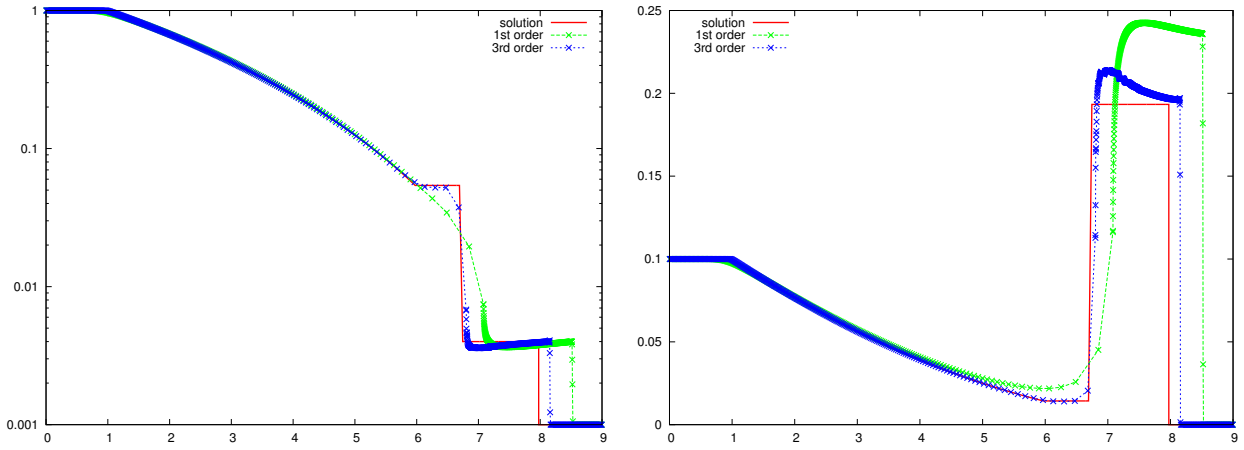

(a) Density profiles. (b) Internal energy profiles.

Figure 10: Comparison between first and third-order schemes on the Leblanc problem at time $t = 6$ on a 1000 cells mesh.

are approached in a lot better way when the high-order scheme is used. Furthermore, due to the too large numerical dissipation produced through a first-order computation, the numerical solution will be very slow to converge to the correct shock localization, regardless the solver employed. Figure 11 depicts this phenomenon for the Godunov acoustic solver. The high-order extension permits to overcome this difficulty. Indeed, in Figure 12, one can clearly see the shock convergence

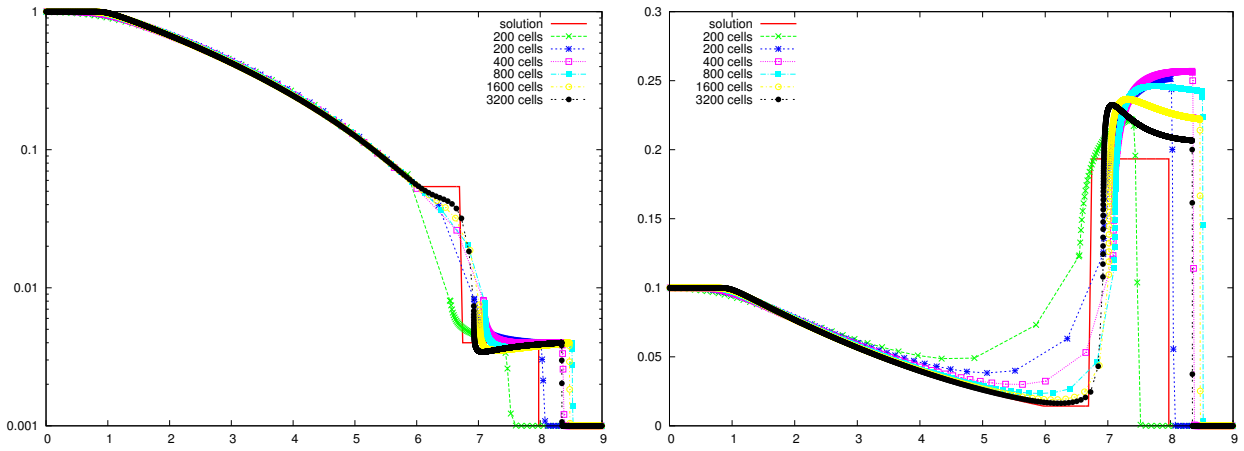

(a) Density profiles. (b) Internal energy profiles.

Figure 11: Convergence of the first-order scheme on the Leblanc problem at time $t = 6$.

to the expected position.

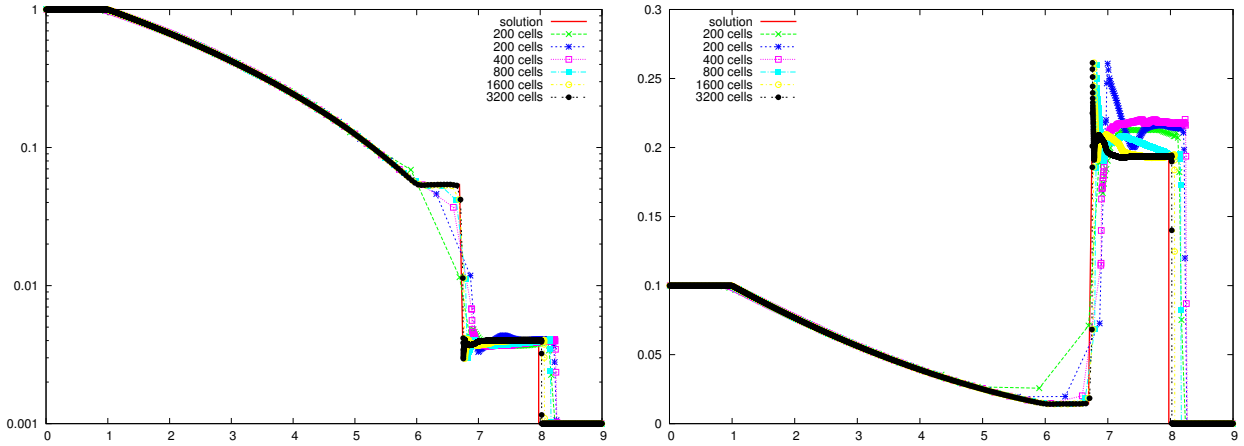

(a) Density profiles.

(b) Internal energy profiles.

Figure 12: Convergence of the third-order scheme on the Leblanc problem at time $t = 6$.

Thanks to this extreme shock tube problem, we were able to point out slight differences in the discontinuity resolution between the different solvers presented. Nonetheless, such difference only appear in problems involving very severe shocks or expansion waves, and further become insignificant when the mesh is refined or when the scheme is upgraded to high-order accuracy. In most cases, the difference yielded by the solver choice being very slight, we make use of the simplest and most computational efficient one of the three, namely the Godunov acoustic solver.

4.1.3. The 123 problem - double rarefaction

We now consider the following low density and low pressure problem on the initial domain $[-4, 4]$, where the initial condition writes

$$(\rho^0,\, u^0,\, p^0) = \begin{cases} (1,\, -2,\, 0.4), & -4 < X < 0, \\ (1,\, 2,\, 0.4), & 0 < X < 4. \end{cases}$$

The fluid considered is described through the ideal gas EOS with $\gamma = 1.4$. The left and right domain boundaries are enforced to move at a velocity respectively equal to -2 and 2. As it has been done in the Leblanc shock tube problem, we compare at time $t = 1$ the exact solution with the first-order numerical solutions obtained on a 400 cells grid with the different solvers, see Figure 13. One can see the quite bad resolution of the Lagrangian schemes near the vacuum. This strong heating phenomenon is well known, and come from the scheme entropy production even in rarefaction waves, along with the very few number of grid points near the origin in this case. However, in the light of Figure 13, the acoustic solver clearly yields a better resolution compared to the Dukowicz solver in the strong expansion problem. Like in the Leblanc test case, this difference becomes insignificant with high-order approximations, see Figure 14. Without the positivity-preserving limitation introduced in Section 2.9, the high-order Lagrangian schemes blow up for this example. Finally, to assess the benefit of the high-order extension, we compare the first-order and third-order numerical solutions, see Figure 15. We can distinctly see how the high-order extension improves the global resolution of the solution and reduces the heating phenomenon observed on the internal energy in the vicinity of vacuum.

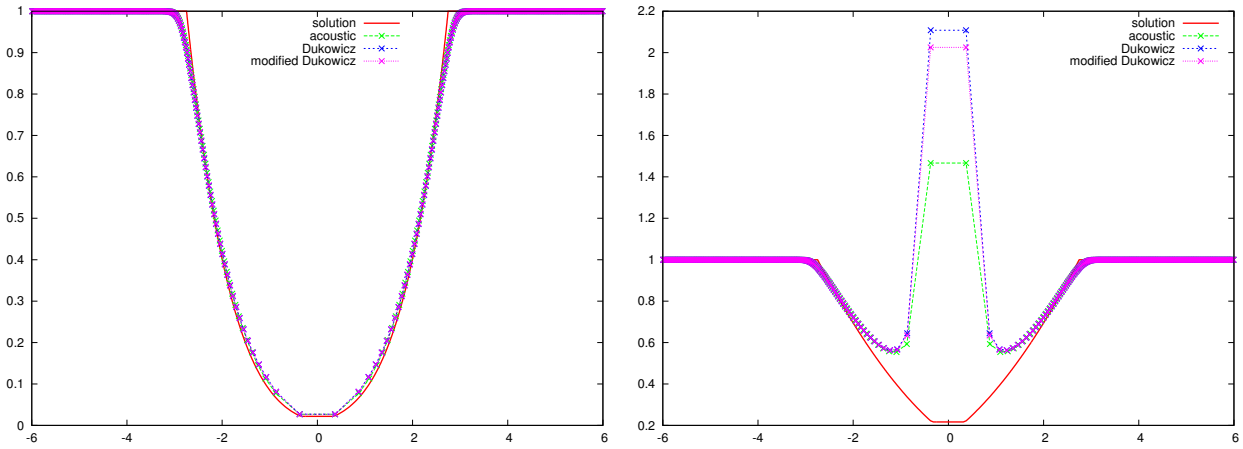

(a) Density profiles. (b) Internal energy profiles.

Figure 13: Comparison between solvers on the 123 problem at time $t = 1$ on a 400 cells mesh with first-order schemes.

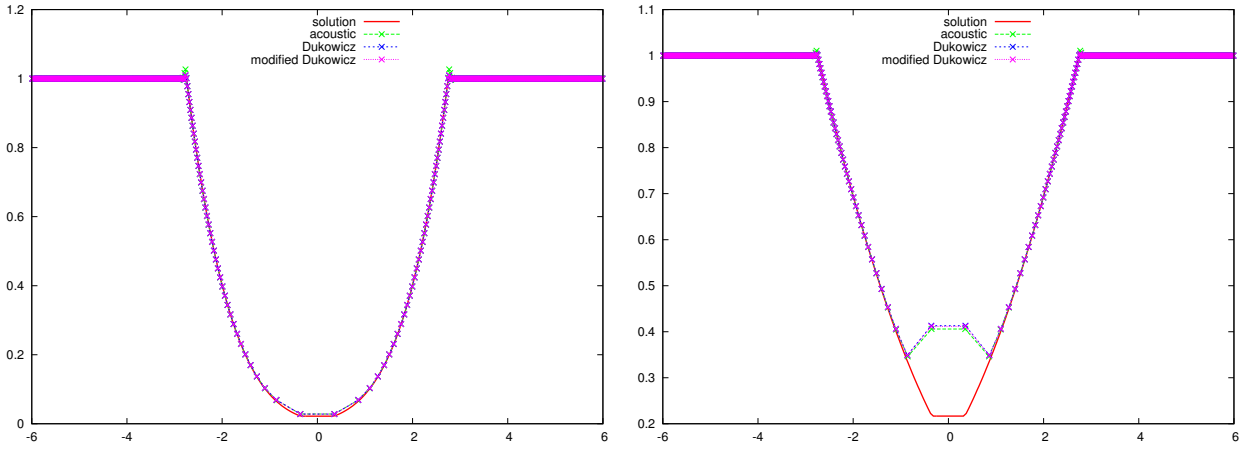

(a) Density profiles. (b) Internal energy profiles.

Figure 14: Comparison between solvers on the 123 problem at time $t = 1$ on a 400 cells mesh with third-order DG schemes.

4.1.4. Interaction of blast waves

The blast waves interaction problem is a standard low energy problem involving shocks, generally used to assess the robustness of gas dynamics schemes. The initial data read

$$\rho^0(X) = 1, \quad u^0(X) = 1, \quad p^0(X) = \begin{cases} 10^3, & 0 < X < 0.1, \\ 10^{-2}, & 0.1 < X < 0.9, \\ 10^2, & 0.9 < X < 1.0. \end{cases}, \quad X \in [0, 1].$$

The fluid under consideration is described by the ideal gas EOS with $\gamma = 1.4$, and reflective conditions are applied to the left and right boundaries of the domain. In Figure 16, the density and internal energy computed with 400 uniform cells at time $t = 0.038$, respectively with the first-order and third-order schemes, are compared with the reference "exact" solution. This reference

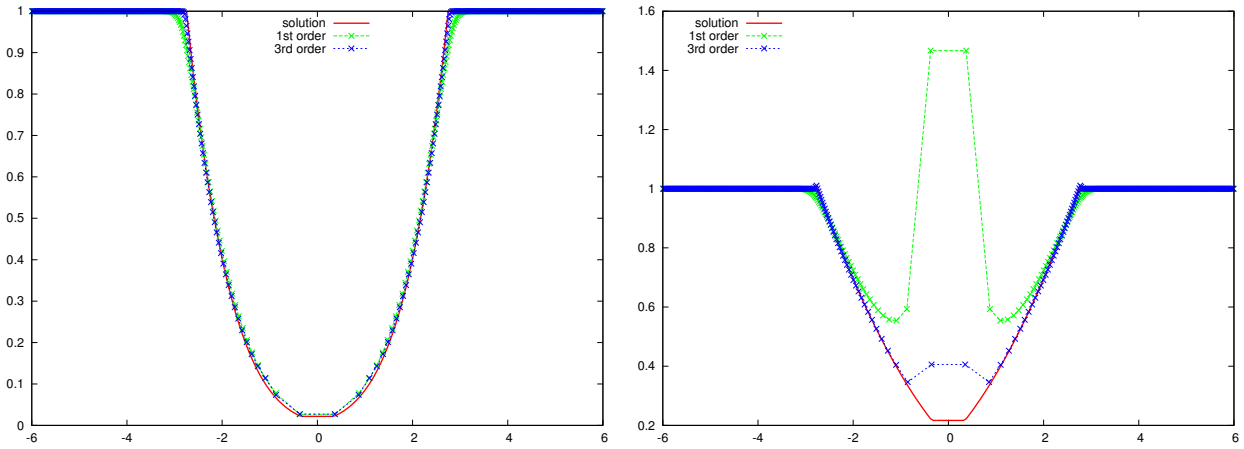

(a) Density profiles. (b) Internal energy profiles.

Figure 15: Comparison between first and third-order schemes on the 123 problem at time $t = 1$ on a 400 cells mesh.

solution has been obtained using a first-order scheme with 10000 grid points. In this strong shocks problem, we make use of the additional limitation described in the introduction of this section to avoid to occurrence of extremely small time steps, as well as improve the global quality of the third-order numerical solution. It is clear in Figure 16 that the density as well as the internal

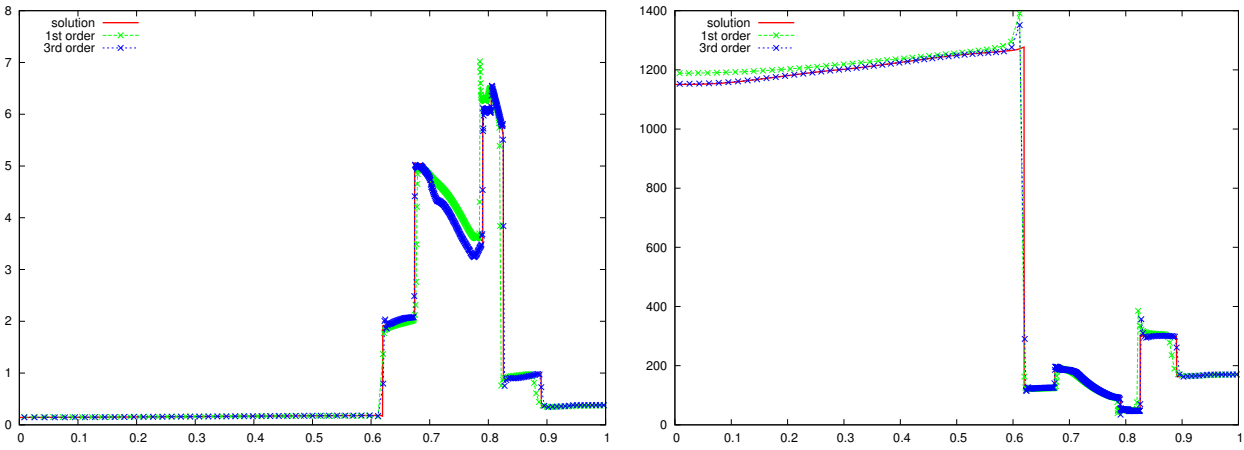

(a) Density profiles. (b) Internal energy profiles.

Figure 16: Comparison between first and third-order on a blast wave problem at time $t = 0.038$ on a 400 cells mesh.

energy remain positive for both first-order and high-order schemes. One can also distinctly observe the better resolution yielded by the third-order scheme in comparison with the first-order one. The overshoots visible in the numerical solution are independent of the limitation, being present from the first-order. This phenomenon is inherent to the Lagrangian formulation used, and is due to the very strong difference in the cell aspect ratio before and after discontinuities.

4.1.5. The gas-liquid shock tube

So far, only the case of the ideal gas equation of state has been issued. To address the case of the stiffened gas EOS, we make use the following severe water-air shock tube. This problem yields a density ratio of 200 and will enable us to illustrate the performance of the Lagrangian schemes presented for multi-material flows presenting strong interfacial contact discontinuity. In this shock tube test case, the fluid on the left side of the membrane located at $x = 0.3$ is considered to be a perfect gas, while on the right side water is considered. The perfect gas is modeled by the ideal EOS with $\gamma = 1.4$, while the water is described through the stiffened gas EOS with $\gamma = 4.4$ and $p_s = 6 \times 10^8$. The initial states of the two fluids are defined as follows

$$(\rho^0,\, u^0,\, p^0) = \begin{cases} (5,\, 0,\, 10^5), & 0 < X < 0.3, \\ (10^3,\, 0,\, 10^9), & 0.3 < X < 1.0. \end{cases}$$

We display in Figure 17 the numerical solutions at time $t = 0.00024$ obtained by means of the first-order scheme and the limited DG third-order scheme provided with the acoustic solver, on a grid made of 200 cells. These results prove the good agreement between the exact solution and the

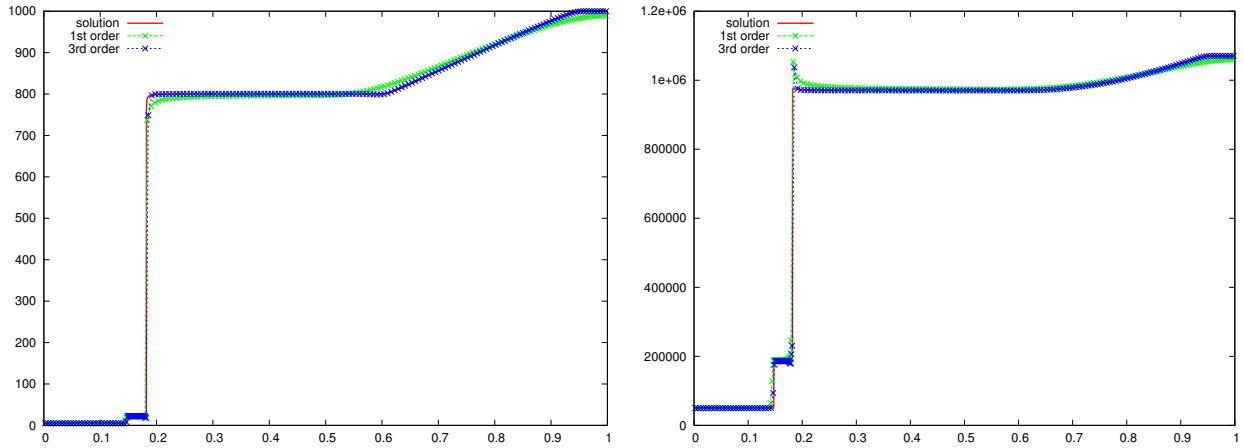

(a) Density profiles. (b) Internal energy profiles.

Figure 17: Comparison between first and third-order on the water-air shock tube problem at time $t = 0.00024$ on a 200 cells mesh.

numerical ones, despite of the extreme initial conditions. In both first-order and high-order cases, the density and internal energy are maintained positive at all time. Furthermore, the third-order scheme again demonstrate to yield a better resolution than the first-order one, as expected.

4.1.6. The underwater TNT explosion

To assess the case of the Jones-Wilkins-Lee equation of state, we make use the multi-material test case initially introduced in [30]. This problem has been modified in [15] to increase the stiffness of the problem and thus to produce a more challenging problem, namely where the appearance of negative density and internal energy are more likely. In this latter case, the initial data read

$$(\rho^0,\, u^0,\, p^0) = \begin{cases} (1.63 \times 10^{-3},\, 0,\, 8.381 \times 10^3), & 0 < X < 0.16, \\ (1.025 \times 10^{-3},\, 0,\, 1), & 0.16 < X < 3.0. \end{cases}$$

On the left of the interface initially located at $x = 0.3$, the gaseous product of the detonated explosive is modeled by the JWL EOS with $A_1 = 3.712 \times 10^5$, $A_2 = 3.23 \times 10^3$, $R_1 = 4.15$, $R_2 = 0.95$, $\rho_0 = 1.63 \times 10^{-3}$ and $\gamma = 1.3$. On the right of the interface, the water is described through the stiffened gas EOS with $\gamma = 7.15$ and $p_s = 3.309 \times 10^2$. In Figure 18, the density and pressure profiles of the first-order and limited third-order Lagrangian schemes with 400 cells are compared to the reference "exact" solution obtained using the first-order scheme with 5000 grid points. The use of a Lagrangian formulation permits the sharp capture of the interface of the gas

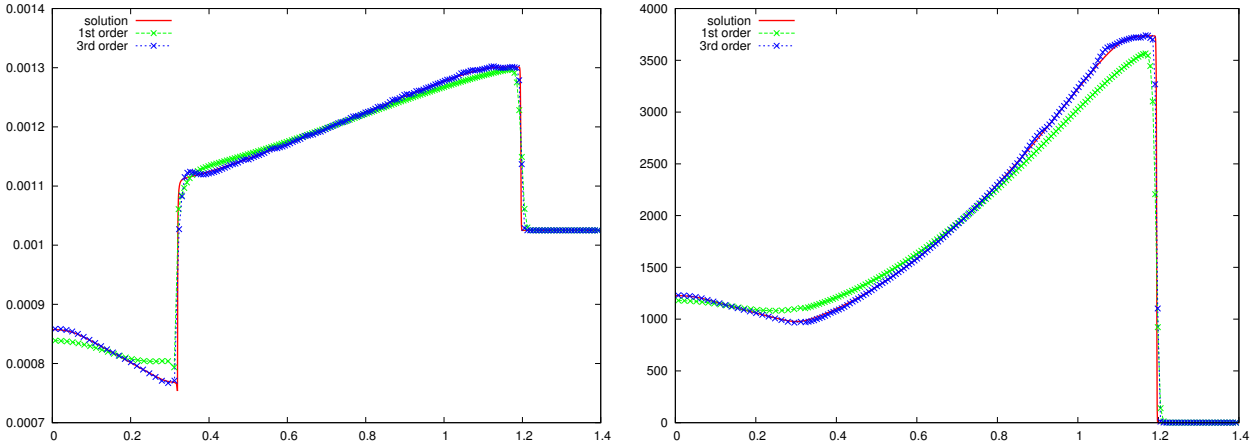

(a) Density profiles.

(b) Pressure profiles.

Figure 18: Comparison between first and third-order on the one-dimensional underwater TNT explosion at time $t = 0.00025$ on a 400 cells mesh.

and condensed phases of this underwater explosion. Furthermore, in the light of the analytical demonstrations and constraints developed in this paper, the Lagrangian schemes presented are ensured to produce admissible solutions. Again, the third-order scheme produces better resolution for both density and pressure.

4.1.7. The Wilkins problem

To end with the one-dimensional numerical results, we consider the Wilkins test case. This problem has been introduced in [73] and addressed in a Lagrangian frame in [54]. It consists in computing the flow resulting from a flying aluminum plate that strikes a target aluminum plate. The equation of state used to describe the material under consideration is the Mie-Grüneisen EOS, with the following parameters: $\rho_0 = 2785$, $a_0 = 5328$, $\Gamma_0 = 2$ and $S_m = 1.338$. The computational domain is $[0, 0.05]$ and the initial data are prescribed by

$$\rho^0(X) = 2785, \quad p^0(X) = 10^{-6}, \quad u^0(X) = \begin{cases} 800, & 0 < X < 0.005, \\ 0, & 0.005 < X < 0.05. \end{cases}$$

A free boundary condition is impose at the left domain boundary, while at the right domain boundary a wall condition is enforced. We run this test case until the final time $t = 5 \times 10^{-6}$. Analytically, the flying plate impact produces a flow that will be characterized at the final time by an elastic rarefaction wave followed by a plastic rarefaction wave, and an elastic shock followed by a plastic shock, see for instance [54]. Obviously, because the schemes presented in this paper

are meant to resolve the gas dynamics system of equations, there are not able to capture the elastic waves, see Figure 19. We only use this elastic-plastic test case to assess to robustness of the presented schemes in the case of the Mie-Grüneisen EOS. In Figure 19, we compare the first-order

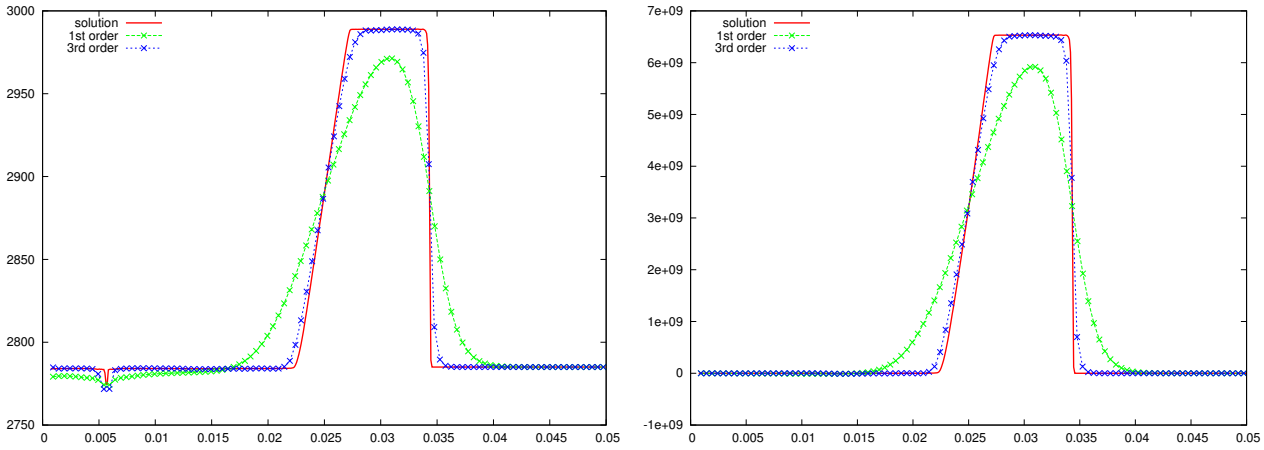

(a) Density profiles.

(b) Internal energy profiles.

Figure 19: Comparison between first and third-order on the one-dimensional flying plate impact problem at time $t = 5 \times 10^{-6}$ on a 100 cells mesh.

and limited third-order numerical solutions with a reference "exact" solution computed with the first-order scheme with 5000 cells. As expected, even using complex equation of state as the Mie-Grüneisen one, these Lagrangian schemes are able to produce admissible numerical solution and thus to run the computation through the final time without any crash of the code. Furthermore, one can see how the high-order scheme improves the captures of the shock and rarefaction wave. Obviously, this accuracy is limited by the model used, here the compressible gas dynamics one.

4.2. Two-dimensional case

For the two-dimensional case, we study the first-order and second-order versions of the cell-centered discontinuous Galerkin Lagrangian schemes presented in [72], for different equations of state. In its first-order version on straight line polygonal mesh, the LCCDG scheme reduces to EUCCLHYD scheme. We will not addressed the third-order case on curved geometries in this two-dimensional section since the third-order LCCDG scheme still produces some non-physical deformations in the presence of very intense shock waves due to the limitation, see [72].

Because the LCCDG have already proved to yield expected accuracy, we refer the interested reader to [72] for a complete convergence analysis on the smooth Taylor-Green vortex test case.

4.2.1. The Sedov blast wave problem

We consider the Sedov problem for a point-blast in a uniform medium. An exact solution based on self-similarity arguments is available, see for instance [43]. The initial density is set to $\rho^0 = 1$, and the fluid at rest as $\boldsymbol{u}^0 = 0$. The pressure is considered to be zero over the domain except at the origin. Thus, we set an initial delta-function energy source at the origin prescribing the pressure in the cell containing the origin as follows, $p_{or} = (\gamma - 1)\rho_{or}\frac{\varepsilon^0}{v_{or}}$, where v_{or} denotes the volume of the

cell containing the origin and ε^0 is the total amount of release energy. By choosing $\varepsilon^0 = 0.244816$, as suggested in [43], the solution consists of a diverging infinite strength shock wave whose front is located at radius $r = 1$ at $t = 1$, with a peak density reaching 6. The fluid is modeled by the ideal gas EOS with $\gamma = 1.4$. Generally, because one cannot simulate vacuum, the initial pressure is set to 10^{-6} over the domain, except at the origin. Here, to make it more challenging, we set the initial pressure to 10^{-14}.

Now, similarly to what has been done in the 1D case with the Leblanc shock tube test case, we assess the resolution of the different solvers, namely the acoustic, Dukowicz and modified Dukowicz solvers, in this point blast problem. Let us point out that, as expected through the analysis presented in this paper, the use of the acoustic solver without the additional time step constraint on the volume variation leads to a crash of the code in this Sedov test case. In this perfect gas problem, consistently with the theory presented, the Dukowicz solver, as well as the modified version of it, will succeed to run until the final time with only the CFL condition enforced. In Figure 20, with the first-order scheme with a 30×30 Cartesian grid on the domain $(X, Y) = [0, 1.2] \times [0, 1.2]$, the density maps as well as the density and pressure profiles of the three different solvers are displayed. In

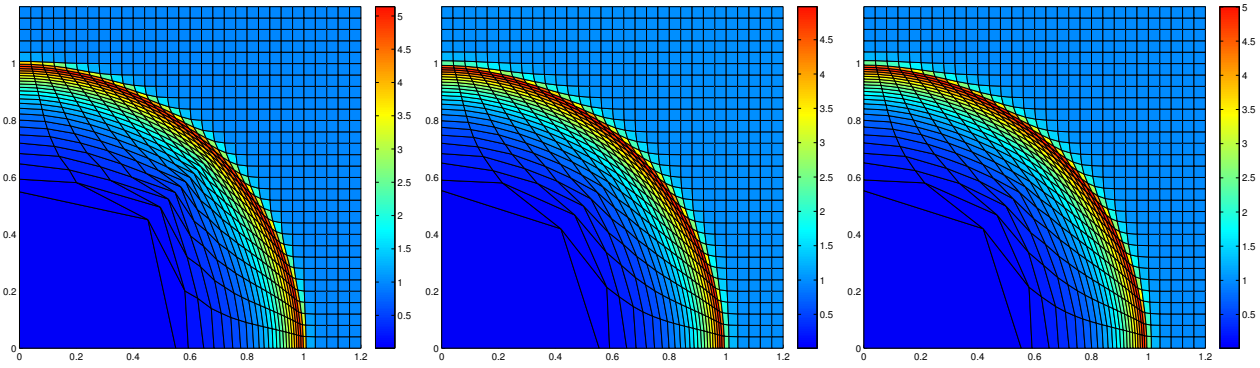

(a) Acoustic solver. (b) Dukowicz solver. (c) Modified Dukowicz solver.

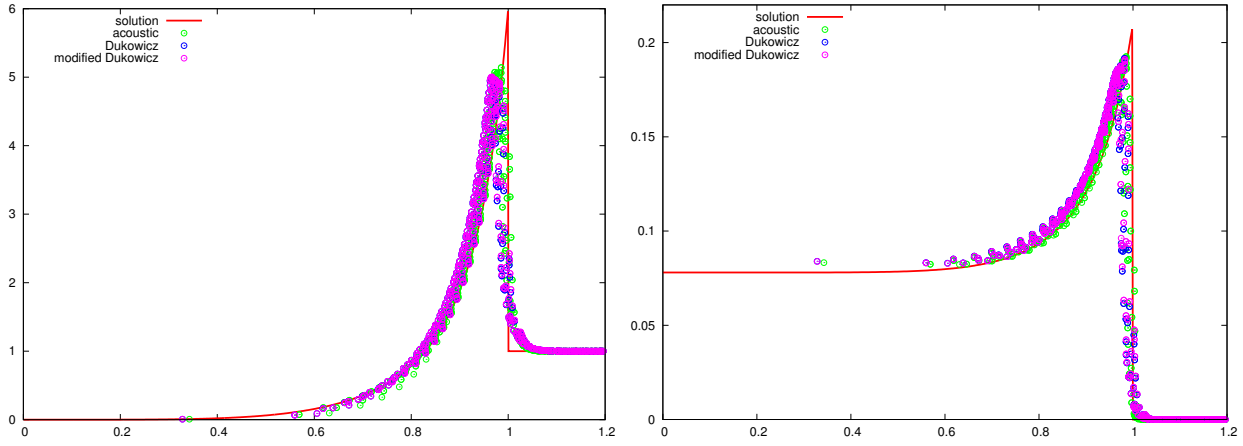

(d) Density profiles. (e) Pressure profiles.

Figure 20: Comparison between solvers on the Sedov problem at time $t = 1$ on a 30×30 Cartesian mesh with first-order schemes.

the light of Figure 20, regardless the solver used, the numerical solution proves a good agreement with the one-dimensional analytical solution, and the shock wave front is correctly located and almost cylindrical. Further, the density peak almost reaches 6. However, the overall quality of the final grids obtained with original and modified Dukowicz solvers, Figures 20(b) and 20(c), is superior to the quality of the final grid get in the case of the acoustic solver, see Figure 20(a). Indeed, in Figure 20(a), the grid presents non-convex cells in the 45 degrees direction, while it is not the case on Figures 20(b) and 20(c). Nonetheless, plotting the density and pressure in all cells versus the cell center radius, Figures 20(d) and 20(e), one can observe the relative equivalence of the results obtained through the different solvers, even if the acoustic solver seems to be slightly less diffusive. The non-convex cell appearance in the first-order acoustic scheme case is prevented going the second-order. Indeed, the second-order DG scheme provided with the acoustic solver

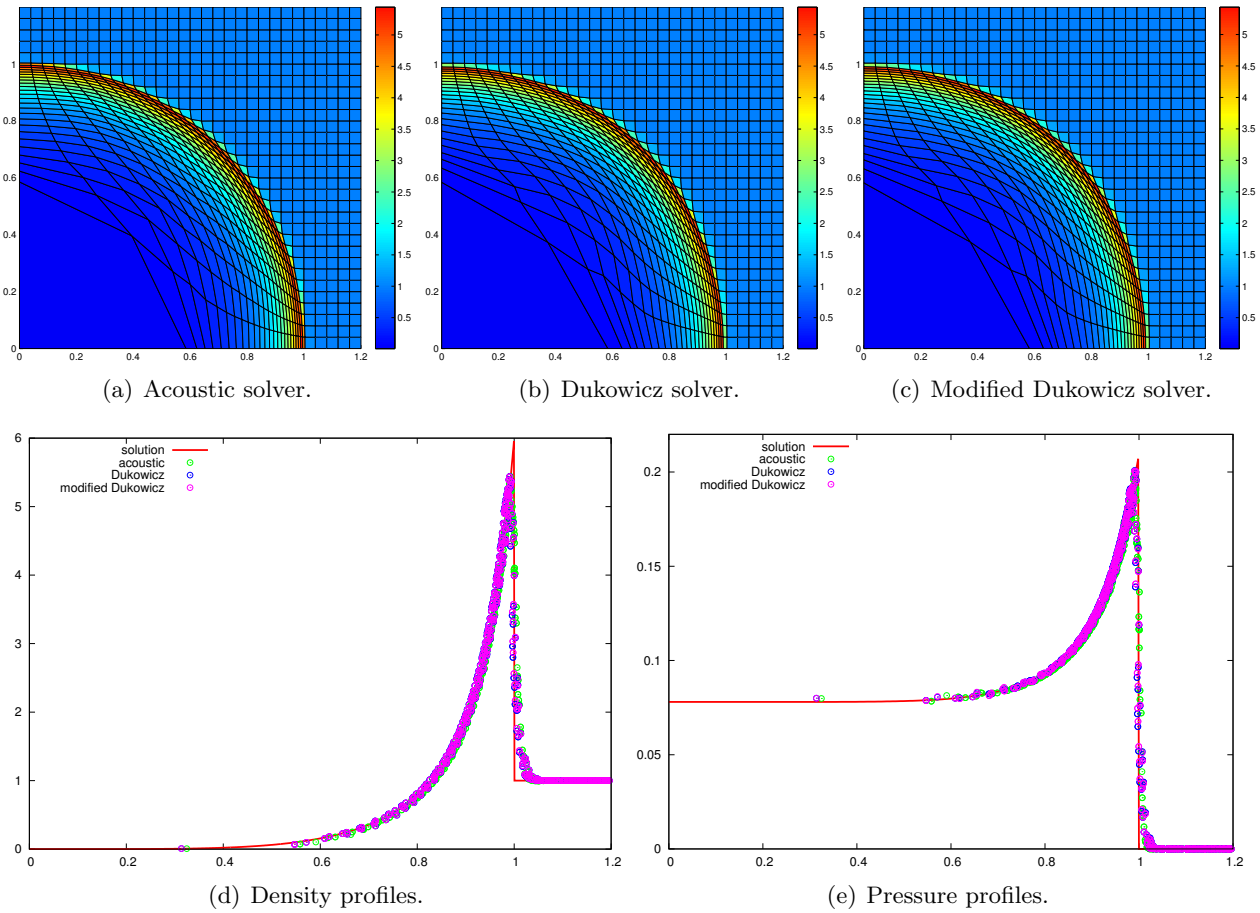

(a) Acoustic solver. (b) Dukowicz solver. (c) Modified Dukowicz solver.

(d) Density profiles. (e) Pressure profiles.

Figure 21: Comparison between solvers on the Sedov problem at time $t = 1$ on a 30×30 Cartesian mesh with limited second-order schemes.

produces a final grid of very good overall quality, see Figure 21(a). Similarly to the 1D cases, the high-order extension dramatically reduces the difference in the results between the different solvers. Finally, we assess the difference in the resolution between the first-order scheme and the limited second-order scheme in this Sedov point blast problem, using the acoustic solver. As expected,

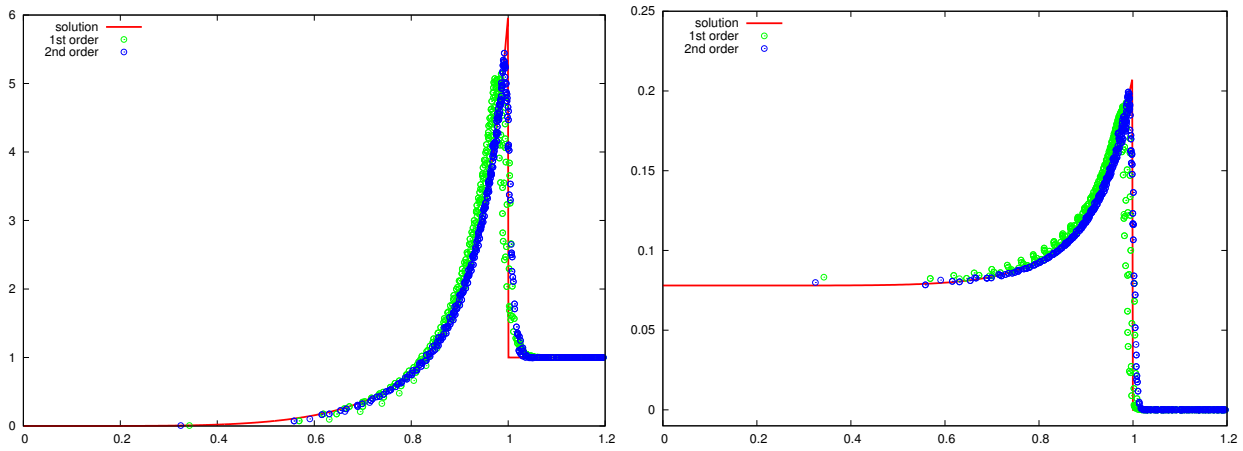

(a) Density profiles. (b) Pressure profiles.

Figure 22: Comparison between first and second-order schemes on the Sedov problem at time $t = 1$ on a 30×30 Cartesian mesh.

given the profiles depicted in Figure 22, and comparing the final meshes obtained, Figures 20(a) and 21(a), it is clear how the high-order scheme captures more accurately the cylindrical and sharp aspect of the front shock.

4.2.2. The 123 problem - double rarefaction

Now, we make use of the two-dimensional extension of the 123 problem presented previously. The initial domain is defined as $(X, Y) \in [0, 4]^2$, wherein the fluid is considered perfect with $\gamma = 1.4$, the initial density $\rho^0 = 1$ and the initial pressure $p^0 = 0.4$. The fluid velocity is initialized as being outward radial of magnitude 2. Similarly to the 1D case, we compare the final solutions obtained at time $t = 1$ with the first-order scheme provided with the three different solvers presented, see Figure 23(b). Given Figure 23(a), one can clearly see the spurious heating phenomenon near the vacuum in this cylindrical rarefaction problem. Like in 1D, in the light of Figure 23(b), we can state that in this case the acoustic solver yields the better resolution. In Figure 24, we plot the computation time steps for the three different solvers. As one may have expected, the acoustic solver seems optimal in simplicity and time step in this case. Finally, to observe the benefits of the high-order discretizations, we compare the numerical solutions obtained by means of the first-order scheme and the second-order scheme in this 123 rarefaction problem, using the acoustic solver. As expected, the second-order scheme prove to yield a better resolution than the first-order one, see Figure 25.

4.2.3. The Noh problem

The Noh problem [60] is a well known test case used to validate Lagrangian schemes in the regime of infinite strength shock wave. In this test case, a cold gas modeled by the ideal EOS with $\gamma = 5/3$ and unit density is given an initial inward radial velocity of magnitude 1. Generally, the initial pressure is given by $p^0 = 10^{-6}$. But, as in the previous Sedov problem, to yield a more challenging test case we internalize the pressure to $p^0 = 10^{-14}$. A diverging cylindrical shock wave is generated which propagates at speed $D = \frac{1}{3}$. The density plateau behind the shock wave reaches the value 16. The initial computational domain is defined by $(X, Y) = [0, 1] \times [0, 1]$. The

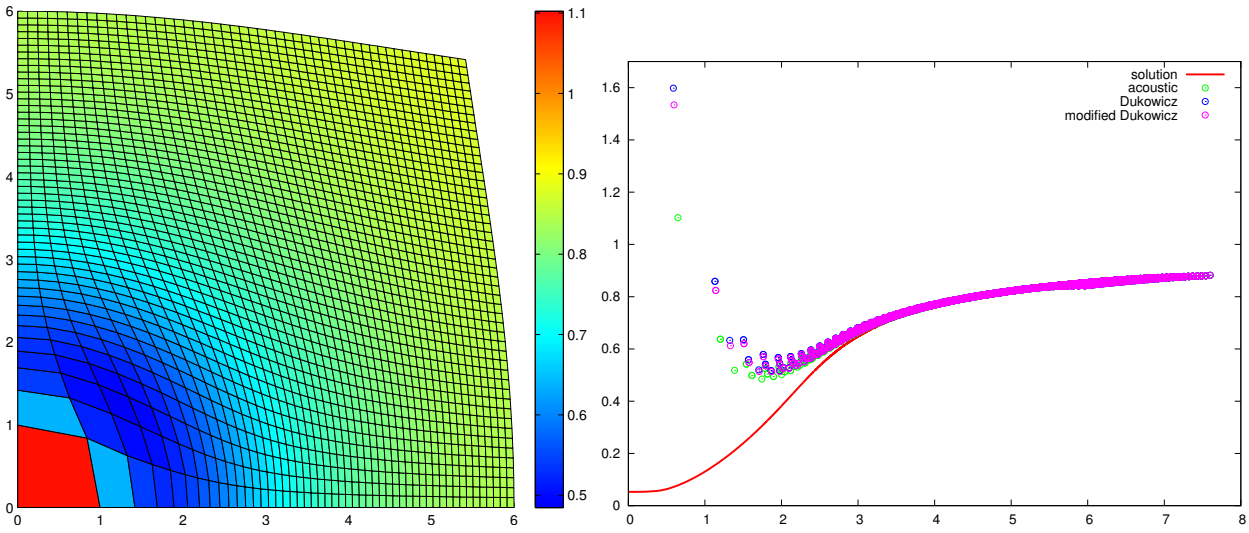

(a) Internal energy map. (b) Internal energy profiles

Figure 23: Comparison between solvers on the 123 problem at time $t = 1$ on a 50×50 Cartesian mesh with first-order schemes.

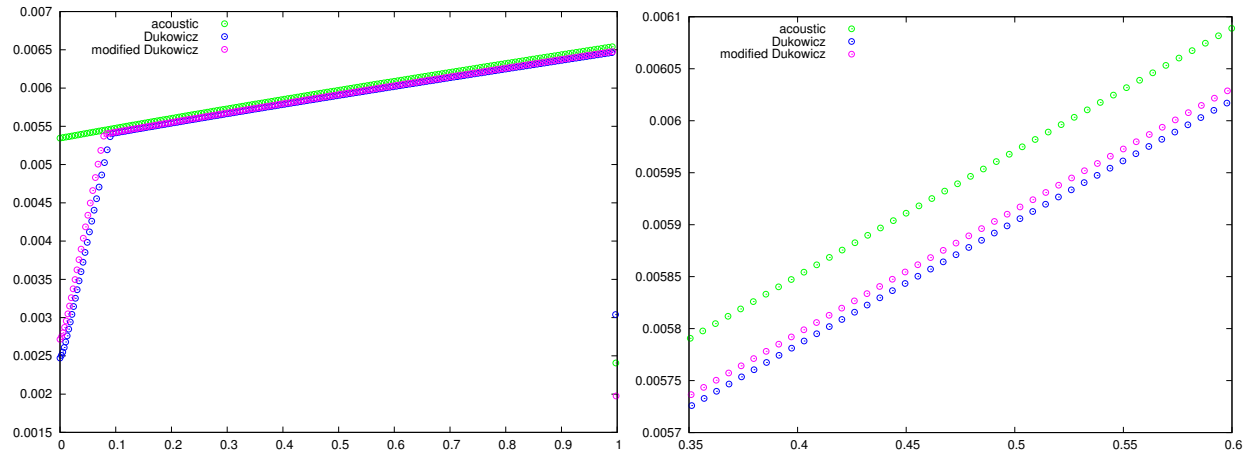

(a) Time steps. (b) Time steps - zoom.

Figure 24: Time steps of the first-order scheme with different solvers for the 123 problem on a 50×50 Cartesian mesh.

boundary conditions on the X and Y axis are symmetry conditions whereas a pressure given by $p^\star = p^0$ is prescribed at $X = Y = 1$. We run the Noh problem on a 50×50 Cartesian grid. This configuration leads to a severe test case since the mesh is not aligned with the flow, and produce some spurious mesh deformations in the 45 degrees direction, see Figure 26(a). This well-known phenomenon can be corrected by using the Dukowicz solver, see Figure 26(b), of the modified Dukowicz one, Figure 26(c). Another remedy will be the use of an high-order approximation. We note on Figure 27(a), where the acoustic solver is used, how the limited second-order scheme

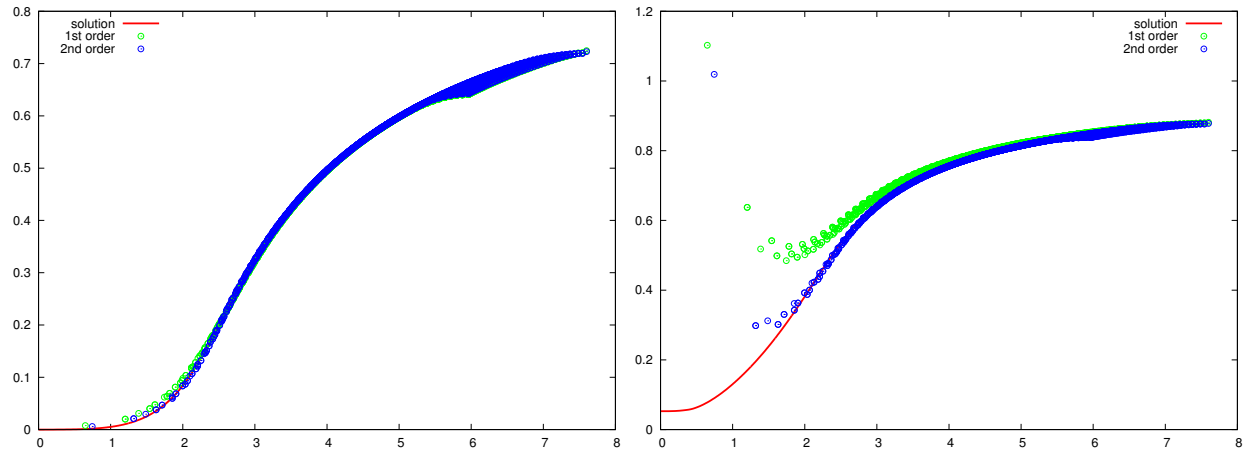

(a) Density profiles. (b) Internal energy profiles.

Figure 25: Comparison between first and second-order schemes on the 123 problem at time $t = 1$ on a 50×50 Cartesian mesh.

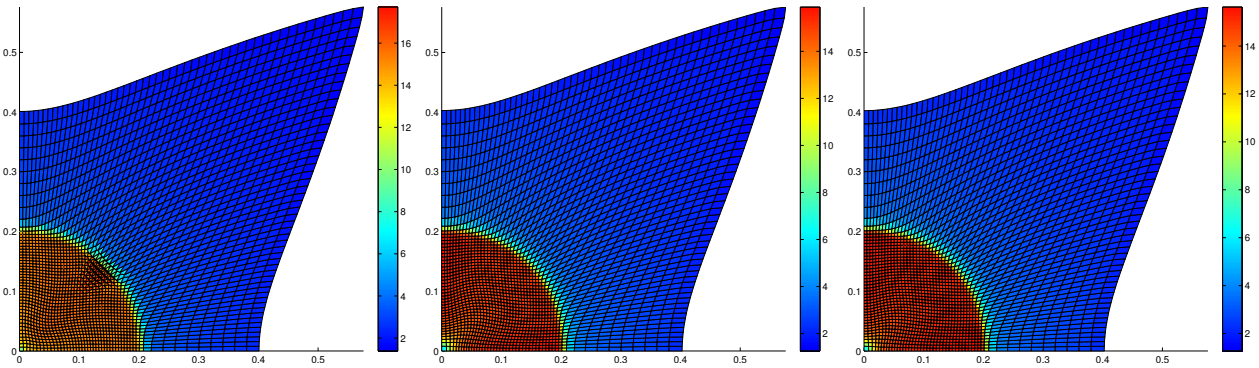

(a) Acoustic solver. (b) Dukowicz solver. (c) Modified Dukowicz solver.

Figure 26: Comparison between solvers on the Noh problem at time $t = 0.6$ on a 50×50 Cartesian mesh with first-order schemes.

produces a smooth and cylindrical solution, as well as a shock located at a circle whose radius is approximately 0.2. On Figure 27(b), we observe that the second-order plot is very sharp at the shock wave front and very similar to the one-dimensional cylindrical solution. Moreover the density at the shock plateau is not far from the analytical value. This shows the ability of theses schemes to preserve the radial symmetry of the flow, as well as ensure an admissible numerical solution even in severe test cases as the Noh problem.

4.2.4. The air-water-air problem

We make use of the cylindrical two-phase problem presented in [15]. A domain defined in polar coordinates by $(r, \theta) \in [0, 1.2] \times [0, 2\,\pi]$ is considered. The inner and outer parts ($r \in [0, 0.2] \bigcup [1.0, 1.2]$) of the domain are filled by air, modeled by the ideal EOS with $\gamma = 1.4$, while the central part ($r \in [0.2, 1.0]$) contains water described through the stiffened gas EOS with $\gamma = 7$ and $p_s = 3000$.

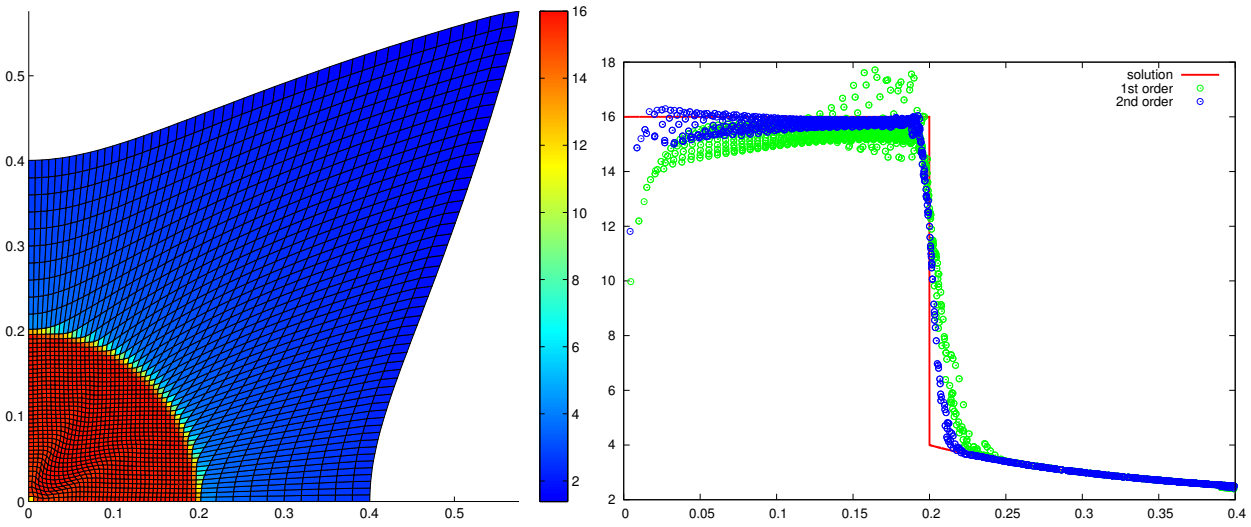

(a) Density map. (b) Density profiles.

Figure 27: Comparison between first and second-order schemes on the Noh problem at time $t = 0.6$ on a 50×50 Cartesian mesh.

The initial data are prescribed as follows

$$(\rho^0,\, \boldsymbol{u}^0,\, p^0) = \begin{cases} (0.001,\, \mathbf{0},\, 1000), & 0 < r < 0.2, \\ (1,\, \mathbf{0},\, 1), & 0.2 < r < 1.0, \\ (0.001\,\mathbf{0},\, 0.001), & 1.0 < r < 1.2. \end{cases}$$

Because of the symmetry of the solution, we only simulate a 1/8 part of the full domain, namely $(r, \theta) \in [0, 1.2] \times [0, \frac{\pi}{4}]$. In Figure 28, we display the numerical results obtained with the second-order DG scheme with the acoustic solver on a 120×9 polar grid at the final time $t = 0.007$. In

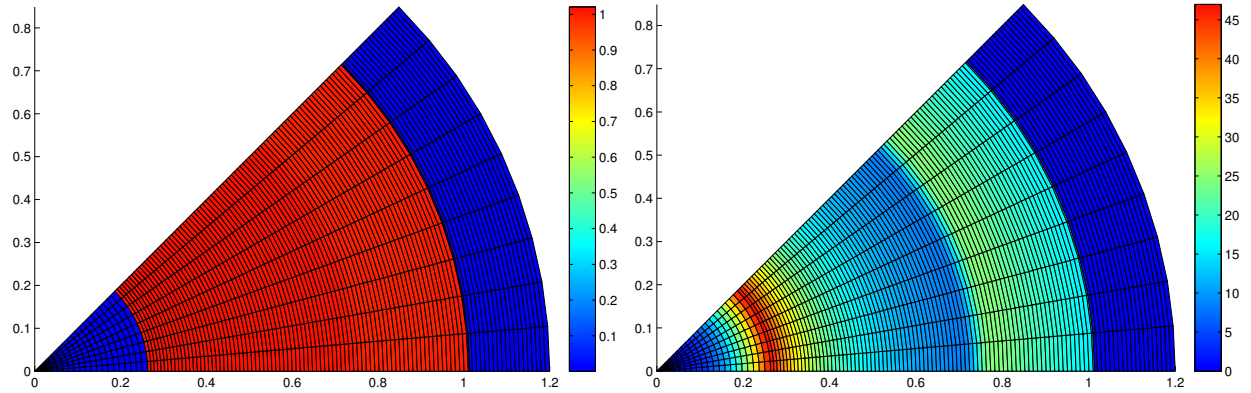

(a) Density map. (b) Kinetic energy map.

Figure 28: The air-water-air problem at time $t = 0.007$ on the polar domain $[0, 1.2] \times [0, \frac{\pi}{4}]$ made of 120×9, with the second-order DG scheme.

Figures 28(a) and 28(b), one can clearly that the cylindrical features of the solution are well captured

by the numerical scheme. Furthermore, no negative density nor negative internal energy appear during this quite severe problem. In Figures 29(a) and 29(b), the numerical solutions obtained by

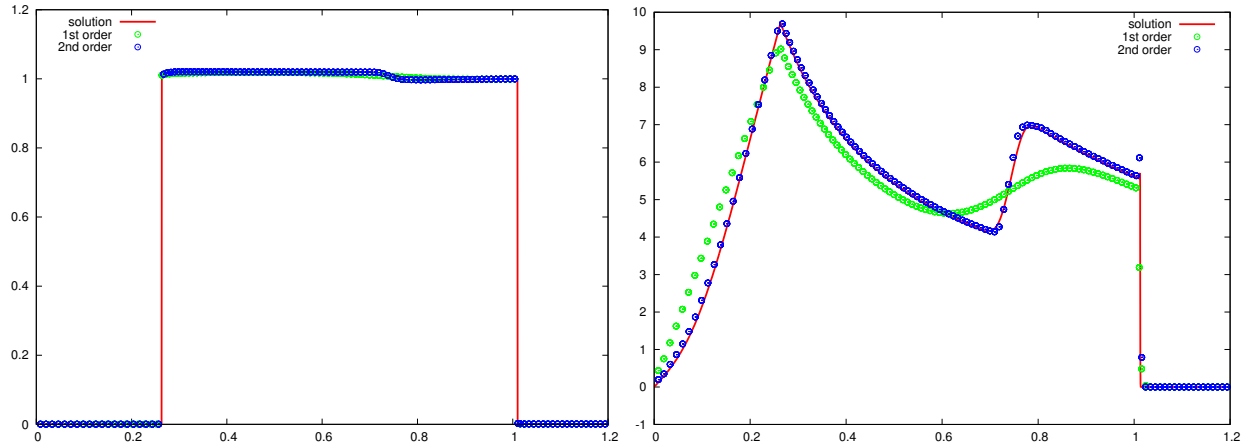

(a) Density profiles.

(b) Radial velocity profiles.

Figure 29: Comparison between first and second-order schemes on the air-water-air problem at time $t = 0.007$ on the polar domain $[0, 1.2] \times [0, \frac{\pi}{4}]$ made of 120×9.

means of the first-order and second-order schemes are compared with the reference "exact" solution obtained with 2500×1 cells on the radial symmetric domain $(r, \theta) \in [0, 1.2] \times [0, 1]$. In the end, the second-order scheme is shown to have a better resolution.

4.2.5. The underwater TNT explosion

We assess now the two-dimensional case of the underwater TNT explosion presented previously. We make use of exactly the same data described in Section 4.1.6, but this time on the polar domain $(r, \theta) \in [0, 1.2] \times [0, 2\,\pi]$. The gaseous product of the detonated explosive are initially contained in $r \in [0, 0.16]$ and modeled by the JWL EOS, while the rest of the domain is filled by water described through the stiffened gas EOS. As before, thanks to the symmetry of the solution, we only simulate a 1/8 part of the full domain, namely $(r, \theta) \in [0, 1.2] \times [0, \frac{\pi}{4}]$. In Figure 30, we display the numerical results obtained with the limited second-order DG scheme with the acoustic solver on a 120×9 polar grid at the final time $t = 2.5 \times 10^{-4}$. In Figures 30(a) and 30(b), one can clearly see that the cylindrical features of the solution are well captured by the numerical scheme. Furthermore, no negative density nor negative internal energy appears during this severe multi-material problem. In Figures 31(a) and 31(b), the numerical solutions obtained by means of the first-order and second-order schemes are compared with the reference "exact" solution obtained with 3000×1 cells on the radial symmetric domain $(r, \theta) \in [0, 1.2] \times [0, 1]$. As expected, the second-order scheme proves to have a better resolution. Furthermore, these results are consistent with the ones presented in [30, 15].

4.2.6. The two-dimensional projectile impact problem

To end with the numerical results section, we make use of the two-dimensional projectile impact problem introduced and described in [44]. The initial projectile is a rectangular plate of length

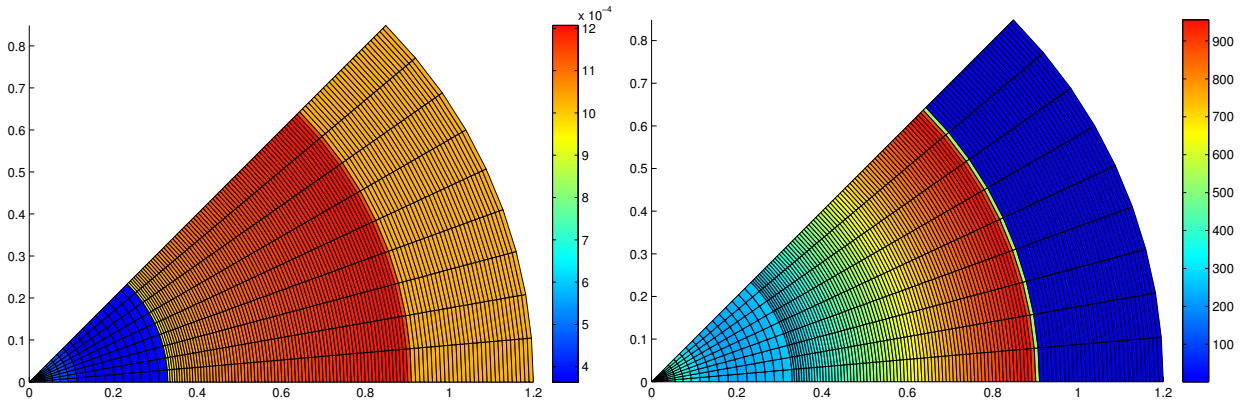

(a) Density map. (b) Pressure map.

Figure 30: The spherical underwater TNT charge explosion problem at time $t = 2.5 \times 10^{-4}$ on the polar domain $[0, 1.2] \times [0, \frac{\pi}{4}]$ made of 120×9, with the second-order DG scheme.

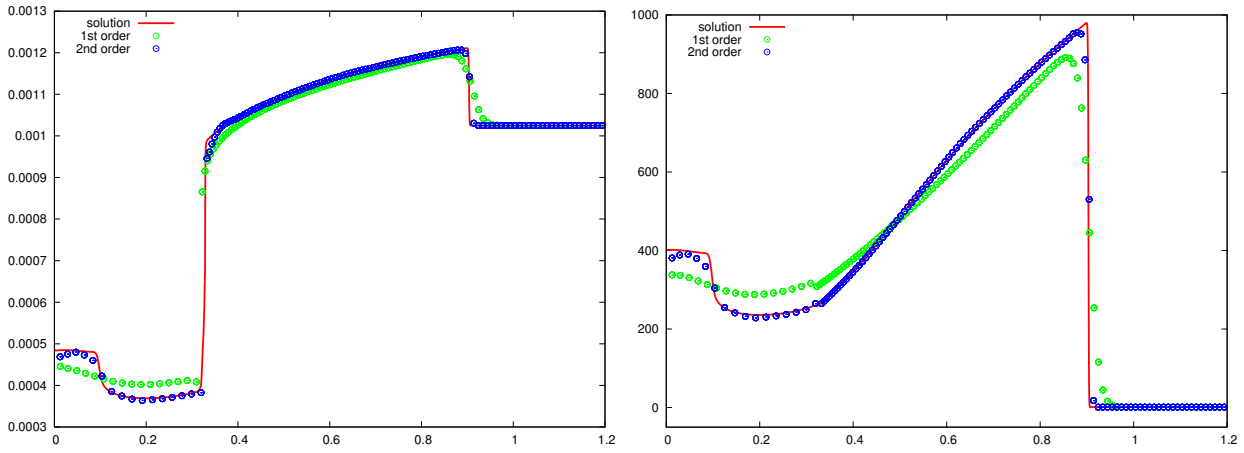

(a) Density profiles. (b) Pressure profiles.

Figure 31: Comparison between first and second-order schemes on the spherical underwater TNT charge explosion problem at time $t = 2.5 \times 10^{-4}$ on the polar domain $[0, 1.2] \times [0, \frac{\pi}{4}]$ made of 120×9.

5 and height 1. The material under consideration is aluminum and is thus modeled by the Mie-Grüneisen equation of state. The value of the parameters are the same as the one used in the one-dimensional Wilkins problem, see Section 4.1.7. Due the axial symmetry of this problem, we focus in the half problem of the initial domain $(X, Y) \in [0, 5] \times [0, 0.5]$. The initial velocity is given by $\boldsymbol{u}^0 = (-150, 0)^{\mathrm{t}}$. We take the free traction boundary conditions for all the domain boundaries except the left one which is enforced to be a wall boundary. We recall this problem has neither an analytical solution nor experimental results. However, it is a good test to assess the robustness of our numerical method, while keeping in mind that the numerical solution accuracy will be limited by equations model studied, which is in our case the compressible gas dynamics system. In Figure 32, we have displayed the initial grid and the final density maps obtained at

time $t = 0.005$ by means of the first-order and limited second-order DG schemes, with the acoustic solver, on a 100×10 Cartesian grid. Comparing Figures 32(b) and 32(c), we clearly see the second-

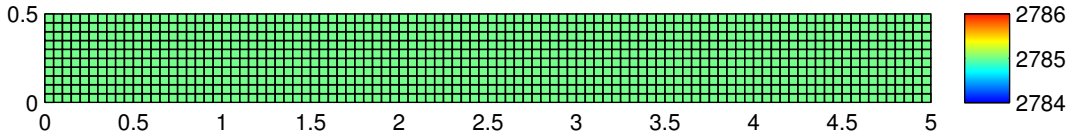

(a) Initial density map.

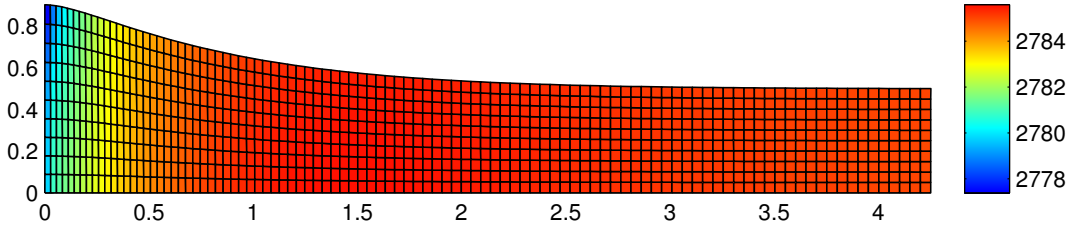

(b) First-order density map.

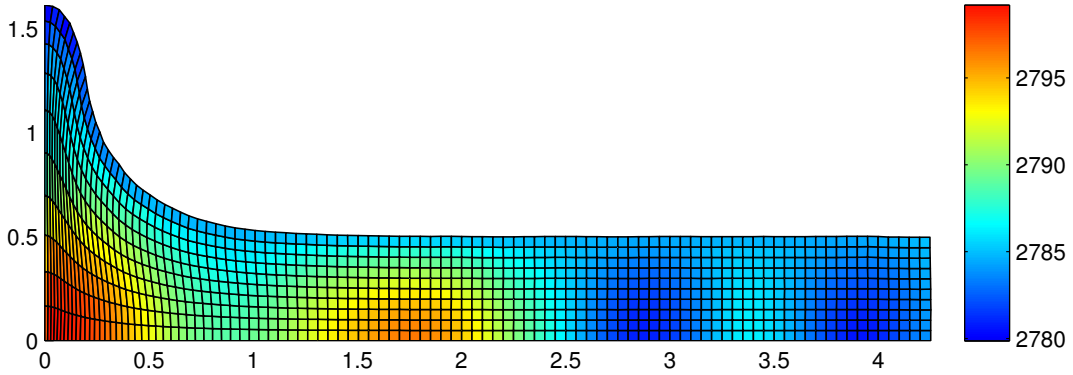

(c) Second-order density map.

Figure 32: Two-dimensional projectile impact problem at time $t = 0.005$ on a 100×10 Cartesian grid.

order final solution grid a lot more deformed than the first-order one. This phenomenon can be explained by the large amount of numerical diffusion inherent of the first-order scheme. As it has been demonstrated in [72] in the case of a Gresho-like vortex problem, in some extreme cases the first-order scheme is unable to simulate appropriately the problems to the final time due to the large numerical diffusion. But obviously, resolving the compressible gas dynamics equations, the numerical schemes presented are not able to capture elastic waves and features. This is the reason why the second-order results, Figure 32(c), are quite far from the ones obtained in [54] with an elastic-plastic second-order cell-centered Lagrangian scheme. Nevertheless, this test case permitted us once more to prove the robustness of the cell-centered Lagrangian schemes presented, as no negative density or negative internal energy appears during the calculation.

5. Conclusion

The aim of this paper is to determine different conditions and constraints under which a wide class of cell-centered Lagrangian schemes solving the compressible gas dynamics equations would

be positivity-preserving, and thus be assured to produce admissible solution. This study has been first tackled in the one-dimensional case, for both first-order finite volume scheme with different approximate Riemann solvers and high-order numerical methods. This analysis has then been extended to the two-dimensional case, and has proved to fit a large number of already existing Lagrangian schemes, as for instance those presented in [12, 55, 8, 72]. Basically, this positivity-preserving property relies on two different techniques: either a particular definition of the local approximation of the acoustic impedances arising from the approximate Riemann solver, or an additional time step constraint relative to the cell volume variation. The first-order proofs have been extended to the high-orders of accuracy by means of the positivity-preserving theory developed in [74, 75, 78]. This work has addressed both ideal and non-ideal equations of state. A wide number of challenging test cases have been used to depict the good performance and robustness of the Lagrangian schemes presented.

In the future, we intend to improve the third-order limiting procedure, in the particular case of moving curved geometries, to remedy the appearance of spurious grid deformation found in [72]. This will enable us to demonstrate once more the relevance of the theory developed in this paper, even in the case of third-order scheme based on curving geometries. Then, the whole positivity-preserving theory developed here, as well as the generic discretization introduced for the two-dimensional gas dynamics equations, will be generalized to the 3D case, as it is done for instance in [57, 12]. We also plan to develop a positive DG discretization of the gas dynamics equations written under the updated Lagrangian formulation and to extend its capability to the non-linear elasticity equations.

Acknowledgment

Research is partially supported by NASA grant NNX12AJ62A and NSF grant DMS-1418750.

Appendices

A. Equations of state

This appendix aims at giving further details related to the equations of state employed in this article, as well as deriving the corresponding domains of validity.

A.1. Gamma gas law for perfect gas

For perfect gas, the thermodynamic pressure is defined as

$$p = \rho(\gamma - 1)\varepsilon, \tag{A.1}$$

where $\gamma > 1$ is the polytropic index of the gas. In this particular case, the sound speed writes

$$a^2 = \gamma \frac{p}{\rho} = \gamma(\gamma - 1)\varepsilon. \tag{A.2}$$

With these particular definitions, it is clear that:

Remark A.1. *If* $\rho \in]0, \infty[$ *then* $\varepsilon > 0 \iff a^2 > 0 \quad (\iff p > 0)$.

The domain of validity of such EOS is $(\rho, \varepsilon) \in]0, +\infty[\times]0, +\infty]$. Thus, we would like to ensure the numerical scheme produces solutions lying in this validity domain.

A.2. Stiffened gas EOS

For stiffened gas, the pressure reads

$$p = \rho(\gamma - 1)\varepsilon - \gamma\, p_s, \tag{A.3}$$

where p_s is a positive constant representing the molecular attraction between water molecules. The sound speed now writes

$$a^2 = \gamma\, \frac{p + p_s}{\rho} = \gamma(\gamma - 1)(\varepsilon - p_s\, \tau). \tag{A.4}$$

The existence of real a is such that:

Remark A.2. *If* $\rho \in]0, \infty[$ *then* $\widehat{\varepsilon} = \varepsilon - p_s\, \tau > 0 \iff a^2 > 0 \quad (\iff \widehat{p} = p + p_s > 0)$.

The domain of validity of such EOS is then $(\rho, \widehat{\varepsilon}) \in]0, +\infty[\times]0, +\infty]$.

A.3. Jones-Wilkins-Lee (JWL) EOS for detonation-product gas

This equation of state is used to describe explosions. Here, the pressure reads

$$p = \rho(\gamma - 1)\varepsilon + f_j(\rho), \tag{A.5}$$

where the positive function $f_j(\rho)$ writes

$$f_j(\rho) = A_1 \left(1 - \frac{(\gamma - 1)\rho}{R_1 \rho_0}\right) \exp^{-\frac{R_1 \rho_0}{\rho}} + A_2 \left(1 - \frac{(\gamma - 1)\rho}{R_2 \rho_0}\right) \exp^{-\frac{R_2 \rho_0}{\rho}}, \tag{A.6}$$

with A_1, A_2, R_1, R_2 being constants depending on the material. ρ_0 is the density of the explosive before detonation, and thus the solution should ensure that $\rho \leq \rho_0$ at all time. With this definition of the pressure, the sound speed writes

$$a^2 = \frac{\gamma p - f_j(\rho) + \rho f_j'(\rho)}{\rho} = (\gamma - 1)(\gamma\varepsilon + \frac{f_j(\rho)}{\rho} + \frac{f_j'(\rho)}{\gamma}). \tag{A.7}$$

It follows that the sound speed is defined if and only if, for $\rho \neq 0$, the internal energy yields

$$\varepsilon \geq -\frac{1}{\gamma}(\frac{f_j(\rho)}{\rho} + \frac{f_j'(\rho)}{\gamma}) = -\frac{g_j(\rho)}{\gamma}. \tag{A.8}$$

The function $g_j(\rho)$ is positive for $\rho > 0$. Similarly to the work presented in [15], we restrict ourselves to the case where $\varepsilon > 0$ and thus, one can state:

Remark A.3. *If* $\rho > 0$ *then* $\varepsilon > 0 \implies a^2 > 0 \quad (\implies p > 0)$.

The chosen domain of validity is then $(\rho, \varepsilon) \in]0, \rho_0]\times]0, +\infty]$. The condition $\rho \leq \rho_0$ comes from a physical interpretation of the studied problems and thus can be relaxed without risking any crash of the code. For example, in the numerical applications this condition can be relaxed as $\rho \leq \rho_0\,(1+\epsilon)$, where $\epsilon \geq 0$ is small. This can be useful in some extreme applications to avoid having too small time steps in the early computational time.

A.4. Mie-Grüneisen EOS for solids

For shock-compressed solids, the pressure reads

$$p = \rho_0 \, \Gamma_0 \, \varepsilon + \rho_0 \, a_0^2 \, f_m(\eta), \tag{A.9}$$

where the function $f_m(\eta)$ writes

$$f_m(\eta) = \frac{(\eta - 1)[\eta - \frac{1}{2}\Gamma_0(\eta - 1)]}{[\eta - S_m(\eta - 1)]^2}, \tag{A.10}$$

with $\eta = \frac{\rho}{\rho_0}$, ρ_0 being the density of the unstressed material, Γ_0 the Grüneisen constant, and a_0 and S_m being the coefficients relating the shock speed and the particle velocity, see [58, 54] for more details. Because the Mie-Grüneisen EOS gives thermodynamic relations for compressed solids, we can without loss of generality assume that $\eta \geq \eta_m$ at all time, with η_m a positive constant. By the definition of the function $f_m(\eta)$, we also consider $\eta < \frac{S_m}{S_m - 1}$ under the assumption that $S_m > 1$. Using definition (A.9), one can write the sound speed definition as

$$a^2 = a_0^2 \, f_m'(\eta) + \frac{\Gamma_0 \, p}{\rho_0 \, \eta^2} = \frac{1}{\eta^2} \left(\Gamma_0^2 \, \varepsilon + a_0^2 \left(\Gamma_0 \, f_m(\eta) + \eta^2 \, f_m'(\eta) \right) \right). \tag{A.11}$$

It follows that the sound speed is defined if and only if, for $\eta < \frac{S_m}{S_m - 1}$, the internal energy yields

$$\varepsilon \geq -\frac{a_0^2}{\Gamma_0^2} \left(\Gamma_0 \, f_m(\eta) + \eta^2 \, f_m'(\eta) \right) = -\frac{a_0^2}{\Gamma_0^2} \, g_m(\eta). \tag{A.12}$$

In (A.12), the function $g_m(\eta)$ can yield negative values for small η. Actually, $g_m(\eta) \geq 0$ if $\eta \in [\eta^\star, \frac{S_m}{S_m - 1}[$, where $g_m(\eta^\star) = 0$. We assume here that $\eta_m \geq \eta^\star$. Similarly to what has been done for the JWL equation of state, we restrict our study to the case $\varepsilon > 0$. Consequently, if $g_m(\eta) \geq 0$, $\varepsilon > 0 \Longrightarrow a^2 > 0$. It immediately follows that:

Remark A.4. *If* $\rho \in [\eta^\star \, \rho_0, \frac{S_m}{S_m - 1} \, \rho_0[$ *then* $\varepsilon > 0 \implies a^2 > 0 \quad (\Longleftrightarrow p > \rho_0 \, a_0^2 \, f(\eta))$.

In the compression case, *i.e.* $\eta \geq 1$, the pressure remains positive. For this particular equation of state, we set the domain of validity to be $(\rho, \varepsilon) \in [\eta^\star \, \rho_0, \frac{S_m}{S_m - 1} \, \rho_0 \, [\times]0, +\infty]$. The evaluation of $\eta^\star$ involves very complex algebra. Thus, for the sake of simplicity we give the definition of $\eta^\star$ in the special case where $\Gamma_0 = 2$. This is the value of the Grüneisen constant used in our numerical applications, or in those presented in [54]. In this case, $\eta^\star$ writes

$$\eta^\star = \frac{4 - 3S_m + \dfrac{10 - 6S_m - 3S_m^2}{C_m} + C_m}{3(S_m - 1)}, \tag{A.13}$$

where $C_m = \left(-28 + 36S_m - 9S_m^2 + 3\sqrt{3}\sqrt{S_m^6 + 6S_m^5 + 5S_m^4 - 56S_m^3 + 60S_m^2 - 8S_m - 8} \right)^{\frac{1}{3}}$. Here are some values of $\eta^\star$ for different S_m used in the literature: $S_m = 1.49 \rightarrow \eta^\star = 0.766531905...$, $S_m = 1.338 \rightarrow \eta^\star = 0.756983366...$, $S_m = 1.124 \rightarrow \eta^\star = 0.741878192....$

References

[1] R. Abgrall, R. Loubère, and J. Ovadia. A Lagrangian Discontinuous Galerkin-type method on unstructured meshes to solve hydrodynamics problems. *Int. J. Numer. Meth. Fluids*, 44:645–663, 2004.

[2] F. L. Adessio, J R Baumgardner, J. K. Dukowicz, N. L. Johnson, B. A. Kashiwa, R. M. Rauenzahn, and C. Zemach. CAVEAT: a computer code for fluid dynamics problems with large distortion and internal slip. Technical Report LA-10613-MS, Rev. 1, UC-905, Los Alamos National Laboratory, 1992.

[3] A.J. Barlow. A high order cell centred dual grid Lagrangian Godunov scheme. *Computers and Fluids*, 83:15–24, 2013.

[4] P. Batten, N. Clarke, C. Lambert, and Causon. On the choice of wavespeeds for the hllc riemann solver. *SIAM J. Sci. Comput.*, 18:1553–1570, 1997.

[5] M. Ben-Artzi and J. Falcovitz. *Generalized Riemann problems in Computational Fluids Dynamics*. Cambridge University press, 2003.

[6] C. Berthon, B. Dubroca, and A. Sangam. A local entropy minimum principle for deriving entropy preserving schemes. *SIAM J. Numer. Anal.*, 50(2):468–491, 2012.

[7] W. Boscheri and M. Dumbser. Arbitrary-lagrangian-eulerian one-step weno finite volume schemes on unstructured triangular meshes. *Commun. Comput. Phys.*, 14:1174–1206, 2013.

[8] B. Boutin, E. Deriaz, P. Hoch, and P. Navaro. Extension of ALE methodology to unstructured conical meshes. *ESAIM: Proceedings*, 32:31–55, 2011.

[9] D.E. Burton, T.C. Carney, N.R. Morgan, S.K. Sambasivan, and M.J. Shashkov. A cell-centered Lagrangian Godunov-like method for solid dynamics. *Computers and Fluids*, 83:33–47, 2013.

[10] E.J. Caramana, D.E. Burton, M.J. Shashkov, and P.P. Whalen. The construction of compatible hydrodynamics algorithms utilizing conservation of total energy. *J. Comput. Phys.*, 146:227–262, 1998.

[11] E.J. Caramana and M.J. Shashkov. Elimination of artificial grid distorsion and hourglass–type motions by means of Lagrangian subzonal masses and pressures. *J. Comp. Phys.*, 142:521–561, 1998.

[12] G. Carré, S. Delpino, B. Després, and E. Labourasse. A cell-centered Lagrangian hydrodynamics scheme in arbitrary dimension. *J. Comp. Phys.*, 228:5160–5183, 2009.

[13] J. Cheng and C.-W. Shu. A high order eno conservative lagrangian type scheme for the compressible euler equations. *J. Comp. Phys.*, 227(2):1567–1596, 2007.

[14] J. Cheng and C.-W. Shu. A third-order conservative Lagrangian type scheme on curvilinear meshes for the compressible Euler equations. *Commun. Comput. Phys.*, 4:1008–1024, 2008.

[15] J. Cheng and C.-W. Shu. Positivity-preserving lagrangian scheme for multi-material compressible flow. *J. Comp. Phys.*, 257:143–168, 2014.

[16] J. Cheng and C.-W. Shu. Second order symmetry-preserving conservative Lagrangian scheme for compressible Euler equations in two-dimensional cylindrical coordinates. *J. Comp. Phys.*, 272:245–265, 2014.

[17] B. Cockburn, S.-Y. Lin, and C.-W. Shu. TVB Runge-Kutta local projection discontinuous Galerkin finite element method for conservation laws III: One-dimensional systems. *J. Comp. Phys.*, 84:90–113, 1989.

[18] B. Cockburn and C.-W. Shu. The Runge-Kutta discontinuous Galerkin method for conservation laws V: Multidimensional systems. *J. Comp. Phys.*, 141:199–224, 1998.

[19] P. Collela. Glimm's method for gas dynamics. *SIAM J. Sci. Statist.*, 3:76–110, 1982.

[20] B. Després. Lagrangian systems of conservation laws. *Numer. Math.*, 89:99–134, 2001.

[21] B. Després. *Lois de Conservation Euleriennes, Lagrangiennes et méthodes numériques.* Mathématiques et Applications. Springer, 2010.

[22] B. Després and C. Mazeran. Lagrangian Gas Dynamics in Two Dimensions and Lagrangian systems. *Arch. Rational Mech. Anal.*, 178:327–372, 2005.

[23] J. K. Dukowicz. A general, non-iterative Riemann solver for Godunov's method. *J. Comput. Phys.*, 61:119–137, 1984.

[24] M. Dumbser and W. Boscheri. High-order unstructured lagrangian one-step weno finite volume schemes for non-conservative hyperbolic systems: applications to compressible multi-phase flows. *Computers and Fluids*, 86:405–432, 2013.

[25] W. Boscheriand M. Dumbser. A direct arbitrary-lagrangian-eulerian ader-weno finite volume scheme on unstructured tetrahedral meshes for conservative and non-conservative hyperbolic systems in 3d. *J. Comp. Phys.*, 275:484–523, 2014.

[26] E.N. Dvorkin and M.B. Goldschmit. *Nonlinear Continua.* Springer, 2005.

[27] B. Einfeldt. On godunov-type method for gas dynamics. *SIAM J. Sci. Comput.*, 9:445–473, 1988.

[28] B. Einfeldt, C.-D. Munz, P. L. Roe, and B. J. Sjöogreen. On godunov-type methods near low densities. *J. Comp. Phys.*, 92:273–295, 1991.

[29] J. L. Estivalezes and P. Villedieu. High-order positivity preserving kinetic schemes for the euler compressible euler equations. *SIAM J. Numer. Anal.*, 33:2050–2067, 1996.

[30] C. Farhat, J.-F. Gerbeau, and A. Rallu. Fiver: a finite volume method based on exact two-phase riemann problems and sparse grids for multi-material flows with large density jumps. *J. Comp. Phys.*, 231:6360–6379, 2012.

[31] G. Gallice. Positive and Entropy Stable Godunov-type Schemes for Gas Dynamics and MHD Equations in Lagrangian or Eulerian Coordinates . *Numer. Math.*, 94:673–713, 2003.

[32] P. Germain. *Mécanique*, volume I. Ellipses, 1986.

[33] W.B. Goad. WAT: A Numerical Method for Two-Dimensional Unsteady Fluid Flow. Technical Report LAMS 2365, Los Alamos National Laboratory, 1960.

[34] E. Godlewski and P.-A. Raviart. *Hyperbolic Systems of Conservation Laws*. Springer Verlag, 2000.

[35] S.K. Godunov, A. Zabrodine, M. Ivanov, A. Kraiko, and G. Prokopov. *Résolution numérique des problèmes multidimensionnels de la dynamique des gaz*. Editions Mir, 1979.

[36] M.E. Gurtin, E. Fried, and L. Anand. *The Mechanics and Thermodynamics of Continua*. Cambridge University Press, 2009.

[37] A. Harten, B. Engquist, S. Osher, and S. Chakravarthy. Uniformly high order essentially non-oscillatory schemes, III. *J. Comp. Phys.*, 71:231–303, 1987.

[38] A. Harten, P. D. Lax, and B. Van Leer. On upstream differencing and godunov-type schemes for hyperbolic conservation laws. *SIAM Rev.*, 25:35–62, 1983.

[39] C.W. Hirt, A. Amsden, and J.L. Cook. An arbitrary Lagrangian–Eulerian computing method for all flow speeds. *J. Comp. Phys.*, 14:227–253, 1974.

[40] R. A. Horn and C. R. Johnson. *Matrix analysis*. Cambridge University Press, 1985.

[41] Z. Jia and S. Zhang. A new high-order discontinuous Galerkin spectral finite element for Lagrangian gas dynamics in two-dimensions. *J. Comp. Phys.*, 230(7):2496–2522, 2011.

[42] G.-S. Jiang and C.-W. Shu. Efficient implementation of weighted eno schemes. *J. Comp. Phys.*, 126:202–228, 1996.

[43] J.R. Kamm and F.X. Timmes. On efficient generation of numerically robust Sedov solutions. Technical Report LA-UR-07-2849, Los Alamos National Laboratory, 2007.

[44] G. Kluth and B. Després. Discretization of hyperelasticity on unstructured mesh with a cell-centered Lagrangian scheme. *J. Comp. Phys.*, 229(24):9092–9118, 2010.

[45] Tz.V. Kolev and R.N. Rieben. A tensor artificial viscosity using a finite element approach. *J. Comp. Phys.*, 228:8336–8366, 2010.

[46] B. Van Leer. Towards the ultimate conservative difference scheme. V-A second-order sequel to Godunov's method. *J. Comput. Phys.*, 32:101–136, 1979.

[47] R. J. LeVeque. *Finite Volume Methods for Hyperbolic Problems*, volume 31. Cambridge Texts in Applied Mathematics, 2002.

[48] T. Linde and P. L. Roe. Robust euler codes. Thirteenth computational fluid dynamics conference, AIAA paper 97-2098, 2007.

[49] W. Liu, J. Cheng, and C.-W. Shu. High order conservative lagrangian scheme with lax-wendroff type time discretization for the compressible euler equations. *J. Comp. Phys.*, 228(23):8872–8891, 2009.

[50] X.-D. Liu, S. Osher, and T. Chan. Weighted essentially non-oscillatory schemes. *J. Comp. Phys.*, 115:200–212, 1994.

[51] R. Loubère. *Une Méthode Particulaire Lagrangienne de type Galerkin Discontinu. Application à la Mécanique des Fluides et l'Interaction Laser/Plasma.* PhD thesis, Université Bordeaux I, 2002.

[52] P.-H. Maire. A high-order one-step sub-cell force-based discretization for cell-centered Lagrangian hydrodynamics on polygonal grids . *Computers and Fluids*, 46(1):479–485, 2011.

[53] P.-H. Maire. Contribution to the numerical modeling of Inertial Confinement Fusion, 2011. Habilitation à Diriger des Recherches, Bordeaux University, available at `http://tel.archives-ouvertes.fr/docs/00/58/97/58/PDF/hdr_main.pdf`.

[54] P.-H. Maire, R. Abgrall, J. Breil, R. Loubère, and B. Rebourcet. A nominally second-order cell-centered Lagrangian scheme for simulating elastic-plastic flows on two-dimensional unstructured grids. *J. Comp. Phys.*, 235:626–665, 2013.

[55] P.-H. Maire, R. Abgrall, J. Breil, and J. Ovadia. A cell-centered Lagrangian scheme for two-dimensional compressible flow problems. *SIAM J. Sci. Comput.*, 29:1781–1824, 2007.

[56] P.-H. Maire and J. Breil. A second-order cell-centered Lagrangian scheme for two-dimensional compressible flow problems. *Int. J. Numer. Meth. Fluids*, 56:1417–1423, 2008.

[57] P.-H. Maire and B. Nkonga. Multi-scale Godunov-type method for cell-centered discrete Lagrangian hydrodynamics. *J. Comp. Phys.*, 228:799–821, 2009.

[58] R. Menikoff. Equations of state and fluid dynamics. Technical Report LA-UR-07-3989, Los Alamos National Laboratory, 2007.

[59] C. D. Munz. On Godunov-type schemes for Lagrangian gas dynamics. *SIAM J. Numer. Anal.*, 31:17–42, 1994.

[60] W. F. Noh. Errors for calculations of strong shocks using artificial viscosity and an artificial heat flux. *J. Comp. Phys.*, 72:78–120, 1987.

[61] B. Perthame. Second-order boltzmann schemes for compressible euler equations in one and two space dimensions. *SIAM J. Numer. Anal.*, 29:1–19, 1992.

[62] B. Perthame and C.-W. Shu. On positivity preserving finite volume schemes for euler equations. *Numer. Mat.*, 73:119–130, 1996.

[63] S. Del Pino. A curvilinear finite-volume method to solve compressible gas dynamics in semi-Lagrangian coordinates. *Comptes Rendus Mathématique*, 348:1027–1032, 2010.

[64] B. J. Plohr and D. H. Sharp. A Conservative Eulerian Formulation of the Equations for Elastic Flows. *Advances in Applied Mathematics*, 9:481–499, 1988.

[65] R. D. Richtmyer and K. W. Morton. *Difference methods for initial-value problems.* John Wiley, 1967.

[66] P. L. Roe. Approximative riemann solvers, parameter vectors, and difference schemes. *J. Comp. Phys.*, 43:357–372, 1981.

[67] J. Salençon. *Mécanique des milieux continus*, volume I, Concepts généraux. Editions de l'Ecole Polytechnique, 2005.

[68] C.-W. Shu and S. Osher. Efficient implementation of essentially non-oscillatory shock-capturing schemes. *J. Comp. Phys.*, 77:439–471, 1988.

[69] E. F. Toro, M. Spruce, and W. Spear. Restoration of the contact surface in the hll riemann solver. *shock waves*, 4:25–34, 1994.

[70] F. Vilar. A discontinuous Galerkin discretization for solving thetwo-dimensional gas dynamics equations written under total Lagrangian formulation on general unstructured grids. *Computers and Fluids*, 64:64–73, 2012.

[71] F. Vilar, P.-H. Maire, and R. Abgrall. Cell-centered discontinuous Galerkin discretizations for two-dimensional scalar conservation laws on unstructured grids and for one-dimensional Lagrangian hydrodynamics. *Computers and Fluids*, 46(1):498–604, 2010.

[72] F. Vilar, P.-H. Maire, and R. Abgrall. Cell-centered discontinuous Galerkin discretization for two-dimensional Lagrangian hydrodynamics. *J. Comp. Phys.*, 276:188–234, 2014.

[73] M.L. Wilkins. *Methods in Computational Physics*, volume 3, chapter Calculation of elastic-plastic flows, pages 211–263. Academic Press, 1964.

[74] X. Zhang and C.-W. Shu. On maximum-principle-satisfying high order schemes for scalar conservation laws. *J. Comp. Phys.*, 229:3091–3120, 2010.

[75] X. Zhang and C.-W. Shu. On positivity preserving high order discontinuous galerkin schemes for compressible euler equations on rectangular meshes. *J. Comp. Phys.*, 229:8918–8934, 2010.

[76] X. Zhang and C.-W. Shu. Positivity preserving high order discontinuous galerkin schemes for compressible euler equations with source term. *J. Comp. Phys.*, 230:1238–1248, 2011.

[77] X. Zhang and C.-W. Shu. Positivity preserving high order finite difference weno schemes for compressible euler equations. *J. Comp. Phys.*, 231:2245–2258, 2012.

[78] X. Zhang, Y. Xia, and C.-W. Shu. Maximum-principle-satisfying and positivity-preserving high order discontinuous galerkin schemes for conservation laws on triangular meshes. *J. Sci. Comput.*, 50:29–62, 2012.